A disformally coupled quintessence mimicking the ΛCDM background

Author: Mr. Avishek Dusoye

Supervisors: Dr. A. de la Cruz-Dombriz

Prof. P.K.S. Dunsby

Prof. N. J. Nunes

Thesis presented for the degree of Doctor of Philosophy
in the Department of Mathematics and Applied Mathematics,
University of Cape Town

Date: 14 February 2022

Declaration

I, Mr. Avishek Dusoye, understand what plagiarism is. I have not plagiarized any part of this Ph.D thesis and all references therein indicate where the work of others are quoted. I hereby declare that the work presented here has not previously been submitted to this or any other university for a degree, and that it represents my own work.

The work presented in this thesis is based partly on collaborations with my supervisors Dr. Alvaro de la Cruz-Dombriz (University of Cape Town), Prof. Peter Dunsby (University of Cape Town), and Prof. Nelson Nunes (University of Lisbon). I confirm that, I have been granted permission by the University of Cape Town's Doctoral Degrees Board to include the following publications in my PhD thesis, and where co-authorships are involved, my co-authors have agreed that I may include the publications:

1. *Disformal couplings in a ΛCDM background cosmology*,
   Avishek Dusoye, Alvaro de la Cruz-Dombriz, Peter Dunsby, Nelson Nunes,
   (Published to JCAP (2021) Vol. 3, arXiv:2006.16962v3).

2. *Constraining disformal couplings with Redshift Space Distortion*,
   Avishek Dusoye, Alvaro de la Cruz-Dombriz, Peter Dunsby, Nelson Nunes,
   (Submitted to JCAP - Dec 2021, arXiv:2112.04736v1).

All the computational codes and data files pertaining to those two publications and the body of work presented in Chapters 3 and 4 can be accessed via this Dropbox hyperlink: https://bit.ly/AviPhDCodes.

Avishek Dusoye

Acknowledgement

I am very grateful for this journey which has caused me to stretch beyond my capabilities. It has been a roller-coaster experience, where the difficult moments have taught me resilience, grit, wisdom, equipoise and patience.

I am forever thankful to my supervisors. I appreciate Prof. Peter Dunsby for his patience and guidance. I render gratitude towards Dr. Alvaro de la Cruz-Dombriz for his expertise, accessibility and advices, and for being more than just a mentor in my life. I acknowledge Prof. Nelson Nunes for all the discussions, the constructive criticisms, and for teaching me what is expected in a research of good standard.

I feel indebted towards the National Research Foundation (NRF) for the Doctoral Innovation Scholarship 2016 (Ref. SFH150727131568) and the UCT International Scholarship 2017, which provided financial support for three years, as well as for the equipment and the travel grant to Corfu Summer School in Greece. I also appreciate all the research grants, which have been allocated to me by my supervisors from the NRF grants (No.120390, Ref. BSFP190416431035 and No.120396, Ref. CSRP190405427545) and from the UCT National Astrophysics Space Science Program (NASSP). A special thought is given to the NRF post-graduate funding administrator Late Ms. Bongiwe Ndamane.

I would like to thank the hospitality of the Institute of Theoretical Astrophysics, University of Oslo (Norway) during my research visit over there.

A big shout out goes to my mom, my brother Anshul and my best friend Aditi for all their emotional sustenance in light and darkness. I am grateful for having the support of great friends within the Cosmology Gravity Group, especially from Mariam, Simthembile and Miguel.

Abstract

Although the currently-accepted Concordance model of the Universe has been very successful observationally, it cannot resolve two main issues. Firstly, it cannot untangle the unknown nature of the cosmological constant in the Einstein Field Equations, which is responsible for the accelerated cosmological expansion. Secondly, it cannot explain the σ_8 tension, which occurs because the constraints upon galactic clustering by the Cosmic Microwave Background Planck experiments diverge from the large-scale measurement by the Dark Energy Survey. As an alternative to the cosmological constant, this thesis will be using a scalar field, namely the quintessence. Our studied cosmological model assumes that the quintessence is coupled with a generic fluid. It also assumes a theory of gravity with two geometries. The gravitational geometry describes the curvature of space-time while the physical geometry describes the propagation of matter fields. The conformal transformation, which relates the gravitational metric and the physical metric, is extended here to a disformal transformation. In this thesis, the disformally coupled quintessence model mimics the expansion history of the Concordance model, in order to reproduce its observational success and yet have additional degrees of freedom to attempt to address those two issues. Using this approach, the quintessential potential is not specified. The dynamical system for our model is analysed using phase portraits for various studied scenarios. We investigate the expansion history of the DCQ model, where the quintessence couples disformally with dark matter (Scenario I). Our investigation confirms that the quintessential mass influences the disformal characteristics of the dynamical system. Furthermore, the evolution of the density perturbations for the disformally coupled dark matter is reviewed. A disformal effect due to the quintessential mass is seen in the growth rate of the cosmological structures on large scales. The disformal parameter renders no appreciable effect on the evolution of total matter perturbation. A Bayesian analysis of the relevant parameters for the perturbative model (i.e., conformal parameter and quintessential mass) is then carried out using the Redshift Space Distortion data to constrain the best-fit parameters, which might elucidate the σ_8 tension. The best fit set of parameters indicates that the data prefers the model to behave conformally.

Contents

List of Tables

List of Figures

Table 1: **Notations and Conventions**

COVARIANT COORDINATE	x_μ
CONTRAVARIANT COORDINATE	x^μ
METRIC	$g_{\mu\nu}$
INVERSE METRIC	$g^{\mu\nu}$
AFFINE CONNECTION	$\Gamma^\alpha_{\mu\nu}$
CHRISTOFFEL SYMBOLS	$\{^\alpha_{\mu\nu}\}$
RIEMANN TENSOR	$R^\alpha{}_{\mu\beta\nu} = g^{\alpha\lambda}R_{\lambda\mu\beta\nu}$
RICCI TENSOR	$R_{\mu\nu} = R^\alpha{}_{\mu\alpha\nu}$
RICCI SCALAR	$R = g^{\mu\nu}R_{\mu\nu}$
EINSTEIN TENSOR	$G_{\mu\nu} \equiv R_{\mu\nu} - \frac{1}{2}g_{\mu\nu}R$
ENERGY MOMENTUM TENSOR	$T_{\mu\nu}$
PARTIAL DERIVATIVES	$\partial_\mu f \equiv f_{,\mu} = \frac{\partial f}{\partial x^\mu}$
COVARIANT DERIVATIVES	$\nabla_\mu f \equiv f_{;\mu}$
D'ALEMBERTIAN	$\Box \equiv g^{\mu\nu}\nabla_\mu\nabla_\nu$
TORSION TENSOR	$T^\alpha_{\mu\nu} \equiv \Gamma^\alpha_{\mu\nu} - \Gamma^\alpha_{\nu\mu}$
NON-METRICITY TENSOR	$Q^\alpha_{\mu\nu} \equiv \nabla^\alpha g_{\mu\nu}$

Table 2: **Acronyms**

ΛCDM	Lambda Cold Dark Matter
GR	General Relativity
DE	Dark Energy
DM	Dark Matter
CCQ	Conformally Coupled Quintessence
DCQ	Disformally Coupled Quintessence
RSD	Redshift Space Distortion
EOS	Equation Of State
IC	Initial Conditions

Chapter 1

Introduction

This chapter provides the background and the motivation for this thesis. It includes an overview of General Relativity in section 1.1, a general description of the Universe in section 1.2, the evidence of dark energy as well as dark matter in section 1.3 and the overview of the ΛCDM model with its current issues in sections 1.4-1.6.

1.1 The premises of General Relativity

General Relativity (GR), also known as Einstein's theory of gravity, is considered as one of the most successful theories because it remains largely valid even a century after its formulation [1, 2]. It conceptualises gravity as the geometric property of spacetime in a four dimensional (4D) manifold. The Lagrangian formulation of GR is usually described by the Einstein-Hilbert (EH) action, which is given by [1]:

$$S_{\rm EH} = \frac{1}{16\pi G}\int (R - 2\Lambda)\,\sqrt{-g}\,d^4x + \int \mathcal{L}_m(g_{\mu\nu}, \psi)\,d^4x\ , \tag{1.1}$$

where the first term is the Lagrangian density from the gravitational contribution and $\mathcal{L}_m$ is the Lagrangian density for the matter fields, ψ. The signature of the diagonalised metric is assumed to be of the form $(-,+,+,+)$ and the variation of the EH action (1.1) is carried out with respect to the metric to give the Einstein field equations [1]:

$$G_{\mu\nu} \equiv R_{\mu\nu} - \frac{1}{2}g_{\mu\nu}R = \frac{8\pi G}{c^4}T_{\mu\nu} + \Lambda g_{\mu\nu}\ , \tag{1.2}$$

where $G_{\mu\nu}$ is the Einstein tensor, $T_{\mu\nu}$ is the energy-momentum tensor, Λ is the cosmological constant, $g_{\mu\nu}$ is the metric of the 4D manifold, G is the Newton's constant and c is the speed of light. In the thesis, we shall choose to use units such that c is unity. GR allows us to understand 1) how the dynamic expansion of the Universe occurs, 2) the nature of neutrons stars and black holes, 3) the existence of gravitational waves, 4) the growth

of structures, and 5) Cosmological Singularities. GR couples universally with all matter fields in the Universe and provides a geometric description of gravity, which embodies the principle of general covariance*. One of the important premises of GR is the universality of freefall [2]. The Equivalence Principles, which are the foundational postulates of GR, are mentioned [2]:

1. **Weak Equivalence Principle (WEP)**; Any uncharged test particle which is free-falling from a given initial position and with a given velocity, should follow the same path of motion.

2. **Einstein Equivalence Principle (EEP)**; In addition to the validity of WEP, an observer at rest in any free-falling frame should find the laws of special relativistic physics to remain valid (locally, and up to tidal gravitational forces), irrespective of the position and the velocity of such a frame.

3. **Strong Equivalence Principle (SEP)**; Massively gravitating objects as well as test particles are subject to the postulate of WEP, and furthermore, an observer at rest in any free-falling frame should find the laws of special relativistic physics to remain valid (locally, and up to tidal gravitational forces), regardless of the position and the velocity of such a frame.

The WEP has been tested through the E*ö*tvos Experiments [3]. The Hugh-Drever Experiment validates the EEP and concludes that the matter fields can only couple with a single rank-2 metric tensor [4]. There are also three classic observational tests of GR which are successful at the scale of the solar system [1, 2]: (i) the gravitational redshifting of light (ii) the bending of the path of light by the Sun (iii) the precession of perihelion of Mercury. Furthermore, there are three theorems which provide us with a better understanding of GR, and they are iterated in the following:

1. **Birkhoff's theorem** [5]; It states that the spherical symmetric solutions of the Einstein field equations (1.2) in vacuum must be static and asymptotically flat (in absence of cosmological constant).

2. **Lovelock's theorem** [6, 7]; It states that the only second-order Euler-Lagrange expression which can be obtained from the variation of a scalar density of the form $\mathcal{L} = \mathcal{L}(g_{\mu\nu})$ in 4D space-time is given below, where ε_1 and ε_2 are arbitrary constants:

$$E_{\mu\nu} = \varepsilon_1\sqrt{-g}G_{\mu\nu} + \varepsilon_2\sqrt{-g}g_{\mu\nu} \ , \tag{1.3}$$

*General covariance refers to the invariance of laws of physics under differentiable coordinate transformations [1].

3. The **No-hair theorem** [8]; It states that the final state for any gravitational collapse is a black hole which is described by its charge, mass and spin only.

Assuming a Riemannian geometry (i.e., vanishing torsion), it can be said that the metric is the key structure in describing the geometry. In GR, it is assumed that the geometry describing curvature is identical to the geometry describing the propagation of the matter fields. However, one of the main ideas behind this thesis involves generalising this assumption by considering those two geometries as distinct, but related to each other (See the conformal and disformal transformation in equation (2.2) and equation (3.1) respectively). Any dually geometric theory of gravity will break the SEP [9], but those transformations are still constrained by the WEP and causality [9]. The extended theories of gravity, which are discussed later in Chapter 2, 3 and 4, are constructed so as to preserve the Lovelock's theorem (1.3), by considering the addition of a scalar field, namely the quintessence.

1.1.1 Affine connection and Riemann Curvature tensor

Any general vector V with its components V^μ can be expressed in terms of basis vectors e_μ as in $V = V^\mu e_\mu$. In Minkowski space-time, the derivative of such a basis do not vary, i.e., $\dfrac{\partial e_\alpha}{\partial x_\beta} = 0$. But in general space-time, the derivative of that basis is not zero but is actually a vector, which can be re-expressed in terms of a new set of basis vector. The components preceding the new bases are called the affine connection [1]:

$$\frac{\partial e_\nu}{\partial x^\mu} = \Gamma^\alpha_{\mu\nu}\, e_\alpha \ , \qquad \text{such that} \qquad \Gamma^\alpha_{\mu\nu} = \left\{{\alpha \atop \mu\nu}\right\} = \frac{1}{2} g^{\alpha\beta}(g_{\mu\beta,\nu} + g_{\nu\beta,\mu} - g_{\mu\nu,\beta}) \ , \tag{1.4}$$

where the affine connection $\Gamma^\alpha_{\mu\nu}$ have same components as the Christoffel symbols $\left\{{\alpha \atop \mu\nu}\right\}$, when the torsion tensor $T^\alpha_{\mu\nu}$ and the non-metricity tensor $Q^\alpha_{\mu\nu}$ are assumed to vanish. Thus, $\Gamma^\alpha_{\mu\nu}$ can be calculated from the metric components. In any local inertial frame, one should recollect $\Gamma^\alpha_{\mu\nu} = 0$ since the derivative of the metric would be zero. The use of the affine connection in GR is relevant because one is working with non-inertial frames.

There is a famous quote by John A. Wheeler; "Space-time tells matter how to move; matter tells spacetime how to curve", which attempts roughly to describe gravity as in equation (1.2). The Riemann Curvature tensor $R^\mu{}_{\nu\alpha\beta}$ is a measure of how curved the space-time can be in the presence of mass-energy and can be defined in terms of the affine connection [1]:

$$R^\alpha{}_{\mu\beta\nu} \equiv \Gamma^\alpha_{\mu\beta,\nu} - \Gamma^\alpha_{\mu\nu,\beta} + \Gamma^\alpha_{\varepsilon\beta}\Gamma^\varepsilon_{\mu\nu} - \Gamma^\alpha_{\varepsilon\nu}\Gamma^\varepsilon_{\beta\mu} \ . \tag{1.5}$$

It can even be observed by the deviation of the geodesics of light in a curved space-time, which is given by equation (1.6)[1], whereby u^μ and u^ν are the velocities of two relativistic particles following their own geodesics and ξ^β is a vector separating the two particles.

$$\nabla_\lambda \nabla^\lambda \xi^\alpha = R^\alpha{}_{\mu\nu\beta} u^\mu u^\nu \xi^\beta \ . \tag{1.6}$$

In flat space-time, we find $\nabla_\lambda \nabla^\lambda \xi^\alpha = 0$ as expected since the geodesics would reduce to parallel paths and this would imply $R^\alpha{}_{\mu\nu\beta} = 0$. But in presence of mass-energy, $R^\alpha_{\mu\nu\beta} \neq 0$. The traceless component of the Riemann Curvature tensor is commonly known as the Weyl tensor $W_{\mu\nu\alpha\beta}$. The projections of the Weyl tensor, with respect to a co-moving observer with velocity u^α, yield the electric curvature part $E_{\mu\nu} = W_{\mu\nu\alpha\beta} u^\alpha u^\beta$ and magnetic curvature part $H_{\mu\nu} = \frac{1}{2} \eta_{\mu\lambda\varepsilon} W^{\lambda\varepsilon}{}_{\nu\beta} u^\beta$ [10], where $\eta_{\mu\lambda\varepsilon}$ is the 3D volume element.

1.1.2 Ricci identity and Bianchi Identity

The Ricci identity is a more general form of the geodesic equation (1.6). In the subsection 1.1.2, a derivation of the two identities is reviewed, by taking the parallel transport of a general vector field around a closed loop in a curved space-time.

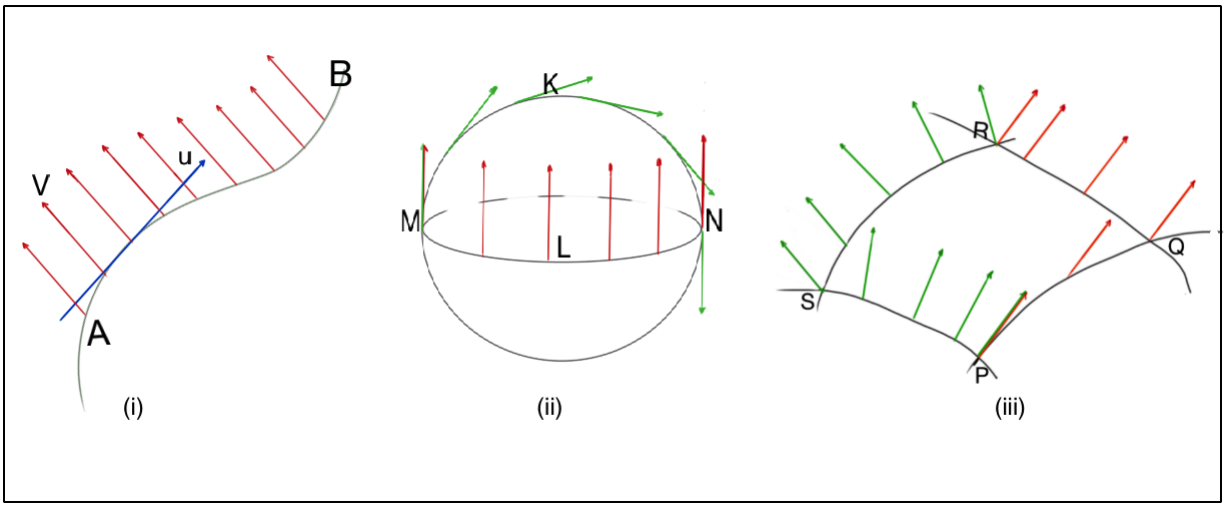

Figure 1.1: The parallel transport of a vector field V in three cases: (i) along a timelike curve with tangent u, (ii) on a spherical space-time by two pathways, (iii) around a closed loop by two pathways. The picture was inspired by Ref. [11] and P. Dunsby's GR Lecture notes.

First, let us define how the parallel transport works in the simplest cases. The left panel of Figure 1.1 shows for the case of a vector field V^α which is transported along the worldline of a curve AB. This curve has also a tangent $u^\alpha = \dfrac{\partial x^\alpha}{\partial \lambda}$ where λ is an affine parameter on the curve. The parallel transport of V^α is only valid if it satisfies

$\frac{dV^\alpha}{d\lambda} = \frac{dx^\beta}{d\lambda}\nabla_\beta V^\alpha = 0$, which also implies that $u^\beta \nabla_\beta V^\alpha = 0$. In a Minkowski flat space, the parallel transport of a vector would simply bring a translation of the vector from one point to another. But in case of the curved space-time, one finds that the direction of the transported vector is not the same as at its original point. This is illustrated in the central panel of Figure 1.1, where the same vector which gets transported through two pathways (MLN and MKN) on a sphere but ends up in opposite direction.

Let us now consider a infinitesimal loop PQRS (see the right panel of Fig 1.1) on the surface of the same sphere, which has both intrinsic and extrinsic curvature. Since the direction of the transported vector V^α will change on this loop, we can calculate the variation produced for V^α. Taking from P to Q, we obtain $\delta V^\alpha = dx^\beta \nabla_\beta V^\alpha = dV^\alpha + \Gamma^\alpha_{\beta\sigma} V^\sigma dx^\beta$. If one now takes the transported vector from the Q to R, we have to parallel transport once again $(V^\alpha + \delta V^\alpha)$. The new variation becomes $\delta(\delta V^\alpha) = dx^\beta dx^\mu \nabla_\beta \nabla_\mu V^\alpha$. The full expression is given by equation (1.7)[11]:

$$\delta(\delta V^\alpha)_{PQR} = d^2 V^\alpha + 2\Gamma^\alpha_{\beta\sigma} dx^\beta dV^\sigma + (\partial_\mu \Gamma^\alpha_{\beta\sigma} + \Gamma^\alpha_{\mu\lambda}\Gamma^\lambda_{\beta\sigma}) dx^\beta dx^\mu V^\sigma \tag{1.7}$$

We can then repeat the same process for the parallel transport of the same vector V^α via PSR and obtain a similar expression as well for $\delta(\delta V^\alpha)_{PSR}$ (See GR in Ref. [11] for more details). By comparing expressions for $\delta(\delta V^\alpha)_{PQR}$ and $\delta(\delta V^\alpha)_{PSR}$, one finds that the only terms containing $dx^\beta dx^\mu$ are different, and that substracting both expressions leads to the Ricci Identity [1, 11]:

$$(\nabla_\beta \nabla_\mu - \nabla_\mu \nabla_\beta) V^\alpha = R^\nu{}_{\alpha\beta\mu} V^\alpha \ , \tag{1.8}$$

Where $R^\nu{}_{\alpha\beta\mu}$ is the Riemann Tensor such that $R_{\nu\alpha\beta\mu} = g_{\nu\lambda} R^\lambda{}_{\alpha\beta\mu}$, as introduced by equation (1.5). The Bianchi Identity comes from the cyclic and symmetric properties of the Riemann Tensor. For instance, if we permutate the indices, we find $R_{\alpha\beta\mu\nu} = R_{\mu\nu\alpha\beta}$ and $R_{\alpha\beta\mu\nu} = -R_{\beta\alpha\mu\nu} = R_{\alpha\beta\nu\mu}$. Therefore, $R_{\alpha\beta\mu\nu} + R_{\alpha\mu\beta\nu} + R_{\alpha\nu\beta\mu} = 0$, can be inferred and its covariant derivative would provide for the Bianchi Identity [1, 11]:

$$\nabla_\lambda R_{\alpha\beta\mu\nu} + \nabla_\mu R_{\alpha\beta\nu\lambda} + \nabla_\nu R_{\alpha\beta\lambda\mu} = 0 \ . \tag{1.9}$$

These two identities basically summarise the properties of curvature in a 4D manifold.

1.2 A general covariant description of the Universe

We shall now provide the mathematical setup for the description of a general model of the Universe, which evolves through space-time from inflation until today. In this section, we are assuming that GR is sufficient enough to describe the interaction between the geometry and the cosmological contents on large scales. The section 1.2 has been mainly inspired by the Cargèse Lectures* on cosmological models [10].

The most fundamental way to describe a manifold is by its space-time metric $g_{\mu\nu}$. Within such a 4D manifold, all events happen at a particular temporal and spatial coordinates. Therefore most of the variables describing an event can be expressed of the metric. The term "1 + 3" refers to the splitting of one temporal and three spatial components of all the cosmological quantities for any defined model.

Let us consider a simple model of the Universe, in which the content is expanding like an inflating balloon. The overall motion of matter can be described as radially outward and by its 4-velocity tensor $u^\mu = \dfrac{dx^\mu}{dt}$. t is proper time and we define $u^\mu u_\mu = -1$. We assume to be observers that are in the same rest frame as matter and assume that we are also moving with 4-velocity u^μ. Therefore it is useful to project the cosmological variables parallel and orthogonal to the 4-velocity. The projection tensors are defined as $U^\mu_\nu = -u^\mu u_\nu$ and $h_{\mu\nu} = g_{\mu\nu} + u_\mu u_\nu$. In addition, other mathematical objects e.g., the covariant derivative can also be projected spatially and denoted as $\tilde{\nabla}^a = h^a_i \nabla^i$.

1.2.1 The Kinematic and Dynamical quantities

Since we are considering an expanding Universe, it is in our interest to find the covariant derivative of the 4-velocity. The derivative of u_ν (i.e.$\nabla_\mu u_\nu$) being a tensor also exhibits symmetric properties and we will have to decompose it into the trace, symmetric and anti-symmetric parts [10], as per equation (1.10). The reason for this is that these parts have different interpretations and physical meanings. They can be treated and evolved separately for the sake of clarity in our model. In this section, the overdot for e.g., in $\dot{x}$ refers to the derivative of an arbitrary variable x with respect to proper time.

$$\begin{aligned}\nabla_\mu u_\nu = -u_\mu \dot{u}_\nu + \tilde{\nabla}_\mu u_\nu &= -u_\mu \dot{u}_\nu + \tilde{\nabla}_\mu u_\nu + \tilde{\nabla}_{\langle\mu} u_{\nu\rangle} + \tilde{\nabla}_{[\mu} u_{\nu]} \\ &= -u_\mu \dot{u}_\nu + \frac{1}{3}\Theta h_{\mu\nu} + \sigma_{\mu\nu} + \omega_{\mu\nu} \ ,\end{aligned} \tag{1.10}$$

*The treatment and evolution of electro-gravitational quantities are omitted from this section because they are not quite relevant for this thesis. Any interested reader may refer to [10] for further details.

where the acceleration $\dot{u}_\nu$, the rate of volume expansion $\Theta = \tilde{\nabla}_\mu u^\mu$, the rate of fluid distortion i.e., shear $\sigma_{\mu\nu} = \tilde{\nabla}_{\langle\mu} u_{\nu\rangle}$ and rate of rotational velocity i.e., vorticity $\omega_{\mu\nu} = \tilde{\nabla}_{[\mu} u_{\nu]}$ are the only *kinematic quantities* for this model. Since these kinematic quantities describe the average motion of the cosmological contents, it would be relevant to decompose their energy-momentum tensor $T_{\mu\nu}$ into trace, symmetric and anti-symmetric parts as well [10]:

$$T_{\mu\nu} = \rho u_\mu u_\nu + P h_{\mu\nu} + 2q_{(\mu} u_{\nu)} + \pi_{\mu\nu} \ , \tag{1.11}$$

where the energy density $\rho = T_{\mu\nu} u^\mu u^\nu$, the isotropic pressure $P = T_{\mu\nu} h^{\mu\nu}/3$, the heat flux $q^\mu = -T_{\nu\lambda} u^\nu h^{\lambda\mu}$ and the anisotropic stress $\pi_{\mu\nu}$ are known as the *dynamical quantities*. The equation (1.11) is general and could apply to many types of cosmological fluids. For example, $P = 0$ in the case of pressureless matter such as dust and cold dark matter. $q^\mu = 0$ and $\pi_{\mu\nu} = 0$ in the case of a perfect fluid. The relation between the dynamical quantities ρ and P specifies the nature of the fluid, usually in the form:

$$P = w\rho \ , \tag{1.12}$$

where w is the parameter for the equation of state (EOS). For instance, we have $w = 1/3$ for radiation and $w = 0$ for baryons or dark matter.

1.2.2 Propagation and Constraint Equations

The Ricci identity (1.8) and Bianchi identity (1.9) are quite general and apply to many models of the Universe. Since the observer is in the rest frame of matter (moving with 4-velocity u^α in this cosmological model), it therefore makes sense to project these identities parallel and orthogonal to the 4-velocity to consider the effect of gravity as relevant in that frame. Moreover, these identities are written in terms of Riemann curvature, whose components* i.e., $R^{\mu\nu}_{\alpha\beta} = R^{\mu\nu}_{\alpha\beta}|_{\rm P} + R^{\mu\nu}_{\alpha\beta}|_{\rm I}$ could be expressed in terms of the kinematic and the dynamic quantities [10]:

$$R^{\mu\nu}_{\alpha\beta}|_{\rm P} = \frac{2}{3}(\rho + 3P - 2\Lambda) u^{[\mu} u_{[\alpha} h^{\nu]}_{\beta]} + \frac{2}{3}(\rho + \Lambda) h^\mu_{[\alpha} h^\nu_{\beta]} \ , \tag{1.13}$$

$$R^{\mu\nu}_{\alpha\beta}|_{\rm I} = -2u^{[\mu} h^{\nu]}_{[\alpha} q_{\beta]} - 2u_{[\alpha} h^{[\mu}_{\beta]} q^{\nu]} - 2u^{[\mu} u_{[\alpha} \pi^{\nu]}_{\beta]} + 2h^{[\mu}_{\ [\alpha} \pi^{\nu]}_{\ \beta]} . \tag{1.14}$$

The projection of the identities (1.8)-(1.9) allows us to find out how the kinematic and dynamic quantities evolve as the Universe expands. The relations which are obtained after such projections are referred to as the set of propagation and constraint equations.

*P denotes perfect fluids with both $q^\mu = 0$ and $\pi_{\mu\nu} = 0$ while I denotes imperfect fluids.

The propagation equations represent the evolution of the those quantities while constraint equations manifest the laws of conservation for those quantities. Every vector field obeys the Ricci identity (1.8) and when we apply the identity for the velocity field of matter u^α, we have $(\nabla_\nu\nabla_\mu - \nabla_\mu\nabla_\nu)u^\alpha = R^\alpha{}_{\beta\mu\nu}u^\beta$. To project this identity along the direction of u^μ, we multiply the identity with u^μ and contract it to obtain the following form [10]:

$$(\nabla_\nu u^\alpha)^{\cdot} - \nabla_\nu \dot{u}^\alpha + \nabla_\mu u^\alpha \nabla_\nu u^\mu = R^\alpha{}_{\beta\mu\nu}u^\beta u^\mu. \tag{1.15}$$

One can insert equation (1.10) to substitute $\nabla_\nu u^\alpha$ in the equation (1.15). Then after multiplying the equation (1.15) with the metric g^ν_α to contract all the indices, one obtains the general Raychaudhuri equation [10]:

$$\dot{\Theta} - \tilde{\nabla}_\lambda \dot{u}^\lambda - \dot{u}_a\dot{u}^a + \frac{1}{3}\Theta^2 + 2\sigma^2 - 2\omega^2 = -\frac{\kappa}{2}(\rho + 3P) + \Lambda \ . \tag{1.16}$$

This equation is fundamental because $\dot{\Theta}$ represents the accelerating rate of volume expansion of the Universe. It is mainly sourced by the content of the Universe $(\rho + 3P)$ and the cosmological constant Λ. It also has some contributions from the shear σ and the vorticity w. Those terms account for the cases when the Universe is stretching and rotating respectively.

However, the rate of shear σ and rate of vorticity ω are evolving with time as well. On one hand, one can obtain the following vorticity propagation equation (1.17) by starting with the skew part of the equation (1.15). Knowing that $R_{[\alpha|\beta\mu|\nu]}u^\beta u^\mu = 0$ is useful here. Then one can project the skewed part of equation (1.15) orthogonal to u^μ by multiplying with $h^\alpha_\beta h^\nu_\lambda$. After the re-arrangements of some terms, one reaches to the expression [10];

$$\dot{\omega}^{\langle\mu\rangle} - \eta^{\mu\lambda\gamma}\tilde{\nabla}_{[\lambda}\dot{u}_{\gamma]} = -\frac{2}{3}\Theta\omega^\mu + \sigma^\mu{}_\nu\omega^\nu \ , \tag{1.17}$$

where the vorticity vector is usually defined as $\omega^\rho = \eta^{\sigma\rho\kappa\tau}\omega_{\kappa\tau}u_\sigma$ and $\eta^{\sigma\rho\kappa\tau}$ represents the 4-D volume element. On the other hand, the shear propagation equation can be deduced as follows. The shear can be expressed as $\sigma_{\kappa\lambda} = h^\mu_\kappa h^\nu_\lambda \nabla_\mu u_\nu - \frac{1}{3}\Theta h_{\kappa\lambda}$. By taking the time derivative of this expression and by projecting orthogonally to u^μ, one obtains[10];

$$\dot{\sigma}_{\langle\mu\nu\rangle} - \tilde{\nabla}_{\langle\mu}\dot{u}_{\nu\rangle} = -\frac{2}{3}\Theta\sigma_{\mu\nu} + \dot{u}_{\langle\mu}\dot{u}_{\nu\rangle} - \sigma_{\langle\mu\lambda}\sigma^\lambda{}_{\nu\rangle} - \omega_{\langle\mu\lambda}\omega^\lambda{}_{\nu\rangle} - (E_{\mu\nu} - \frac{1}{2}\pi_{\mu\nu}). \tag{1.18}$$

The constraint equations (1.19)-(1.20) usually arise from the symmetric properties of the Bianchi identity (1.9). One can obtain the conservation equation of vorticity (1.19), after having multiplied $R^\alpha{}_{[\beta\mu\nu]} = 0$ with $u_\alpha u^\nu$ and the 4D volume element $\eta^{\alpha\beta\mu\nu}$. The

conservation equation of shear (1.20) can be obtained by similarly projecting $R^{\alpha}{}_{[\beta\mu\nu]} = 0$ orthogonal to u^{α} and making use of $R_{\beta\nu}u^{\beta}h^{\nu\mu} = -q^{\mu}$ [10]:

$$\tilde{\nabla}_{\alpha}\omega^{\alpha} = (\omega^{\beta}\dot{u}_{\beta}) , \tag{1.19}$$

$$\tilde{\nabla}_{\beta}\sigma^{\alpha\beta} = +\frac{2}{3}\tilde{\nabla}^{\alpha}\Theta - \eta^{\alpha\beta\mu}(\tilde{\nabla}_{\beta}\omega_{\mu} + 2\dot{u}_{\beta}\omega_{\mu}) - q^{\alpha}. \tag{1.20}$$

In addition to the conservation of the kinematic quantities, one can also find the conservation equations of the dynamical quantities. By contracting the Bianchi identity (1.9) twice, one finds that the Einstein tensor is conserved, $\nabla_{\mu}G^{\mu\nu} = 0$. From Einstein field equations (1.2), the conservation of energy-momentum that $\nabla_{\mu}T^{\mu\nu} = 0$ is also implied. Therefore in this context of projecting the Bianchi identity (1.9) alongside and orthogonal to the 4-velocity u^{μ}, it makes sense to evaluate $u_{\nu}\nabla_{\mu}T^{\mu\nu}$ as well as $h^{\lambda}_{\nu}\nabla_{\mu}T^{\mu\nu}$. Those evaluations would produce the following conservation equations of the energy density and the heat flux respectively [10]:

$$\dot{\rho} + \tilde{\nabla}_{\lambda}q^{\lambda} = -\Theta(\rho + P) - 2(\dot{u}_{\lambda}q^{\lambda}) - \sigma_{\mu\nu}\pi^{\mu\nu} , \tag{1.21}$$

$$\dot{q}^{\langle\lambda\rangle} + \tilde{\nabla}^{\lambda}P + \tilde{\nabla}_{\kappa}\pi^{\lambda\kappa} + \frac{4}{3}\Theta q^{\lambda} + q^{\kappa}(\sigma^{\lambda}_{\kappa} + \omega^{\lambda}_{\kappa}) + \dot{u}_{\kappa}\pi^{\lambda\kappa} + (\rho + P)\dot{u}^{\lambda} = 0 , \tag{1.22}$$

where $\dot{\rho}$ is the flux of energy-mass with isotropic pressure P and q^{μ} is the heat flux with anistropy pressure $\pi^{\mu\nu}$ if we include the contribution for an imperfect fluid. For perfect fluids, the equation (1.21) reduces as follows with $\Theta = 3\dot{a}/a$:

$$\dot{\rho} = -3\dot{a}/a(\rho + P). \tag{1.23}$$

1.3 Evidence for Dark Energy and Dark matter

One of the simplest ways to conceptualise Dark Energy (DE) is the idea of a cosmological fluid with a negative EOS, which might explain the effects of the cosmological constant. The cosmological constant Λ acts as a source term in the Einstein equations (1.2) and therefore contributes to the effect of gravity and the evolution of our Universe. The late-time accelerated cosmological expansion justifies the cosmological constant to be positive and non-zero value [12]. The DE is referred as dark mainly because this form of mass-energy does not interact directly with light and its nature is unknown. The main supporting reasons for DE to exist, are iterated below:

1. Planck's latest results [13] combined with Type Ia Supernovae, measures an EOS parameter for DE of $w_{\mathrm{DE}} = -1.03 \pm 0.03$.

2. The Dark Energy Survey [14] measures $w_{\rm DE} = -1.031^{+0.218}_{-0.379}$, after combining those two-point functions, using a magnitude-limited lens sample for the first time.

3. The Seven-Year Wilkinson Microwave Anisotropy Probe (WMAP) Observations points toward $w_{\rm DE} = -1.10 \pm 0.14$ [15].

4. The Ref.[16] shows a cosmological constraint of $w_{\rm DE} \approx -1$ using the Cosmic Microwave Background (CMB) data, the Baryonic Acoustic Oscillation (BAO) data and the Combined Supernova Datasets 2008. This is illustrated in Figure 1.2 below:

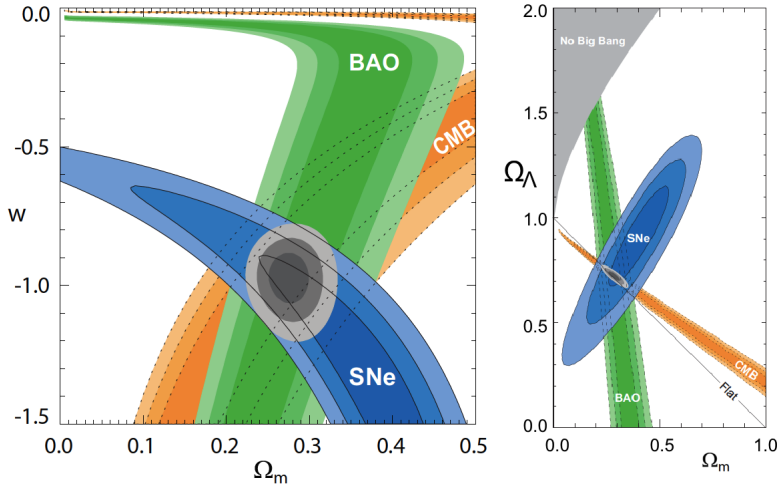

Figure 1.2: The right panel and left panel show the contours plot of w versus Ω_m and Ω_Λ versus Ω_m respectively for a flat Universe [16], whereby the reader can refer to equation (1.27) for the definition of energy densities Ω_Λ and Ω_m.

The "missing" amount of luminous matter in galaxies and clusters seems to be justified by the non-relativistic cold dark matter (CDM)[17]. Although the CDM does not interact with light, it still has a gravitational influence on luminous matter. The effects of the CDM have been found in the following cases:

1. The rotation curves of galaxies tend to have a plateau of constant velocity at large radii. This is counter-intuitive to what is predicted by Kepler's law, unless there is more matter which is not detected [18].

2. The lensing effects due to cluster of galaxies are stronger than what is expected by the presence of its luminous mass only [19].

3. The diffusion damping, which is a phenomenon that happens during recombination, tends to cause the small-scale structure in baryons to be reduced significantly. This is also why galaxy formation does not happen at late times. However, CDM can resist such a damping mechanism and seeds for the formation of galaxies [20].

1.4 The ΛCDM Concordance model

The currently accepted cosmological model, which includes about 68.89% dark energy in the form of a cosmological constant and 31.11% dark matter [13], is known as the ΛCDM Concordance model. The background formalism is based on the well-known cosmological principle that the Universe is homogeneous and isotropic. The geometry of the ΛCDM model utilises the Friedmann-Lemaître-Robertson Walker (FLRW) metric which is described in the Cartesian cordinates below [11]:

$$ds^2 = g_{\mu\nu}dx^\mu dx^\nu = -dt^2 + a^2(t)\gamma_{ij}dx^i dx^j \quad \text{such that } \gamma_{ij} = \frac{\delta_{ij}}{\left(1 + \frac{1}{4}\mathcal{K}\delta_{ab}x^a x^b\right)}\,, \tag{1.24}$$

where t is the cosmic time, $a(t)$ is the scale factor, and the indices $i, j = 1, 2, 3$ denote the spatial coordinates. δ_{ij} is the Kronecker delta and $\mathcal{K}$ is the spatial curvature of the FLRW geometry. Given the FLRW metric (1.24), one can compute the components of the affine connections, the Ricci Tensor, the Einstein Tensor and the energy-momentum tensor [11], as shown in the Appendix A.1. Thus, the 00^{th} and ij^{th} components of the Einstein field equations (1.2) provide the Friedmann and the Raychaudhuri equations respectively in cosmic time [11]:

$$H^2 = \frac{\kappa^2}{3}\rho - \frac{\mathcal{K}}{a^2} + \frac{\Lambda}{3} \qquad \text{and} \qquad \dot{H} + H^2 = -\frac{\kappa^2}{6}(\rho + 3P) + \frac{\Lambda}{3}\,, \tag{1.25}$$

where $H(t) = \dot{a}/a$ is the Hubble parameter and the overdot denotes the derivative with respect to cosmic time. The conservation equation (1.23) can be re-written for the n^{th} fluid and the energy density ρ evolves with the scale factor as [11]:

$$\dot{\rho}_n = -3H(\rho_n + P_n) = -3H\rho_n(1 + w_n) \quad \Rightarrow \quad \rho \propto a^{-3(1+w_n)}, \tag{1.26}$$

where the index n denotes the cosmological fluids such as baryons, dark matter, and radiation. It is actually useful to define the dimensionless energy density parameters as below, in order to better understand the ΛCDM model, its solutions and observational constraints.

$$\Omega_n = \frac{\kappa^2\rho_n}{3H^2}\,, \qquad \Omega_\Lambda = \frac{\Lambda}{3H^2}\,, \qquad \Omega_\mathcal{K} = -\frac{\mathcal{K}}{H^2a^2}\,. \tag{1.27}$$

These definitions (1.27) simplify the Friedmann equation (1.25) into equation (1.28):

$$\sum_n \Omega_n + \Omega_\Lambda + \Omega_\mathcal{K} = 1. \tag{1.28}$$

The evolution of the energy density parameters Ω_n with scale factor a is given by [11]:

$$\Omega_n = \Omega_{n0} h^2 \left(\frac{a}{a_0}\right)^{-3(1+w_n)}, \tag{1.29}$$

such that h is the reduced Hubble function and is defined as [11]:

$$h^2 \equiv \left(\frac{H}{H_0}\right)^2 = \sum_n \Omega_{n0} \left(\frac{a}{a_0}\right)^{-3(1+w_n)} + \Omega_{\mathcal{K}0} \left(\frac{a}{a_0}\right)^{-2} + \Omega_{\Lambda 0}. \tag{1.30}$$

H_0 is the Hubble constant, i.e., the value of H today. The quantities Ω_{n0}, $\Omega_{\mathcal{K}0}$ and $\Omega_{\Lambda 0}$ represent the energy density parameters, which are measured today for the n^{th} cosmological fluid, the curvature and the cosmological constant respectively. The ratio of the scale factor to its current value is often related to a useful quantity, dubbed as the redshift Z, by $a/a_0 = 1/(1+Z)$. The dynamical system of the ΛCDM model was studied by considering the following set of differential equations [21]:

$$\Omega'_\Lambda = 2\,(1+q)\,\Omega_\Lambda\,, \tag{1.31}$$

$$\Omega'_\mathcal{K} = 2q\Omega_\mathcal{K}\,, \tag{1.32}$$

$$\Omega'_n = [2q + 2 - 3(1+w_n)]\,\Omega_n\,, \tag{1.33}$$

where $'$ is the derivative with respect to e-fold $N \equiv \ln(a/a_0)$. The variable q is the deceleration parameter, which is defined as $q \equiv -(H'/H) - 1$. The solutions of dynamical systems can be categorised as:

1. Fixed points – which correspond to when the dynamical system (1.31)-(1.33) is in equilibrium, i.e., $\Omega'_n = 0$, and/or $\Omega'_\Lambda = 0$, and/or $\Omega'_\mathcal{K} = 0$.

2. Trajectories – which show the evolution of the dynamical system from a given certain initial conditions, the asymptotic behaviour and the boundaries in energy density parameter space.

The three fixed points and three equilibrium lines, which are defined by $\Omega'_\Lambda = \Omega'_\mathcal{K} = 0$ are enumerated below [21]:

1. $(\Omega_\mathcal{K}, \Omega_\Lambda) = (0, 0)$ denotes the Einstein de-Sitter (EdS) space, i.e., where the cosmological constant is absent in a flat geometry.

2. $(\Omega_\mathcal{K}, \Omega_\Lambda) = (0, 1)$ denotes the de-Sitter (dS) space, where the cosmological constant dominates and matter is absent in a geometry with flat geometry. The Universe is expanding exponentially forever.

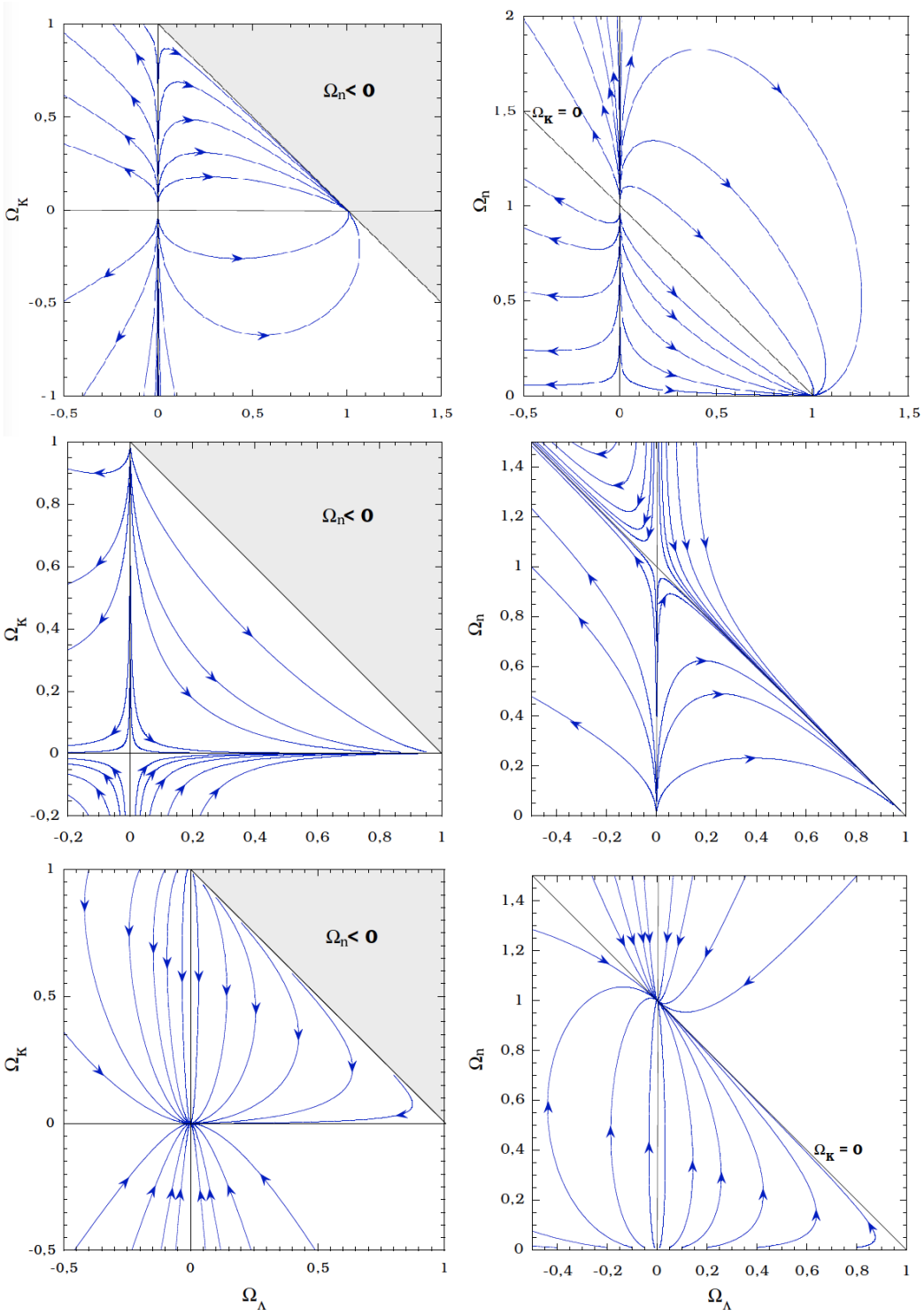

Figure 1.3: The dynamical system analysis of the ΛCDM model [21] is shown. The 3D phase portrait is projected on the $(\Omega_{\mathcal{K}}, \Omega_\Lambda)$ plane (left panels) and on the $(\Omega_n, \Omega_\Lambda)$ plane (right panels). From top to bottom, the panels are for equations of state $\gamma_n = 1,\ 1/3,\ -1$, such that $\gamma_n = w_n + 1$. The interested reader is directed to Ref. [21] for details.

3. $(\Omega_{\mathcal{K}}, \Omega_{\Lambda}) = (1, 0)$ denotes the Milne space (M), where neither matter nor cosmological constant is present in a hyperbolic geometry.

4. $\Omega_{\mathcal{K}} = 0$ is an equilibrium line of fixed points which topologically separate the compact Universes in the $\Omega_{\mathcal{K}} < 0$ region and the infinite Universes in the $\Omega_{\mathcal{K}} > 0$ region.

5. $\Omega_{\Lambda} = 0$ is an equilibrium line of fixed points, connecting the Milne and the EdS fixed points. The dynamical system evolves toward either Milne or EdS fixed point.

6. $\Omega_n = 0$ is a boundary of the parameter space, because the energy density values of Ω_n can only be positive. The dynamical system evolves toward either Milne or de-Sitter fixed points.

Table 1.1 summarises the stability properties for the three fixed points, which can be determined by the linear stability theory [22], as either an attractor (A), or a repeller (R) or a saddle (S). The Figure 1.3 shows the trajectories of the dynamical system (1.31)-(1.33) on the $(\Omega_{\mathcal{K}}, \Omega_{\Lambda})$ plane and the $(\Omega_n, \Omega_{\Lambda})$ plane for three given values of $\gamma_n = 1,\ 1/3,\ -1$, such that $\gamma_n = w_n + 1$. In short, the dynamical system analysis of the ΛCDM model provides different possible evolutions of the Universe, given certain initial conditions and chosen parameters.

γ_n	$]-\infty, 0[$	0	$]0, 2/3[$	$2/3$	$]2/3, +\infty[$
EdS	A	–	S	–	R
dS	S	A	A	A	A
M	S	R	R	R	S

Table 1.1: The stability properties are given for the three ΛCDM fixed points from the dynamical system (1.31)-(1.33) [21]. The nature of the fixed points can be either an attractor (A), or a repeller (R) or a saddle (S) on the phase space.

The spatial curvature of the FLRW geometry is constrained to be nearly flat i.e., its value is compatible with zero within some error bars (See right panel of Fig 1.2) [16]. Therefore for the rest of thesis, all the cosmological models assume a flat geometry. The Figure 1.4 shows the evolution of the energy density parameters of the different cosmological fluids in the ΛCDM model with flat curvature (i.e., assuming $\mathcal{K} = 0$) from an initial redshift $Z_i = 10^7$ to present ($Z = 0$). At very high redshift, the early Universe is in a radiation-dominated epoch and $\Omega_r \approx 1$. The sum of the energy densities is unity as expected from the Friedmann equation (1.28). As the early hot and dense Universe undergoes expansion, the energy density of radiation (photons) dilutes until

present. During that time, since the effect of gravity is at work, so the energy density of matter (baryons and CDM) increases. After matter-radiation equality, the Universe enters into a matter-dominated epoch, i.e., $\Omega_m \to 1$, where the decoupling of electrons and radiation happens and the first atoms are created. Then, the first stars and galaxies are borne and the large-scale structures eventually form. At lower redshift, the energy density of Dark Energy increases and becomes significant. Following from Raychaudhuri equation (1.25), one finds that the accelerated expansion (i.e., $\ddot{a} > 0$) begins before the DE-matter equality. After the DE-matter equality, the Universe enters into a DE dominated epoch, which is still its current state, as shown by the evidence in section 1.3.

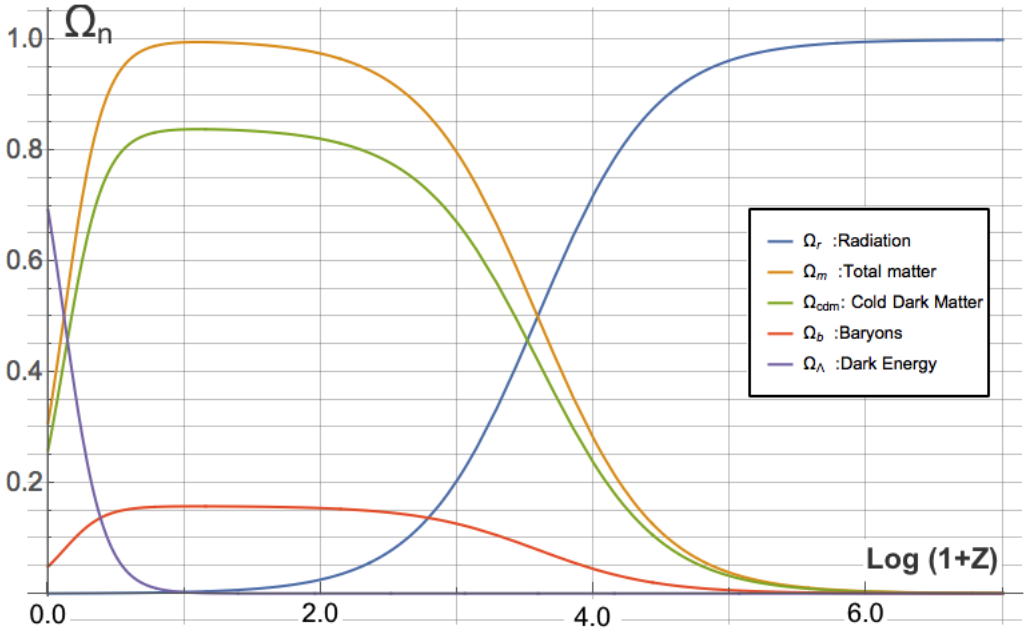

Figure 1.4: The evolution of the energy density parameter is shown for radiation (Blue), Baryons (Red), CDM (Green) and Dark Energy (Purple) respectively in a ΛCDM model with flat spatial curvature (i.e., $\mathcal{K} = 0$) from the early Universe to present. The is inspired from Refs. [23, 24].

1.5 The scalar perturbations of ΛCDM model

The observable Universe is known to have stars, galaxies, superclusters and large-scale structures. This implies that any cosmological model cannot remain entirely isotropic and homogeneous throughout its evolution. In other words, one has to introduce the concept of perturbation for the large-scale structure to emerge eventually. In the ΛCDM model, the spatially flat FLRW metric is perturbed in the Newtonian Gauge by introducing the

Bardeen Potentials (Φ and Ψ). The section 1.5 shall only consider scalar perturbations.

$$g_{\mu\nu} = \bar{g}_{\mu\nu} + \delta g_{\mu\nu} \quad \text{such that} \quad ds^2 = -(1+2\Phi)dt^2 + a^2(t)(1-2\Psi)\gamma_{ij}dx^i dx^j \ . \tag{1.34}$$

The bar over $g_{\mu\nu}$ denotes the background components and the δ preceding $g_{\mu\nu}$ denotes its perturbed components. The perturbed components of the affine connections, Ricci tensor and the Einstein tensor can then be computed as in Appendix A.2. One can also perturb the energy density and pressure of the n^{th} fluids:

$$\rho_n(\vec{x},t) = \bar{\rho}_n(t) + \delta\rho_n(\vec{x},t) \ , \qquad P_n(\vec{x},t) = \bar{P}_n(t) + \delta P_n(\vec{x},t) \ , \tag{1.35}$$

such that it will be useful to define the density contrast $\delta_n \equiv \delta\rho_n/\bar{\rho}_n$ and $c_s^2 \equiv \delta P_n/\delta\rho_n$. The scalar modes of the perturbed Einstein equations (i.e., $\delta G^\mu_\nu = \kappa^2 \delta T^\mu_\nu$) for the ΛCDM model for different combinations of μ and ν are given in cosmic time [25]:

$$a^{-2}\nabla^2\Psi - 3H\left(\dot{\Psi} + H\Phi\right) = \frac{3H^2}{2}\sum \Omega_n\delta_n \ , \tag{1.36}$$

$$\nabla^2\left(\dot{\Psi} + H\Phi\right) = -\frac{3aH^2}{2}\sum \Omega_n(1+w_n)\theta_n \ , \tag{1.37}$$

$$\ddot{\Psi} + \left(2\dot{H} + 3H^2\right)\Phi + H\left(\dot{\Phi} + 3\dot{\Psi}\right) - \frac{\nabla^2(\Psi-\Phi)}{3a^2} = \frac{3H^2c_s^2}{2}\sum \Omega_n\delta_n \ , \tag{1.38}$$

$$\nabla^i\nabla_j(\Psi-\Phi) = 3a^2H^2\sum w_n\Omega_n\pi_n \ , \tag{1.39}$$

where the variable $\theta_n = \nabla^2\mathbf{v}_n$ is the Laplace derivative of the scalar perturbed velocity $\mathbf{v}_n$, and π_n is the divergent scalar of the anisotropic stress tensor $\pi_{\mu\nu}$ of the n^{th} cosmological fluid. In the case of perfect fluids, $\pi_n = 0$. The evaluation of the perturbed conservation equations, i.e., $\delta(\nabla_\mu T^\mu_\nu) = 0$, will render their perturbed Euler and continuity equations for each cosmological fluid for the scalar modes in cosmic time [25]:

$$\dot{\delta}_n = -(1+w_n)\left(\frac{\theta_n}{a} - 3\dot{\Psi}\right) - 3H(c_s^2 - w_n)\delta_n \ , \tag{1.40}$$

$$\dot{\theta}_n = -H(1-3w_n)\theta_n - \frac{\dot{w}_n\theta_n}{(1+w_n)} - \frac{\nabla^2\Phi}{a} - \frac{c_s^2\nabla^2\delta_n}{a(1+w_n)} + \frac{w_n\nabla^2\pi_n}{(1+w_n)a} \ , \tag{1.41}$$

The variable π_n is often related to shear stress σ_n by $\sigma_n = 2\pi_n w_n/3(1+w_n)$ in the literature [25]. For the case where $c_s^2 = w = 0$ (e.g., for pressureless matter), one can obtain the second-order differential equation below [25]:

$$\begin{aligned} \dot{\delta} &= -\theta/a + 3\dot{\Psi} \ , \\ \dot{\theta} &= -H\theta - \nabla^2\Phi/a \ , \end{aligned} \qquad \Rightarrow \quad \ddot{\delta} - 3\ddot{\Psi} - a^{-2}\nabla^2\Phi + 2H(\dot{\delta} - 3\dot{\Psi}) = 0. \tag{1.42}$$

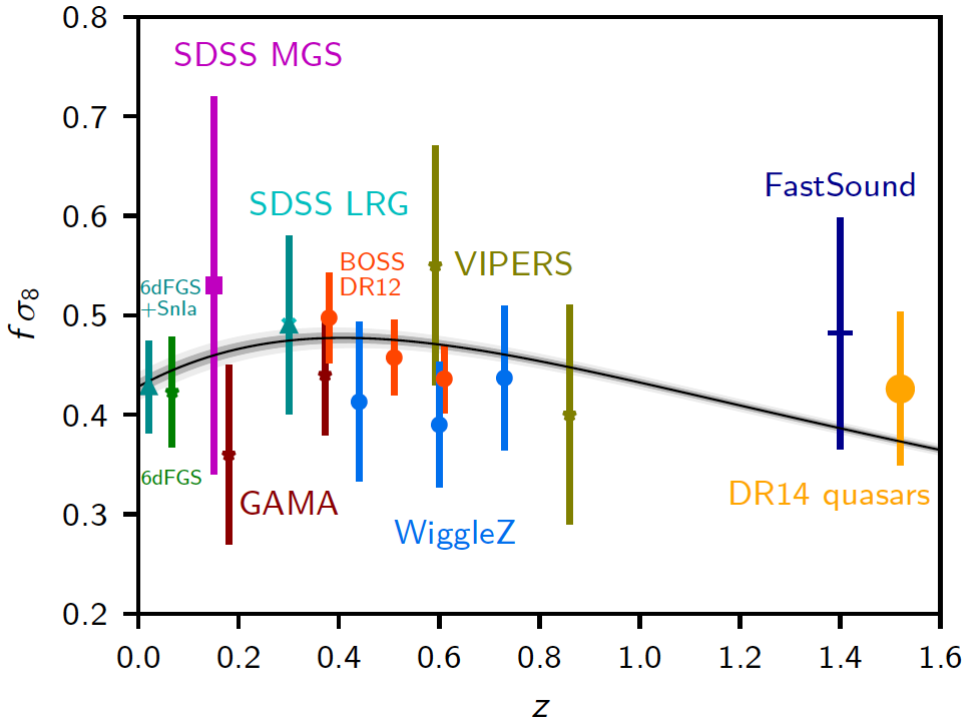

Figure 1.5: The $f\sigma_8(Z)$ curve (black line) for ΛCDM model with $\Omega_m = 0.3158 \pm 0.0073$ and $H_0 = 67.36 \pm 0.54$ kms^{-1}Mpc^{-1} [13]. The two grey bands underneath the black line correspond to the 68% and 95% confidence ranges, which is allowed by the Planck data. The measured $f\sigma_8(Z)$ values from various surveys is also shown [13].

In the ΛCDM model with n cosmological fluids, the total density contrast δ_t and the growth rate f (which indicates rate of evolution of δ_t) can be evaluated by [24]:

$$\delta_t = \frac{\sum \Omega_n \delta_n}{\sum \Omega_n}\,, \quad \text{and} \quad f = \frac{d\ln\delta_t}{d\ln a} = \frac{\delta_t'}{\delta_0} \quad \text{such that} \quad f\sigma_8(Z) = \frac{\delta_t'}{\delta_0}\sigma_8^0\,, \tag{1.43}$$

where the $f\sigma_8(Z)$ function describes the amount of clustering of galaxies at a given redshift Z. From an observational perspective, the structure of the Universe can be studied by using the statistical distribution of matter as a random density field. The length scale $R_8 = 8h^{-1}$ Mpc is defined as the spherical radius within which the linear regime is not valid [11]. σ_8 is the variance of such a matter density field in the sphere of radius R_8 [11]. Assuming a statistical isotropy and homogeneity, a correlation function $\xi(\vec{r}) = \langle\delta_t(\vec{x})\delta_t(\vec{x}+\vec{r})\rangle$ can be defined. After expanding the matter density field in Fourier modes, a matter power spectrum can be computed as below [11]:

$$\delta_t(r) = \int \frac{\delta_t(k)}{(2\pi)^{3/2}} e^{ik.r} d^3\vec{r}\,, \quad \text{and} \quad \mathcal{P}_\delta(k) = \int \xi(\vec{r}) e^{ik.r} d^3\vec{r}\,, \tag{1.44}$$

where the initial matter power spectrum is normalised so that the estimated variance σ_8 is of order unity [11]. The parameter σ_8^0, which is also known as the matter fluctuation amplitude, is the present amplitude of the matter power spectrum at the scale of R_8 [24]. Figure 1.5 shows the various surveys, which have placed constraints on the $f\sigma_8(Z)$ value at given redshift Z for the ΛCDM model.

1.6 The issues with ΛCDM model

The ΛCDM has been one of most successful cosmological models in describing our observational Universe with great precision. However, it cannot explain few important phenomena, and have few unresolved issues which are listed below:

1. Assuming that the Copernican principle to be valid, the *accelerated cosmological expansion* [12, 26] has not been comprehensively explained by any reasonable cause yet. It is often attributed to DE [27] in the form of the cosmological constant in the Einstein field equations (1.2), but the nature of the DE is unknown and unclear to many cosmologists.

2. The σ_8 *tension* arises because the σ_8 constraints upon clustering, which is imposed by the Planck CMB experiments for the early Universe, diverges from the late time measurement by the Dark Energy Survey (DES)[28, 29, 14]. The Planck CMB experiments constrains the matter fluctuation amplitude $\sigma_8^0 = 0.811 \pm 0.006$ [13] for a ΛCDM model. The combination of multiple surveys at the late-times (i.e., KiDs+VIKING-450 and DES-Y1) measures $\sigma_8^0 = 0.762^{+0.025}_{+0.024}$ and indicates a disparity of 2.5σ tension with Planck CMB experiments [30, 31] (See Figure 4.4).

3. The *Coincidence problems* [23] were identified in two instances. The first refers to the present energy density parameter of the cosmological constant and that of average matter to be of the same order of magnitude i.e. $\Omega_\Lambda|_{a=a_0} \sim \Omega_m|_{a=a_0}$. The second refers to the present energy density of baryons and dark matter to be relatively the same, despite the fact that their production mechanisms are different.

4. The *Cosmological Constant problem* [32, 33] refers to the discord between the theoretical and the measured observational value of the cosmological constant by at the least order of magnitude of 10^{60}, and upto 10^{120} if extrapolated to Planck scale.

The ΛCDM issues in the section 1.6 have motivated many cosmologists to find alternatives to GR. A range of theoretical possibilities have been proposed beyond ΛCDM. The

first category makes use of canonical scalar fields [34] or effective fluids [35]. Whether a scalar field or effective fluids are considered, they both have the possibility of interacting with each other. The second category is modified gravity [2], which involves the GR extensions (e.g., by considering a $f(R)$ correction to the gravitational action). In this thesis, we shall consider a cosmological model with an extra scalar field (i.e., the quintessence), which replaces the cosmological constant. In Chapters 2, 3 and 4, we study the quintessence while it interacts with another cosmological fluid. Such interactions (referred to as coupled quintessence) were first introduced by Refs. [36, 37]. The possibility that quintessence interacts with DM is also an interesting avenue to investigate [38].

The outline of the thesis is written in the following order; In Chapter 1, we have reviewed GR as well as the background, the perturbation and the issues of the ΛCDM Concordance model. In Chapter 2, we assume the coupled quintessence in dually geometric theory of gravity with the conformal transformation (2.2), which is simplest relation between the geometry describing curvature and the geometry describing propagation of fields. The couplings of the coupled quintessence are hence conformal by nature. Thus, in Chapter 2, we review few CCQ models with various conformal couplings in the literature, for both background and perturbations. In particular, we revisit a CCQ model which mimics the ΛCDM background, because it was able to alleviate the σ_8 tension [24]. In Chapter 3 and 4, we shall deal with a quintessence that couples and propagates on the physical geometry via a disformal transformation (3.1), which is the extension of the conformal transformation. The cosmological background and perturbations of such a DCQ model which mimics the ΛCDM model, will be studied in Chapter 3 and 4 respectively. The research question in this thesis remains whether any DCQ model in ΛCDM background, can attempt to resolve the first two main issues in section 1.6, since it has additional degrees of freedom compared to ΛCDM model. In Chapter 5, we summarise our results and write the final conclusions about the thesis.

Chapter 2

The Conformally Coupled Quintessence

The concept of quintessence, as an alternative to the cosmological constant, is briefly introduced in this chapter, with the particular focus of being coupled with a fluid. In section 2.1, a short review about the coupled quintessence in the conformal formalism is provided as the foundations for the disformal formalism, which will be presented in Chapter 3. The cosmological background and perturbations of the conformally coupled quintessence (CCQ) model are studied in sections 2.2 and 2.3 respectively. We end the Chapter with section 2.4, which presents how the CCQ model mimics the ΛCDM model, and its implications in the literature.

2.1 Conformal Formalism

From the perspective of extending GR, there is no reason for not allowing the field equations to accommodate other types of scalar field, as well as vector and tensor fields. The Scalar-Tensor theories are one of the well-studied alternative theories of gravity and the general Lagrangian action for their derivations is given by [39, 40, 41]:

$$S = \int \left(\frac{1}{2\kappa^2} \left[\, A(\phi)R - B(\phi)\nabla_\mu\phi\nabla^\mu\phi - 2\Lambda(\phi) \, \right] \, + \, \mathcal{L}_m(\psi, C(\phi)g_{\mu\nu}) \right) \sqrt{-g} \, d^4x \, , \quad (2.1)$$

where $A(\phi)$, $B(\phi)$, and $C(\phi)$ are arbitrary functions of the scalar field ϕ and $\mathcal{L}_m$ denotes the Lagrangian of the matter fields ψ. $\kappa^2 \equiv 8\pi G = M_{\rm pl}^{-2}$, where the Planck's mass is taken as $M_{\rm pl} = 2.4 \times 10^{18}$ GeV and the reduced Planck's constant is assumed to be unity ($\hbar = 1$). The $\Lambda(\phi)$ function generalises the cosmological constant. The $C(\phi)g_{\mu\nu}$ is re-defined into a new metric $\tilde{g}_{\mu\nu}$ by the conformal transformation [42, 43]:

$$\tilde{g}_{\mu\nu} = C(\phi)g_{\mu\nu} \, , \quad (2.2)$$

where $C(\phi)$ is referred as the conformal coefficient. Both the matter and the scalar field couple and propagate on the $\tilde{g}_{\mu\nu}$ metric. The SEP is violated in any dually geometric theory of gravity [9], which will therefore not be valid for massive particles. The WEP remains satisfied for the massless test particles, and the effect of the conformal transformation is to rescale the length of metric $g_{\mu\nu}$[2]. The Einstein frame is defined where the Einstein-Hilbert action (1.1) is recovered but with an added scalar field and the Jordan frame is defined as the frame in which the scalar field is uncoupled from matter [44]. The Einstein and Jordan frames are described by the metrics $g_{\mu\nu}$ and $\tilde{g}_{\mu\nu}$ respectively [44]. The conformal transformation (2.2) essentially connects the Einstein frame and the Jordan frame.

The well-known theoretical idea of the quintessence is to have a scalar field, which can substitute the cosmological constant. Specific choices of $A(\phi)$, $B(\phi)$, $C(\phi)$ and $\Lambda(\phi)$ can reduce the equation (2.1) into the Lagrangian density of the quintessence theory, which can be expressed in the Einstein frame as [24, 36]:

$$\mathcal{L}_{tot} = \frac{R}{2\kappa^2} + \mathcal{L}_{\phi} + \mathcal{L}_m(\psi, \tilde{g}_{\mu\nu}) \ , \quad \text{with} \quad \mathcal{L}_{\phi} = -\frac{1}{2}\nabla_\mu\phi\nabla^\mu\phi - V(\phi) \ , \tag{2.3}$$

where the term $\frac{1}{2}\nabla_\mu\phi\nabla^\mu\phi$ represents a kinetic function and $V(\phi)$ represents the potential for the quintessence. The potential energy of the quintessence can cause the accelerated cosmological expansion, only if it is light enough to vary slowly during the Hubble time [45]. The notion of quintessence being 'coupled' in this framework means that the quintessence is interacting with another general cosmological fluid (referred as the coupled fluid, which could be either dark matter or dust or radiation). For instance, the coupling strength between the quintessence and the ordinary matter is expected to be comparable to the gravitational field strength between them [45]. The conservation equations of the conformally coupled quintessence are described by [24, 45]:

$$\nabla_\mu T^{(\phi)\mu}_{\ \ \ \nu} = C^{(\phi)}_\nu \ , \quad \text{and} \quad \nabla_\mu T^{(c)\mu}_{\ \ \ \nu} = C^{(c)}_\nu \ , \tag{2.4}$$

where $T^{(\phi)\mu}_{\ \ \ \nu}$ and $T^{(c)\mu}_{\ \ \ \nu}$ are the energy-momentum tensors of the quintessence and the coupled fluid respectively. The energy-momentum tensor of the coupled fluid is given by equation (1.11). $C^{(\phi)}_\nu$ and $C^{(c)}_\nu$ are the conformal couplings, such that the flow of the energy-momentum in this interaction is indicated by $C^{(\phi)}_\nu = -C^{(c)}_\nu$.

2.2 The CCQ Background

The conformally coupled quintessence model only extends the ΛCDM model by replacing the cosmological constant with a new scalar field i.e., the quintessence. The addition of the quintessence rather implies that its energy-momentum tensor $T^{(\phi)}_{\mu\nu}$ now contributes as a new source term in the Einstein field equations (1.2). The modified field equations are:

$$G_{\mu\nu} = \kappa^2 T^{(tot)}_{\mu\nu} = \kappa^2 \left(T_{\mu\nu} + T^{(\phi)}_{\mu\nu}\right) \ , \tag{2.5}$$

where the energy-momentum tensor of the quintessence $T^{(\phi)}_{\mu\nu}$ is defined as [11, 46]:

$$T^{(\phi)}_{\mu\nu} = \nabla_\mu \nabla_\nu \phi - g_{\mu\nu} \left(\frac{1}{2} g^{\alpha\beta} \nabla_\alpha \nabla_\beta \phi + V(\phi)\right) \ . \tag{2.6}$$

The spatially flat FLRW background components of the energy-momentum tensor for the quintessence, $T^{\mu(\phi)}_{\nu} = g^{\eta\nu} T^{(\phi)}_{\eta\nu}$, are computed in the Appendix A.7. The 00^{th} and the ij^{th} components of the modified field equation (2.5) for the CCQ model provide the modified Friedmann equation and the modified Raychaudhuri equation in cosmic time as [46]:

$$H^2 = \frac{\kappa^2}{3}(\rho_\phi + \rho_c) \ , \qquad \text{and} \qquad \dot{H} = -\frac{1}{2}\kappa^2 \left[(\rho_\phi + P_\phi) + (1 + w_c)\rho_c\right] \ , \tag{2.7}$$

where the subscript "c" denotes the coupled fluid. The energy density ρ_ϕ and pressure P_ϕ for the quintessence in the Einstein frame are computed from the $T^{(\phi)}_{\mu\nu}$ components:

$$\rho_\phi \equiv \frac{1}{2}\dot{\phi}^2 + V(\phi) \quad \text{and} \quad P_\phi \equiv \frac{1}{2}\dot{\phi}^2 - V(\phi) \ , \quad \text{with} \quad w_\phi = \frac{P_\phi}{\rho_\phi} \ . \tag{2.8}$$

The conservation equations (2.4) can be projected along u^μ to give the continuity and Klein-Gordon equation. Assuming the conformal couplings are $C^{(\phi)}_\nu = -C^{(c)}_\nu = -Q(\phi)\nabla_\nu\phi$ [45], the continuity and Klein-Gordon equations become respectively [45, 46]:

$$\dot{\rho}_c + 3H(\rho_c + P_c) = -Q\dot{\phi} \ , \quad \text{and} \quad \ddot{\phi} + 3H\dot{\phi} + V_{,\phi} = +Q \ , \tag{2.9}$$

where the interaction term $Q(\phi)$ is defined as below and depends on the choice of conformal coefficient $C(\phi)$ from the conformal transformation (2.2)[46]:

$$Q(\phi) = \frac{C_{,\phi}}{2C} T \qquad \text{such that} \qquad T \equiv T^{(c)\mu}{}_{\mu}. \tag{2.10}$$

These conformal couplings are extended to disformal coupling later in Chapter 3 and 4.

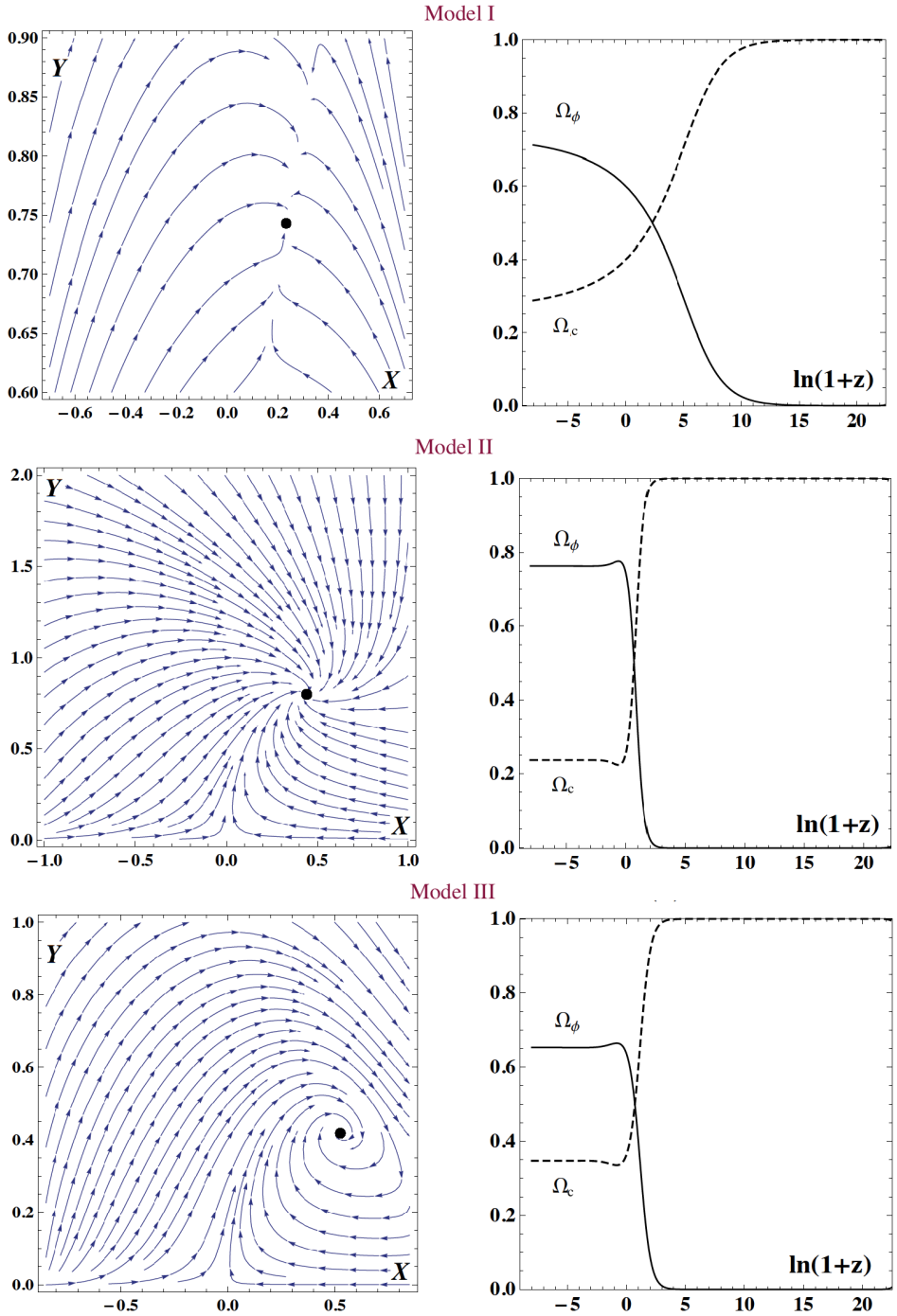

Figure 2.1: The dynamical analysis [47] of three conformally coupled quintessence models (2.11). The right panels (top, middle bottom) correspond to the phase-portraits for model I (with $\varepsilon_1 = -4.6$ and $\lambda = 0.94$), model II (with $\varepsilon_2 = 0.3$ and $\lambda = 1.3$) and model III (with $\varepsilon_3 = 0.1$ and $\lambda = 2.85$) respectively. The black dot is a fixed point. The left (top, middle bottom) panel shows the evolution of the energy density parameters of the quintessence Ω_ϕ and the coupled fluid Ω_c with redshift for the models I, II, III respectively.

The uniqueness of each CCQ model comes from the definition of the conformal couplings $C_\nu^{(\phi)}$. Thus, one can review the dynamical systems of different CCQ models by considering several models for these conformal couplings [47]:

$$\begin{aligned} \text{Model I:} \qquad & C_\nu^{(\phi)} = \varepsilon_1 \partial_\nu \rho_c \\ \text{Model II:} \qquad & C_\nu^{(\phi)} = \varepsilon_2 \partial_\nu \rho_\phi \\ \text{Model III:} \qquad & C_\nu^{(\phi)} = \varepsilon_3 \partial_\nu (\rho_c + \rho_\phi) \end{aligned} \tag{2.11}$$

where $\varepsilon_1, \varepsilon_1$ and ε_1 are constants. Similar to the energy density parameters (1.27), the dimensionless quantities X, Y, and λ were introduced to investigate these models [47]:

$$X^2 = \frac{\kappa^2 \dot{\phi}^2}{6H^2} \,, \qquad Y^2 = \frac{\kappa^2 V}{3H^2} \,, \qquad \lambda = -\frac{V_{,\phi}}{\kappa V} \,, \tag{2.12}$$

By inserting the quantities (2.12), the Friedmann equation (2.7) and the conservation equations (2.9) is expressed as a system of differential equations in terms of e-fold N [47]:

$$X' = -3X + \sqrt{\frac{3}{2}} \lambda Y^2 - X \left(\frac{H'}{H} \right) \quad \text{and} \quad Y' = -\sqrt{\frac{3}{2}} \lambda X Y - \left(\frac{H'}{H} \right) \,, \tag{2.13}$$

For each CCQ model, the ratio $\frac{H'}{H}$ can be deduced from its Raychaudhuri equation (2.7). The total EOS and the energy density parameters for the quintessence are given [47]:

$$w_{tot} = -1 - \frac{2H'}{3H} \,, \qquad \Omega_\phi = \frac{\kappa^2 \rho_\phi}{3H^2} = X^2 + Y^2 \,, \tag{2.14}$$

such that the condition for acceleration is $w_{tot} < -1/3$. The dynamical system (2.13) can be solved numerically. The models I, II , III have five, three, and three fixed points respectively (corrresponding to when $X' = Y' = 0$). Any interested reader is directed to Ref. [47] for details such as the stability analysis for those fixed points. Figure 2.1 shows the XY phase portraits for models I, II, and III with chosen parameters ε and λ. Figure 2.1 also shows the evolution of the energy density parameters Ω_ϕ and Ω_c for each model.

2.3 The CCQ Perturbations

For the perturbation theory of the CCQ model, if the FLRW metric is perturbed as in equation (1.34), then the computation of the affine connections (A.11), the Ricci tensor (A.12), and the Einstein tensor (A.14) also remains the same. And if the cosmological fluids are also perturbed according to equation (1.35), then their perturbed energy-

momentum tensor are same as in equation (A.15). However, one still have to perturb the quintessence ϕ as:

$$\phi(\vec{x},t) = \bar{\phi}(t) + \chi(\vec{x},t) \ . \tag{2.15}$$

The energy-momentum tensor of quintessence in perturbed space-time is computed in Appendix A.16. The scalar modes of the perturbed modified Einstein equations, i.e., $\delta G_{\mu\nu} = \kappa^2 \delta T^{(tot)}_{\mu\nu}$ for the CCQ model for different combinations of μ and ν are given in cosmic time (Inspired from the Refs. [11][25]):

$$\begin{aligned}
\nabla^2\left(\dot{\Psi} + H\Phi\right) &= \frac{\kappa^2\dot{\phi}}{2}\nabla^2\chi - \frac{3aH^2}{2}\sum \Omega_n(1+w_n)\theta_n \ , && (2.16)\\
a^{-2}\nabla^2\Psi - 3H\left(\dot{\Psi} + H\Phi\right) &= \frac{3H^2}{2}\sum \Omega_n\delta_n + \frac{\kappa^2}{2}(\dot{\phi}\dot{\chi} - \Phi\dot{\phi}^2 + V_{,\phi}\chi) \ , && (2.17)\\
\ddot{\Psi} + \left(2\dot{H} + 3H^2\right)\Phi + H\left(\dot{\Phi} + 3\dot{\Psi}\right) &= \frac{3H^2c_s^2}{2}\sum \Omega_n\delta_n + \frac{\kappa^2}{2}(\dot{\phi}\dot{\chi} - \Phi\dot{\phi}^2 - V_{,\phi}\chi) && (2.18)\\
&\quad + \frac{\nabla^2(\Psi-\Phi)}{3a^2} \ , \\
\nabla^i\nabla_j(\Psi - \Phi) &= 3a^2H^2\sum w_n\Omega_n\pi_n \ , && (2.19)
\end{aligned}$$

where n denotes the n^{th} fluids in the model, including the coupled fluid. The interaction term Q is also perturbed as $Q = Q_0 + Q_1$, where Q_0 and Q_1 are the background and the perturbation respectively. Assuming that $C^{(c)}_\nu = -C^{(\phi)}_\nu = +Q(\phi)\nabla_\nu\phi$ [45], the perturbed Euler equation (2.20) and perturbed continuity equation (2.21) can be deduced from the 00^{th} and ij^{th} components of $\delta(\nabla_\mu T^{(c)\mu}{}_\nu) = \delta(Q\nabla_\nu\phi)$ [48], while the perturbed Klein-Gordon equation (2.22) is derived from $\delta(\nabla_\mu T^{(\phi)\mu}{}_\nu) = -\delta(Q\nabla_\nu\phi)$ [48].

$$\begin{aligned}
\dot{\delta}_c &= -(1+w_c)\left(\frac{\theta_c}{a} - 3\dot{\Psi}\right) - 3H(c_s^2 - w_c)\delta_c + \frac{Q_0\,\dot{\phi}}{\rho_c}\delta_c - \frac{Q_0\,\dot{\chi}}{\rho_c} - \frac{Q_1\,\dot{\phi}}{\rho_c} \ , && (2.20)\\
\dot{\theta}_c &= -H(1-3w_c)\theta_c - \frac{\dot{w_c}}{1+w_c}\theta_c - \frac{\nabla^2\Phi}{a} - \frac{c_s^2\nabla^2\delta_c}{(1+w_c)a} + \frac{w_c\nabla^2\pi_c}{(1+w_c)a} && (2.21)\\
&\quad + \frac{Q_0\,\dot{\phi}}{\rho_c}\theta_c + \frac{Q_0\nabla^2\chi}{(1+w_c)\rho_c a} \ , \\
\ddot{\chi} &= -3H\dot{\chi} + a^{-2}\nabla^2\chi - V_{,\phi\phi}\chi + \dot{\phi}(\dot{\Phi} + 3\dot{\Psi}) + \frac{Q_0\dot{\chi}}{\dot{\phi}} + Q_1 + (2\ddot{\phi} + 6H\dot{\phi})\Phi \ , && (2.22)
\end{aligned}$$

where $V_{,\phi\phi}$ is the second derivative of the potential $V(\phi)$ with respect to quintessence. Since the terms Q_0 and Q_1 have dependence on conformal coefficient $C(\phi)$ as in equation (2.10), it implies that the set of equations (2.20)-(2.22) also depends on $C(\phi)$, and will be different for various CCQ models with unique conformal couplings.

2.4 The CCQ mimicking the ΛCDM background

Given the observational constraints with great precision [13], all quintessence models must be able to closely reproduce the evolution of the ΛCDM background. This explains the motivation for a CCQ model [24] to mimic the ΛCDM background, while it attempts to remove the σ_8 tension. The sections 2.4 and 2.5 summarise the work of Ref. [24]. The model in Ref. [24] assumes that the quintessence is conformally coupled with dark matter with a strength of $C_\nu^{(\phi)} = -\kappa\alpha\rho_c\nabla_\nu\phi$. This mimicry of the ΛCDM background requires equating the Friedmann equations as well as the Raychaudhuri equations; from which one can obtain the expressions for ρ_ϕ and P_ϕ [24]:

$$H^2 = H^2_{\Lambda\text{CDM}} \qquad \Rightarrow \qquad \rho_\phi = \rho_\Lambda + \rho_{cdm} - \rho_c \ , \tag{2.23}$$

$$\dot{H} = \dot{H}_{\Lambda\text{CDM}} \qquad \Rightarrow \qquad P_\phi = P_\Lambda = -\rho_\Lambda \ , \tag{2.24}$$

From the definitions (2.8), one can obtain $\dot{\phi}^2 = (\rho_\phi + P_\phi)$ in terms of the energy densities ρ_{cdm} (i.e., CDM from ΛCDM model) and ρ_c (i.e., the coupled fluid from the CCQ model). By using the expression for $\dot{\phi}^2$, one can re-write ρ_ϕ in equation (2.23) in terms of the quintessence ϕ and the energy density of the cosmological constant ρ_Λ [24]:

$$\dot{\phi}^2 = (\rho_\phi + P_\phi) = \rho_{cdm} - \rho_c \qquad \Rightarrow \qquad \rho_\phi = \rho_\Lambda + \dot{\phi}^2 \ . \tag{2.25}$$

One can additionally find an expression for the potential of the quintessence $V(\phi)$ by using the equation (2.24) and the definition (2.8) again [24]:

$$P_\phi = -\rho_\Lambda = \frac{1}{2}\dot{\phi}^2 - V(\phi) \quad \Rightarrow \quad V(\phi) = \frac{1}{2}\dot{\phi}^2 + \rho_\Lambda \ , \tag{2.26}$$

$$\Rightarrow \quad V_{,\phi} = \ddot{\phi}. \tag{2.27}$$

For this model [24], the conformal coefficient in equation (2.2) is defined as $C(\phi) = \exp(-2\kappa\alpha\phi)$ and the interaction term (2.10) is thus computed to be $Q = \kappa\alpha\rho_c$, where α is a conformal parameter. The continuity equations for baryons (b), radiation (r) and the coupled fluid (as in left equation in (2.9)) are given in cosmic time [24]:

$$\dot{\rho}_b + 3H\rho_b = 0 \ , \tag{2.28}$$

$$\dot{\rho}_r + 4H\rho_r = 0 \ , \tag{2.29}$$

$$\dot{\rho}_c + 3H\rho_c = -\kappa\alpha\dot{\phi}\rho_c \ . \tag{2.30}$$

The Klein-Gordon equation (as in right equation in (2.9)) becomes the equation (2.31) in cosmic time, after specifying the interaction term Q and by substituting the derivative of the quintessential potential using equation (2.27) [24].

$$2\ddot{\phi} + 3H\dot{\phi} = +\kappa\alpha\rho_c \, . \tag{2.31}$$

The energy density parameters for the cosmological fluids are defined in the CCQ model;

$$\Omega_c = \frac{\kappa^2\rho_c}{3H^2} \, , \qquad \Omega_\phi = \frac{\kappa^2\rho_\phi}{3H^2} \, , \qquad \Omega_r = \frac{\kappa^2\rho_r}{3H^2} \, , \qquad \Omega_b = \frac{\kappa^2\rho_b}{3H^2} \, , \tag{2.32}$$

such that their evolutions are computed numerically from the early universe to present as shown in Figure 2.2. Figure 2.2 also demonstrates how the conformal parameter α affects the evolution of the density parameters for the quintessence Ω_ϕ and for total matter $\Omega_m = \Omega_c + \Omega_b$. When $\alpha = 0$, the ΛCDM features are recovered (See Figure 1.4).

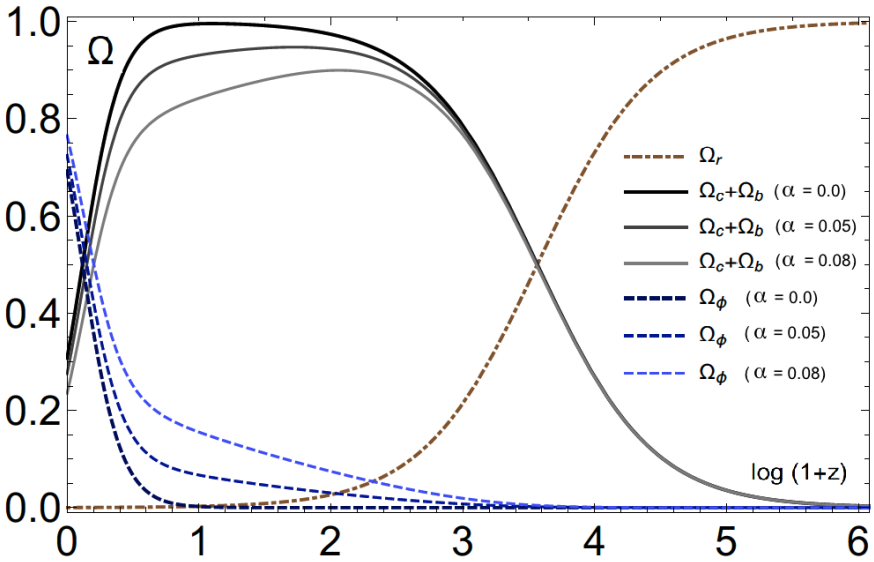

Figure 2.2: The effect of the conformal parameter α upon the evolution of the energy density parameters for quintessence and total matter in the CCQ model [24], mimicking the ΛCDM background. The black solid line ($\alpha = 0$) corresponds to ΛCDM.

2.5 The CCQ perturbations in the ΛCDM background

Although this CCQ model mimics the ΛCDM background, it certainly show deviations at the level of perturbations from the ΛCDM model. Assuming the metric perturbation (1.34), the fluid perturbations (1.35), the scalar field perturbation (2.15), the perturbed

Euler equation (2.20) and continuity equation (2.21) of the coupled fluid simplify as follows (in cosmic time):

$$\dot{\delta}_c = -\frac{\theta_c}{a} + 3\dot{\Psi} - \alpha\kappa\dot{\chi} \,, \tag{2.33}$$

$$\dot{\theta}_c = -\left(H - \alpha\kappa\dot{\phi}\right)\theta_c - a^{-}\left(\nabla^2\Phi - \alpha\kappa\nabla^2\chi\right) \tag{2.34}$$

where the perturbed interaction term is $\delta Q = \kappa\alpha\rho_c\delta_c$ and the CDM is assumed to behave as perfect fluid, i.e., $\pi_c = 0$. It also implies that $\Psi = \Phi$ in the Einstein equation (2.19). The second-order differential equation for the perturbations of the coupled fluid is derived by these next steps. Firstly, the equation (2.34) is inserted into the time derivative of the equation (2.33) which results [24]:

$$\ddot{\delta}_c - 3\ddot{\Psi} + \alpha\kappa\ddot{\chi} + a^{-2}\left(\alpha\kappa\nabla^2\chi - \nabla^2\Phi\right) + \left(\dot{\delta}_c - 3\dot{\Psi} + \alpha\kappa\dot{\chi}\right)\left(2H - \alpha\kappa\dot{\phi}\right) = 0 \,. \tag{2.35}$$

Secondly, the Einstein equation (2.18) is inserted to replace for $3\ddot{\Psi}$ in the equation (2.35). Thirdly, the equation (2.35) makes use of $\Psi = \Phi$ and is approximated within the Newtonian limits for the sub-Hubble scales. Finally, the approximated and perturbed Klein-Gordon equation (2.22) as well as the approximated Einstein equation (2.17) are used to substitute the term $\nabla^2\chi^2$ and $\nabla^2\Psi$ respectively to yield the equation (2.36) [24]:

$$\ddot{\delta}_c + \dot{\delta}_c\left(2H - \alpha\kappa\dot{\phi}\right) - \frac{\kappa^2}{2}\rho_c\delta_c\left(1 + 2\alpha^2\right) - \frac{\kappa^2}{2}\rho_b\delta_b = 0 \,, \tag{2.36}$$

The system of second ODE for the perturbations of the coupled fluid and of the baryons can be then expressed in terms of the e-fold N [24]:

$$\delta_c'' + \delta_c'\left(2 + \frac{H'}{H} - \alpha\kappa\phi'\right) - \frac{3}{2}\Omega_c\delta_c\left(1 + 2\alpha^2\right) - \frac{3}{2}\Omega_b\delta_b = 0 \,, \tag{2.37}$$

$$\delta_b'' + \delta_b'\left(2 + \frac{H'}{H}\right) - \frac{3}{2}\Omega_c\delta_c - \frac{3}{2}\Omega_b\delta_b = 0 \,. \tag{2.38}$$

The system of ODEs (2.37)-(2.38) is solved numerically from the early radiation dominated universe $N_i = -14$ to present with the following initial conditions [24]:

$$\phi(N_i) = \phi'(N_i) = 0 \,, \quad \delta_b(N_i) = \delta_c(N_i) = 10^{-3} \,, \quad \delta_b'(N_i) = \delta_c'(N_i) = 10^{-3} \,. \tag{2.39}$$

The left panel of Figure 2.3 shows the evolution of total matter perturbation δ_t, as defined in equation (1.43), with conformal parameter $\alpha = 0, 0.05$ and 0.08 for the universe at late-time. The positive non-zero value of the conformal parameter α seems to slow down the evolution rate and cause the large-scale structures to cluster more slowly [24].

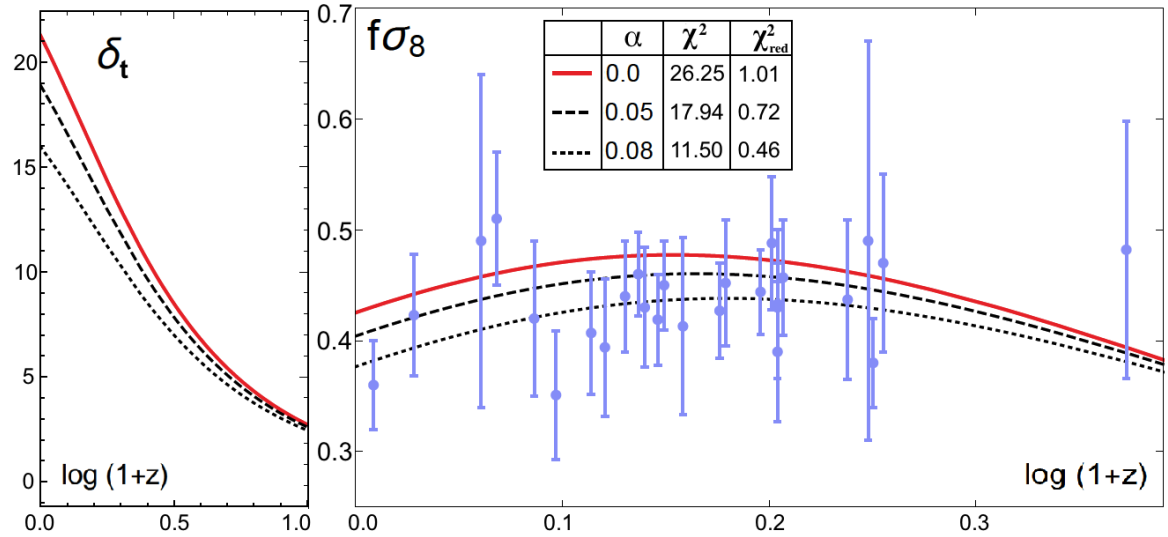

Figure 2.3: The effect of the conformal parameter α on δ_t and $f\sigma_8(Z)$ function are shown for a CCQ model [24], mimicking the ΛCDM background. Red line corresponds to ΛCDM. The RSD data are in Table A.1. We provide the Chi-square estimation (defined in Appendix A.3) for comparison with the DCQ model in Figure 4.2.

The right panel of Figure 2.3 shows how the conformal parameter α in the system of second ODEs (2.37)-(2.38) influences the evolution of the $f\sigma_8(Z)$ function (1.43) with redshift Z in the late universe. The total matter perturbation δ_t and the $f\sigma_8(Z)$ function for the ΛCDM model are recovered with $\alpha = 0$ (see Figure 1.5).

The Ref. [24] performed a Bayesian analysis of the numerical $f\sigma_8(Z)$ curve using the RSD data (Table A.1). In the CCQ model, the $f\sigma_8(Z)$ curve are influenced by two free parameters, which are the conformal parameter α and matter fluctuation amplitude σ_8^0. The surface likelihood function $L(\sigma_8^0, \alpha)$ is evaluated (see Appendix A.3) in the 2D parameter space $\Theta_\mu = \{\sigma_8^0, \alpha\}$ to generate the countour plot as shown in Figure 2.4. Figure 2.4 also provide the best fit set of parameter (i.e., at minimum Chi-square estimation). The best fit value of $\sigma_8^0 = 0.818^{+0.115}_{-0.088}$ by the CCQ model was found to be within 1σ level error margins of Planck (2015)'s constraint $\sigma_8^0 = 0.82 \pm 0.014$ [49] for the ΛCDM based model and therefore alleviate the σ_8 tension [24] (see Figure 4.4 to compare with the constraints from latest Planck data (2018)[13] and DES data [30]).

The Ref. [50] studied the spherical collapse for this CCQ model and investigated the co-moving number of DM halos $\mathcal{N}$ using the Press-Schechter and the Sheth-Tormen mass functions respectively, with the DM halos in mass ranges $10^{14}h^{-1}M_\odot < M_H < 10^{16}h^{-1}M_\odot$. In both cases, the parameter α causes an increase on the number of objects at high redshifts and greater suppression at small redshift, compared to ΛCDM [50].

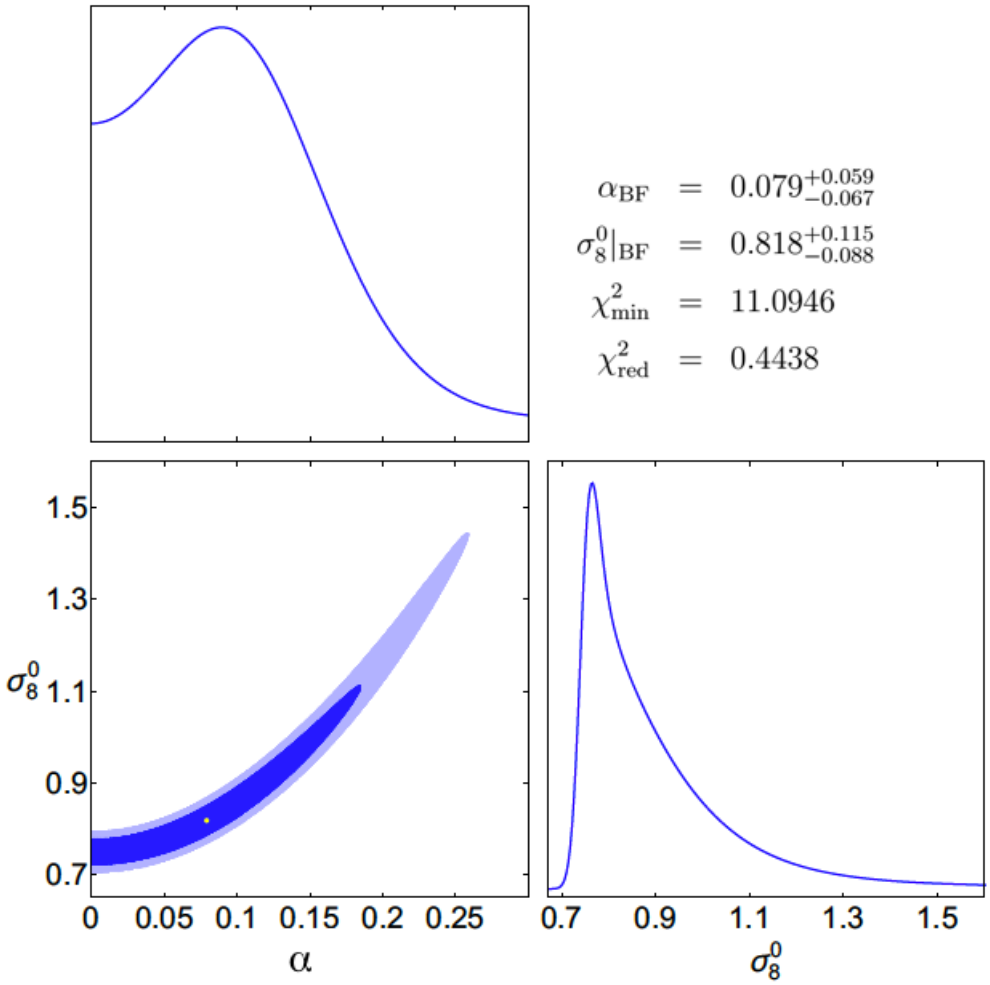

Figure 2.4: Using the RSD data (Table A.1) in a Bayesian analysis, the Ref. [24] constrains the parameters (i.e., α and σ_8^0) of the CCQ model in ΛCDM background. The bottom left panel show the contour plot of the surface likelihood function $L(\sigma_8^0, \alpha)$. The dark and light blue of the contour plot indicate the 68% and 95% confidence level. The top and right panel show the 1D marginalised likelihood function $L(\alpha)$ and $L(\sigma_8^0)$ respectively. The best fit parameters of $\{\sigma_8^0, \alpha\}$ and the minimum chi-square estimation are given.

The main point from the Chapter 2 is that the conformal coefficient $C(\phi)$ from the conformal transformation (2.2) plays an important role in defining the interaction term $Q(\phi)$ as per equation (2.10) and in specifying any particular model. In section 2.1, we retrospect the idea of the quintessence which is conformally coupled to a cosmological fluid. In section 2.2, the cosmological background for the CCQ is constructed and the dynamical system for three models is studied. The perturbed Einstein equations, the perturbed continuity equations, the perturbed Euler equation and the perturbed Klein-Gordon equation for a general CCQ are reviewed in section 2.3 respectively. The methodology and results of Ref. [24] is studied in sections 2.4 and 2.5, because they provide the foundations to

approach a DCQ model, which mimics the ΛCDM background. In Chapter 3, the conformal transformation (2.2) is extended to disformal transformation (3.1), and this will lead the interactions (i.e., couplings) to be of disformal nature. In Chapter 3, we will investigate various disformal couplings of the DCQ model in the ΛCDM background. With a dynamical system analysis and a study of the expansion history of the DCQ model, we shall attempt to shed new light on the issue of the accelerated cosmological expansion. In Chapter 4, we shall explore the DCQ model by studying the evolution of its linear density perturbations and test them against RSD data (Table A.5), in same manner that was carried out in section 2.5.

Chapter 3

The Disformal Couplings in a ΛCDM background cosmology

The coupled quintessence model with disformal couplings is treated here to mimic the ΛCDM background. The quintessential potential is not specified. The studied model considers a quintessence coupled with a generic fluid, which could be either DM or relativistic fluid. The mimicked background consists of a cosmological constant and another uncoupled generic fluid, to cater for various studied scenarios. The cosmological dynamics is investigated for this DCQ model, whose disformal couplings depend on the EOS of both generic fluids. The scenario, whereby both generic fluids are DM, is further analysed via the expansion history of the mimicking DCQ model. The analysis confirms that the quintessential mass influences the disformal characteristics of the dynamical system.

This Chapter is organised in the following order; section 3.1 introduces the disformal transformation. In section 3.2, the Lagrangian description of the DCQ model is provided. Section 3.3 presents how the DCQ mimics the ΛCDM background, which explains the reasoning behind not having to specify the quintessence potential. In section 3.4, the dynamical system of the DCQ model is constructed from the continuity equations. In section 3.5, a brief description of three studied scenarios is given, as well as the suggested approach used to analyse the dynamical systems. Section 3.6 entails the analysis of conformal couplings in the three studied scenarios, which includes the conformal equations, the fixed points, and 2D phase portrait. Sections 3.7 and 3.8 present the analysis of the disformal couplings in the three studied scenarios, which includes the disformal equations, the additional disformal fixed points, the topological features and the investigation of the trajectories on a 3D phase portrait. Finally in section 3.9, we shall present our remarks

about the expansion history of the DCQ model, where both generic fluids are DM and we also investigate the effect of the quintessential mass scale on the interaction.

3.1 Introducing the disformal transformation

In this chapter, we focus on the cosmological dynamics of the quintessence model, under a number of assumptions, which lead to several new perspectives. In what follows, we first assume (for the sake of simplicity) that the quintessence is allowed to interact with a single generic and effective fluid and we investigate the novel phenomenology that arises due to these interactions. The second assumption concerns the geometry in which the quintessence exists. The theory of gravitation might actually require two geometries [9], and they are enumerated as: (i) the gravitational geometry (corresponding to the Einstein frame), which describes the curvature on the fabric of space-time, and (ii) the physical geometry (corresponding to the Jordan frame), which describes how the matter fields propagate. There exist many such examples of dually-geometric theories of gravity [51, 52, 53]. In dually geometric gravitation, the only way to maintain the principle of general covariance is the addition of new fields and hence the use of the quintessence seems convenient [9]. As shown by Ref. [9], the disformal relation is obtained by extending the conformal transformation (2.2) with an extra scaled kinetic term of the scalar field [9]:

$$\tilde{g}_{\mu\nu} = C(\phi) g_{\mu\nu} + D(\phi) \partial_\mu \phi \partial_\nu \phi \ , \tag{3.1}$$

where $D(\phi)$ is the disformal coefficient. The effect of a disformal transformation can be understood as the distortion of angles and lengths in the original metric $g_{\mu\nu}$ due to compression, which occurs in the direction of the gradient of the field. The occurence of the disformal relation happens in many theories such as Horndeski-type scalar tensor theory [54, 55], non-linear massive gravity theory [56, 57], brane cosmology with higher dimensions [58] and this framework has attracted considerable attention [59, 60, 61, 62].

As discussed in sections 2.4 and 2.5, one way to alleviate the σ_8 *Tension* (See section 1.6) is to consider a quintessence conformally coupled with DM, while maintaining a ΛCDM background cosmology [24, 50]. In this Chapter, we extend these studies of sections 2.4 and 2.5 with the addition of disformal couplings, which we explore by performing a dynamical system analysis [47, 63, 64]. We also investigate how the disformal coefficient $D(\phi)$ influences the expansion history of the DCQ model in section 3.9, where quintessence is disformally coupled with DM. The Chapter 3 focuses mainly on the cosmological background of this DCQ model and hence provides the foundations for the disformal perturbations, which will be presented in Chapter 4.

3.2 The disformally coupled quintessence (DCQ) model

The general Scalar-Tensor theory of gravity (2.1) can be simplified to a quintessence theory as in equation (2.3) and the new action in the Einstein frame can be re-expressed as:

$$S = \int \left(\frac{1}{2\kappa^2} R \; - \frac{1}{2} g^{\mu\nu} \partial_\mu \phi \partial_\nu \phi - V(\phi) + \; \mathcal{L}_m(\tilde{g}_{\mu\nu}, \psi) \right) \sqrt{-g} \; d^4x \; , \tag{3.2}$$

The metric variation of (3.2) with respect to the metric $g^{\mu\nu}$ results in the modified Einstein field equations (2.5), which express the quintessence and the coupled fluid as two separate source terms, i.e., $T^{\phi}_{\mu\nu}$ and $T_{\mu\nu}$ respectively. The energy-momentum tensors $T^{\phi}_{\mu\nu}$ as per equation (2.6) and $T_{\mu\nu}$ as per equation (1.11) can be obtained from their Lagrangian density function in the Einstein frame:

$$T^{\phi}_{\mu\nu} = -\frac{2}{\sqrt{-g}} \frac{\delta(\sqrt{-g}\mathcal{L}_\phi)}{\delta g^{\mu\nu}} \;\; \text{and} \;\; T_{\mu\nu} = -\frac{2}{\sqrt{-g}} \frac{\delta(\sqrt{-g}\mathcal{L}_m)}{\delta g^{\mu\nu}} \;\; \text{such that} \;\; \tilde{T}_{\mu\nu} = \frac{\sqrt{-g}}{\sqrt{-\tilde{g}}} \frac{\delta g^{\mu\nu}}{\delta \tilde{g}^{\mu\nu}} T_{\mu\nu} \; , \tag{3.3}$$

where the energy-momentum tensor from the Jordan frame (denoted by $\tilde{T}_{\mu\nu}$) can still be related to its equivalent one from the Einstein frame. The Jacobian of the disformal relation (3.1) provides how the determinants of the metrics are related:

$$J = \frac{\sqrt{-g}}{\sqrt{-\tilde{g}}} = C^2(\phi) \sqrt{1 + \frac{D}{C} g^{\mu\nu} \partial_\mu \phi \partial_\nu \phi} \; . \tag{3.4}$$

Assuming the spatially flat FLRW metric (1.24), the modified Friedmann and Raychaudhuri equation are given by equation (2.7). In our studied model, the quintessence is disformally coupled with a single generic and perfect fluid with EOS parameter $w_{\rm c}$. The energy density, pressure and EOS parameter for the coupled fluid in Einstein frame can be mapped into the Jordan frame as the following (See Appendix of Ref. [65]):

$$\tilde{\rho}_c = \frac{\rho_c}{C^2} \sqrt{1 + \frac{D}{C} g^{\mu\nu} \partial_\mu \phi \partial_\nu \phi} \; , \;\; \tilde{P}_c = \frac{P_c}{C^2 \sqrt{1 + \frac{D}{C} g^{\mu\nu} \partial_\mu \phi \partial_\nu \phi}} \; , \;\; \tilde{w}_c \equiv \frac{\tilde{P}_c}{\tilde{\rho}_c} = \frac{w_c}{\left(1 + \frac{D}{C} g^{\mu\nu} \partial_\mu \phi \partial_\nu \phi \right)} \; . \tag{3.5}$$

Any variable in the Jordan frame is denoted by a tilde over the variable. If we further assume that the quintessence is only a function of time (i.e., $\phi = \phi(t)$), then in the Einstein frame, the EOS parameter for the coupled fluid and its time-derivative are:

$$w_{\rm c} = \left(1 - \frac{D}{C} \dot{\phi}^2 \right) \tilde{w}_c \qquad \text{and} \qquad \dot{w}_{\rm c} = -\tilde{w}_c \dot{\phi} \frac{D}{C} \left[\left(\frac{D_{,\phi}}{D} - \frac{C_{,\phi}}{C} \right) \dot{\phi}^2 + 2\ddot{\phi} \right] \; . \tag{3.6}$$

The variation of the action (3.2) with respect to the quintessence ϕ results in the modified Klein-Gordon equation [44]:

$$\Box\phi = V_{,\phi} - Q(\phi) \ , \tag{3.7}$$

where $V_{,\phi}$ denotes the derivative of $V(\phi)$ with respect to ϕ. The disformal interaction term for the coupling between the quintessence and a single coupled fluid is given by [44]:

$$Q(\phi) = \frac{C_{,\phi}}{2C}T + \frac{D_{,\phi}}{2C}T^{\mu\nu}\nabla_\mu\phi\nabla_\nu\phi - \nabla_\mu\left(\frac{D}{C}T^{\mu\nu}\nabla_\nu\phi\right) \ , \tag{3.8}$$

where $C_{,\phi}$ and $D_{,\phi}$ are the derivatives of conformal and disformal coefficients $C(\phi)$ and $D(\phi)$ respectively. The conservation equations of the energy-momentum tensors $T^{\phi}_{\mu\nu}$ and $T_{\mu\nu}$ for the DCQ model remain of the form (2.4). The total energy-momentum tensor is conserved, although their individual components are not separately conserved. Assuming the disformal couplings are $C^{(\phi)}_\nu = -C^{(c)}_\nu = -Q(\phi)\nabla_\nu\phi$ [45], the conservation equations (2.4) are projected along a co-moving observer u^μ to obtain the continuity and Klein-Gordon equations (2.9). The modified Einstein field equations (2.5), the modified Klein-Gordon equation (3.7) and the disformal interaction term $Q(\phi)$ in equation (3.8) may be applied to general cosmological models.

3.3 The DCQ model mimicking the ΛCDM background

On the one hand, we consider a cosmological background, which has only two fluids, i.e., the cosmological constant and an uncoupled generic fluid. The quantities ρ_u and w_u are the energy density and EOS parameter of the uncoupled generic fluid respectively. In the exact ΛCDM background, the uncoupled generic fluid is simply the CDM, but we rather treat this background with an uncoupled generic fluid in order to investigate other interesting scenarios (See sections 3.6, 3.7 and 3.8). Assuming the spatially flat FLRW metric (1.24), the Friedmann and Raychaudhuri equations for this background are:

$$H^2_{\Lambda\text{CDM}} = \frac{\kappa^2}{3}(\rho_\Lambda + \rho_u) \ , \qquad \text{and} \qquad \dot{H}_{\Lambda\text{CDM}} = -\frac{1}{2}\kappa^2\left[(\rho_\Lambda + P_\Lambda) + (1+w_u)\rho_u\right] \ . \tag{3.9}$$

On the other hand, the quintessence model (constructed in section 3.2) also has two fluids i.e., the quintessence ϕ and the coupled fluid ρ_c (with EOS parameter w_c). As mentioned in the Introduction, the novelty in this Chapter is to extend the CCQ model, mimicking ΛCDM background (in section 2.4 and 2.5), to include disformal couplings. Hence after equating the Friedmann equations (2.7) and (3.9) from the two cosmological backgrounds,

we can express the energy density of the quintessence ρ_ϕ in terms of the energy densities for the cosmological constant ρ_Λ and the coupled fluid ρ_c, and that of uncoupled fluid ρ_u:

$$H^2 = \frac{\kappa^2}{3}(\rho_\phi + \rho_c) = \frac{\kappa^2}{3}(\rho_\Lambda + \rho_u) = H^2_{\Lambda\text{CDM}} \,, \tag{3.10}$$

$$\rho_\phi = \rho_\Lambda + \rho_u - \rho_c \,. \tag{3.11}$$

By equating the Raychaudhuri equations from the two cosmological backgrounds, we can express the pressure of the quintessence in terms of the pressure for the cosmological constant, the uncoupled fluid, and that of coupled fluid:

$$\dot{H} = -\frac{1}{2}\kappa^2\left[(\rho_\phi + P_\phi) + (1+w_c)\rho_c\right] = -\frac{1}{2}\kappa^2\left[(\rho_\Lambda + P_\Lambda) + (1+w_u)\rho_u\right] = \dot{H}_{\Lambda\text{CDM}}, \tag{3.12}$$

$$P_\phi = -\rho_\Lambda + w_u\rho_u - w_c\rho_c \,. \tag{3.13}$$

One can therefore write $(\rho_\phi + P_\phi)$ using equations (3.11) and (3.13) to find an expression for ρ_u:

$$\rho_u = \frac{\dot{\phi}^2}{1+w_u} + \rho_c\,\frac{1+w_c}{1+w_u} \,. \tag{3.14}$$

Then after inserting ρ_u as per equation (3.14) back into equation (3.11), the expression for the energy density ρ_ϕ is obtained in terms of quintessence ϕ :

$$\rho_\phi = \rho_\Lambda + \frac{\dot{\phi}^2}{1+w_u} + \rho_c\,\frac{w_c - w_u}{1+w_u} \,. \tag{3.15}$$

By substituting equation (3.15) and using $\dot{\phi}^2 = \rho_\phi + P_\phi$ into the Friedmann and the Raychaudhuri equations (2.7) respectively, we obtain the following form:

$$H^2 = \frac{\kappa^2}{3}\left[\frac{\dot{\phi}^2}{1+w_u} + \rho_\Lambda + \rho_c\left(\frac{1+w_c}{1+w_u}\right)\right] \,, \qquad \dot{H} = -\frac{1}{2}\kappa^2\left[\,\dot{\phi}^2 + \rho_c(1+w_c)\,\right] \,. \tag{3.16}$$

From equation (3.16), when $\dot{\phi} = 0$, it follows that the coupled system is exactly mimicking ΛCDM with an uncoupled fluid. This assumption of mimicking an uncoupled setup brings the convenience of not having to define a potential. The quintessential potential and its time-derivative, which are obtained by inserting relation (3.15) into $V(\phi) = \rho_\phi - \frac{1}{2}\dot{\phi}^2$, are given as below:

$$V(\phi) = \rho_\Lambda + \frac{\dot{\phi}^2}{2}\left(\frac{1-w_u}{1+w_u}\right) + \rho_c\frac{w_c - w_u}{1+w_u} \,, \tag{3.17}$$

$$\dot{V} = V_{,\phi}\dot{\phi} = \dot{\phi}\ddot{\phi}\,\frac{1-w_u}{1+w_u} + \dot{\rho}_c\frac{w_c - w_u}{1+w_u} + \rho_c\dot{w}_c \,. \tag{3.18}$$

Moreover, the EOS parameter for an uncoupled fluid is the same constant in both Einstein and Jordan frames, i.e. $w_u = \tilde{w}_u = \text{constant} \Rightarrow \dot{w}_u = 0$, whereas for the coupled fluid, the EOS parameter w_c and its time-derivative $\dot{w}_c$ are given by equation (3.6). Therefore by inserting equation (3.6) as well as the continuity equation (2.9) into equation (3.18), and after simplifying some terms, we obtain the derivative of the potential $V_{,\phi}$ as:

$$\begin{aligned} V_{,\phi} &= \frac{\ddot{\phi}}{1+w_u}\left(1-w_u-2\tilde{w}_c\rho_c\frac{D}{C}\right) + \frac{\tilde{w}_c\rho_c}{1+w_u}\left(\frac{D_{,\phi}}{D}-\frac{C_{,\phi}}{C}\right)\frac{D}{C}\dot{\phi}^2 \\ &\quad -\left(\frac{3H\rho_c}{\dot{\phi}}\right)\frac{(w_c-w_u)(1+w_c)}{1+w_u} - \frac{w_c-w_u}{1+w_u}Q(\phi)\,. \end{aligned} \tag{3.19}$$

This $V_{,\phi}$ in equation (3.19) can be inserted into the Klein-Gordon equation (2.9) to find an expression for $\ddot{\phi}$, which is useful when computing the interaction term $Q(\phi)$:

$$\begin{aligned} \ddot{\phi}\left(2-2\tilde{w}_c\rho_c\frac{D}{C}\right) &= (1+w_c)Q(\phi) - 3H\dot{\phi}(1+w_u) + \tilde{w}_c\rho_c\left(\frac{D}{C}\right)\left(\frac{D_{,\phi}}{D}-\frac{C_{,\phi}}{C}\right)\dot{\phi}^2 \\ &\quad + \left(\frac{3H\rho_c}{\dot{\phi}}\right)(w_c-w_u)(1+w_c). \end{aligned} \tag{3.20}$$

Lastly, the interaction term $Q(\phi)$ for a single generic coupled fluid can be computed by evaluating the covariant derivative of time components for the energy-momentum tensor in equation (3.8):

$$Q(\phi) = -\frac{C_{,\phi}}{2C}(1-3w_c)\rho_c - \left(\frac{D_{,\phi}}{2D}-\frac{C_{,\phi}}{C}\right)\frac{D\dot{\phi}^2}{C}\rho_c + Q_0\frac{D\dot{\phi}^2}{C} + 3\frac{D}{C}w_c\rho_c H\dot{\phi} - \frac{D\ddot{\phi}}{C}\rho_c\,. \tag{3.21}$$

After inserting equation (3.20) into the last term of equation (3.21), one can obtain this form for the interaction term:

$$\begin{aligned} Q(\phi) &= \frac{-\rho_c\left(2-2\tilde{w}_c\frac{D}{C}\right)\left[\frac{C_{,\phi}}{2C}(1-3w_c) + \frac{D}{C}\left(\frac{D_{,\phi}}{2D}-\frac{C_{,\phi}}{C}\right)\dot{\phi}^2 - 3Hw_c\frac{D}{C}\dot{\phi}\right]}{\left[\left(1-\frac{D}{C}\dot{\phi}^2\right)\left(2-2\tilde{w}_c\rho_c\frac{D}{C}\right)+\rho_c(1+w_c)\left(\frac{D}{C}\right)\right]} \\ &\quad + \frac{\frac{D\rho_c}{C}\left[3H\dot{\phi}(1+w_u) - \tilde{w}_c\rho_c\left(\frac{D}{C}\right)\left(\frac{D_{,\phi}}{D}-\frac{C_{,\phi}}{C}\right)\dot{\phi}^2 - \left(\frac{3H\rho_c}{\dot{\phi}}\right)(w_c-w_u)(1+w_c)\right]}{\left[\left(1-\frac{D}{C}\dot{\phi}^2\right)\left(2-2\tilde{w}_c\rho_c\frac{D}{C}\right)+\rho_c(1+w_c)\left(\frac{D}{C}\right)\right]}\,. \end{aligned} \tag{3.22}$$

Following the literature, the conformal and disformal coefficients are chosen [44]:

$$C(\phi) = \exp(2\alpha\kappa\phi)\,, \qquad D(\phi) = \frac{\exp\left[2(\alpha+\beta)\kappa\phi\right]}{M^4} = D_m^{-4}\exp\left[2(\alpha+\beta)\kappa\phi\right] \tag{3.23}$$

$$\lambda_C \equiv -\frac{1}{\kappa}\frac{C_{,\phi}}{C} = -2\alpha\,, \qquad \lambda_D \equiv -\frac{1}{\kappa}\frac{D_{,\phi}}{D} = -2(\alpha+\beta)\,, \tag{3.24}$$

where the constants α and β are the conformal and disformal parameters respectively. The variable $M \equiv D_m^{-1}$ is the quintessential mass scale in the disformal coupling. In a purely conformal case, the functions $D(\phi)$ and its derivative $D_{,\phi}$ vanish.

3.4 The dynamical system approach

The dynamical system approach is extensively used in literature to study cosmological models [22, 66]. The dynamical system of any cosmological model can be constructed by considering that certain properties (e.g. energy density) of the different fluids evolve with time t or e-folds N. We shall define the dimensionless dynamical variables [44]:

$$x^2 \equiv \frac{\kappa^2\dot{\phi}^2}{3H^2}, \qquad y^2 \equiv \frac{\kappa^2\rho_\Lambda}{3H^2}, \qquad z^2 \equiv \frac{\kappa^2\rho_c}{3H^2}, \qquad \sigma \equiv \frac{D(\phi)}{\kappa^2 C(\phi)}H^2 \ . \tag{3.25}$$

It follows that the set of equations, governing the evolution of these dynamical variables, can be inferred from the continuity and Klein-Gordon equations (2.9) . At this point, let us emphasise that the dynamical variable σ measures the strength of the disformal coupling. These variables are constrained to obey the Friedmann and Raychaudhuri equations (3.16):

$$1 + w_u = x^2 + (1 + w_u)y^2 + (1 + w_c)z^2 \ , \tag{3.26}$$

$$\frac{H'}{H} = -\frac{3}{2}\left[x^2 + (1 + w_c)z^2\right] = -\frac{3}{2}(1 + w_{\text{eff}}) \ , \tag{3.27}$$

where in equation (3.27), one can define an effective equation of state, i.e w_{eff}, which must satisfy $w_{\text{eff}} < -1/3$ for accelerated expansion and $w_{\text{eff}} > -1/3$ for decelerated expansion. The set of first order differential equations for the dynamical system is obtained by taking the derivative of the dynamical variables (3.25) and then inserting into the continuity and Klein-Gordon equations (2.9) :

$$\begin{aligned} x' &= -\frac{H'}{H}x - \frac{3x}{2}\frac{(1 + w_u)}{(1 - 3\tilde{w}_c z^2\sigma)} + \frac{3\sqrt{3}\tilde{w}_c x^2 z^2\sigma(\lambda_C - \lambda_D)}{2(1 - 3\tilde{w}_c z^2\sigma)} + \frac{3z^2}{2x}\frac{(w_c - w_u)(1 + w_c)}{(1 - 3\tilde{w}_c z^2\sigma)} \\ &\quad + \frac{(1 + w_c)}{(1 - 3\tilde{w}_c z^2\sigma)}\frac{\kappa}{2\sqrt{3}}\frac{Q}{H^2} \ , \end{aligned} \tag{3.28}$$

$$z' = -\frac{H'}{H}z - \frac{3}{2}z(1 + w_c) - \frac{\kappa}{2\sqrt{3}}\frac{Q}{H^2}\frac{x}{z} \ , \tag{3.29}$$

$$y' = -\frac{H'}{H}y \ , \tag{3.30}$$

$$\sigma' = \left((\lambda_C - \lambda_D)\sqrt{3}x + 2\frac{H'}{H}\right)\sigma \ . \tag{3.31}$$

After substituting the dynamical variables (3.25) into the interaction term (3.22), we obtain the following:

$$\hat{Q} \equiv \frac{\kappa Q}{H^2} = \frac{6z^2(1-3\tilde{w}_c\sigma z^2)\left[\frac{\lambda_C}{2}(1-3w_c)+\frac{3}{2}\sigma x^2(\lambda_D-2\lambda_C)+3\sqrt{3}w_c\sigma x\right]}{(1-3\sigma x^2)(2-6\tilde{w}_c\sigma z^2)+3\sigma z^2(1+w_c)} + \frac{9\sqrt{3}\sigma z^2\left[x(1+w_u)+\sqrt{3}\tilde{w}_c\sigma x^2 z^2(\lambda_D-\lambda_C)-(w_c-w_u)(1+w_c)\frac{z^2}{x}\right]}{(1-3\sigma x^2)(2-6\tilde{w}_c\sigma z^2)+3\sigma z^2(1+w_c)} \,. \quad (3.32)$$

The differential equations (3.28)-(3.32) govern the overall behaviour for the DCQ model, mimicking the ΛCDM. The dynamical system (3.28)-(3.32) is a closed because $\left(\frac{H'}{H}\right)$ can be eliminated by using the equation (3.27). The interaction term $Q(\phi)$ is a function of $\lambda_C = -2\alpha$ and $\lambda_D = -2(\alpha+\beta)$. Thus the choice of the functions $C(\phi)$ and $D(\phi)$ determines how the coupled fluid and the quintessence are interacting. Using the Friedmann constraint (3.27), one can express z in terms of $x,\ y$ and then substitute it in the evolution equations (3.28)-(3.32) to reduce the dimensions of the dynamical system, with only $x,\ y$ and σ. The resulting set of equations is then more useful and straightforward to be solved, and we can always recover z through the constraint equation whenever required. Finally, one can write the density parameter Ω_ϕ from equation (3.15):

$$\Omega_\phi \equiv \frac{\kappa^2\rho_\phi}{3H^2} = \frac{x^2}{1+w_u} + y^2 + \frac{w_c-w_u}{1+w_u}z^2 = 1-z^2 \quad \text{and} \quad w_\phi = \frac{x^2+y^2-1}{1-z^2} \,, \quad (3.33)$$

where w_ϕ is the EOS for the quintessence. It is obtained by using equations (3.13) and (3.15), and then expressed in terms of the dynamical variables (3.25), . The solutions of this dynamical system with the differential equations (3.28)-(3.32) can be represented on a phase space of x, z, and σ, where each point denotes a specific state of the system (see Figures 3.2, 3.4 and 3.6). However this phase space cannot be infinite as physical conditions must be imposed, for instance, the energy density can only be positive and therefore the existence of fixed points is limited by $0 < \Omega_\phi < 1$. Although the values of the disformal strength lies between $0 < \sigma < \infty$, it is compactified by defining $\Sigma \equiv \arctan\sigma$. The resulting phase space, therefore, results in a compact set, defined by:

$$\begin{aligned} &-1 < x < 1 \quad \text{and} \quad z > 0 \quad \text{and} \quad 0 < \Sigma < \pi/2 \,, \\ &\text{and } 0 < x^2 + (1+w_u)y^2 + (w_c-w_u)z^2 < (1+w_u) \,. \end{aligned} \quad (3.34)$$

We verify whether the disformal transformation (3.1) is real and invertible, by computing the Jacobian of the equation (3.1), which is expressed in terms of the dynamical variables:

$$J = \frac{\sqrt{-g}}{\sqrt{-\tilde{g}}} = C^2\sqrt{1 + \frac{D}{C}g^{ab}\partial_a\phi\partial_b\phi} = C^2\sqrt{1 - 3\sigma x^2}\ . \tag{3.35}$$

It can be noted that if $3\sigma x^2 > 1$, the Jacobian J is not real and in the limit $\sqrt{1 - 3\sigma x^2} \to 0$, a singularity appears in this phase space. Therefore, the following condition must be imposed on the phase space:

$$3\sigma x^2 \leq 1\ . \tag{3.36}$$

The dynamical system (3.28)-(3.32) is also invariant under the simultaneous transformation of the parameters $(\alpha, \beta) \to (-\alpha, -\beta)$. Thus, the phase space is still fully described by taking only positive (α, β) values.

3.5 Scenarios, Fixed points and Trajectories

The dynamical system is described by the evolution equations (3.28)-(3.32), the Friedmann constraint equation (3.27), two free parameters (α and β), the two fluids (ρ_ϕ and ρ_c) mimicking the cosmological constant Λ and one uncoupled fluid ρ_u. From the perspective of observations, only the EOS parameters from the Jordan frame can be measured, therefore we shall choose the EOS parameters $\tilde{w}_c$ and $\tilde{w}_u$ * for the coupled fluid and uncoupled fluid respectively to cater for different scenarios in our study:

1. Scenario I : $\tilde{w}_c = 0$ and $\tilde{w}_u = 0$, implies that a pressureless fluid (e.g. DM) is coupled to quintessence and both fluids are mimicking a ΛCDM background at late-times.

2. Scenario II: $\tilde{w}_c = 1/3$ and $\tilde{w}_u = 0$, implies that a relativistic fluid is coupled to quintessence and both fluids are mimicking a ΛCDM background.

3. Scenario III: $\tilde{w}_c = 1/3$ and $\tilde{w}_u = 1/3$, implies that a relativistic fluid coupled to quintessence and both fluids are mimicking a background with a cosmological constant Λ and an uncoupled relativistic fluid. An example of this scenario refers to relativistic neutrinos which are coupled to quintessence in the early universe as compared to uncoupled radiation.

Our analysis of the dynamical system in each specific scenario, i.e., after specifying the EOS parameters $\tilde{w}_c$ and $\tilde{w}_u$ is done by investigating two aspects:

1. The nature of the fixed points – which are static solutions of the dynamical system, that correspond to $x' = y' = z' = \sigma' = 0$ [22].

*The gravitational and physical metric are identical in the ΛCDM model, which implies that $w_u = \tilde{w}_u$.

2. The trajectories on the phase space – which are non-static solutions of the dynamical variables. Those trajectories correspond to the evolution of the system from one cosmological state to another on the compactified phase space.

According to linear stability theorem [22], one can then determine how the system behaves around any point, by applying a Taylor expansion. The Jacobian matrix of the set of three evolution equations is first worked out and then its corresponding three eigenvalues of that Jacobian matrix are evaluated for each of the fixed points. The nature of the fixed point is then determined as:

1. If all three eigenvalues $\Re(E_1) < 0$ and $\Re(E_2) < 0$ and $\Re(E_3) < 0$, then the fixed point is stable,

2. If all three eigenvalues $\Re(E_1) > 0$ and $\Re(E_2) > 0$ and $\Re(E_3) > 0$, then the fixed point is unstable,

3. If any combination of three eigenvalues being positive and negative, then the fixed point is saddle,

where $\Re(E_n)$ denote the real part of the n^{th} eigenvalue. These eigenvalues can still have a dependence on the parameters α and β and the conditions for which the fixed points are either stable, unstable or saddle, must be worked out. In other cases, where the eigenvalues are found to be null, the linear stability theorem is inadequate to determine their nature. Then the nature of the point is then evaluated numerically using the Lyapunov theorem [22] to investigate the asymptotic and global stability.

Given certain initial conditions and choice of parameters (α and β), the trajectories of of the relevant dynamical system can be determined on the phase space. In what follows we study the evolution of the dynamical system in each scenario for the two cases:

1. Fixed parameters (α and β) but different Initial Conditions (IC).

2. Fixed IC but different parameters (α and β).

Our approach is to investigate all the different theoretical possibilities for (a) the trajectories, (b) the effect of disformal coupling constant on the evolution of the Universe, and (c) the sensitivity of the dynamical system to the initial conditions. In the upcoming sections 3.6-3.8, we will analyse the nature of the fixed points and trajectories for three different scenarios in both conformal and disformal framework.

3.6 Conformal Framework

We investigate the fixed points and the phase portrait of the dynamical system in a conformal framework (i.e., $C(\phi) \neq 1$ in equation (2.2)) for the three studied scenarios. In a purely conformal framework, the disformal coefficient $D(\phi)$ and its derivative vanish, and the variable σ also vanishes. Compared to the construct of the conformal models (2.11), our dynamical variables (3.25) do not involve a quintessential potential. The differential equations for x and z are obtained as below for the three studied scenarios:

1. In Scenario I ($\tilde{w}_c = 0$ and $\tilde{w}_u = 0$), the interaction between the quintessence and DM, is still present but reduces to $Q = \alpha\rho\nabla^b\phi$ [36]. The differential equations (3.37)-(3.38) are equivalent to dynamical system (2.37)-(2.38) in section 2.5, which have been in expressed in terms of dynamical variables (3.25).

$$x' = \frac{3x}{2}(x^2 + z^2) - \frac{3x}{2} - \frac{\kappa}{2}\sqrt{3}\alpha z^2 , \tag{3.37}$$

$$z' = \frac{3z}{2}(x^2 + z^2) - \frac{3z}{2} + \frac{\kappa}{2}\sqrt{3}\alpha xz . \tag{3.38}$$

2. When $\tilde{w}_c = 1/3$, the quintessence and radiation do not interact at all with each other, and so the interaction term $Q(\phi)$, vanishes as well for both Scenarios II and III. In Scenario II: ($\tilde{w}_c = 1/3$ and $\tilde{w}_u = 0$), the differential equations becomes:

$$x' = \frac{3}{2}x\left(x^2 + \frac{4z^2}{3}\right) - \frac{3x}{2} + \frac{2z^2}{3x} , \tag{3.39}$$

$$z' = \frac{3}{2}z\left(x^2 + \frac{4z^2}{3}\right) - 2z . \tag{3.40}$$

3. In Scenario III ($\tilde{w}_c = 1/3$ and $\tilde{w}_u = 1/3$), the differential equations becomes:

$$x' = \frac{3}{2}x\left(x^2 + \frac{4z^2}{3}\right) - 2x , \tag{3.41}$$

$$z' = \frac{3}{2}z\left(x^2 + \frac{4z^2}{3}\right) - 2z . \tag{3.42}$$

The conformal static solutions (i.e., the fixed points) of the dynamical system (3.37)-(3.38) are detailed below and their Eigenvalues in given in Table A.3, A.5 and A.6.

1. Point A_0, i.e. $(0, 0)$, is a scalar field dominated fixed point which exists in Scenarios I, II, and III. It is located at the origin of the phase space. It is an attractor when

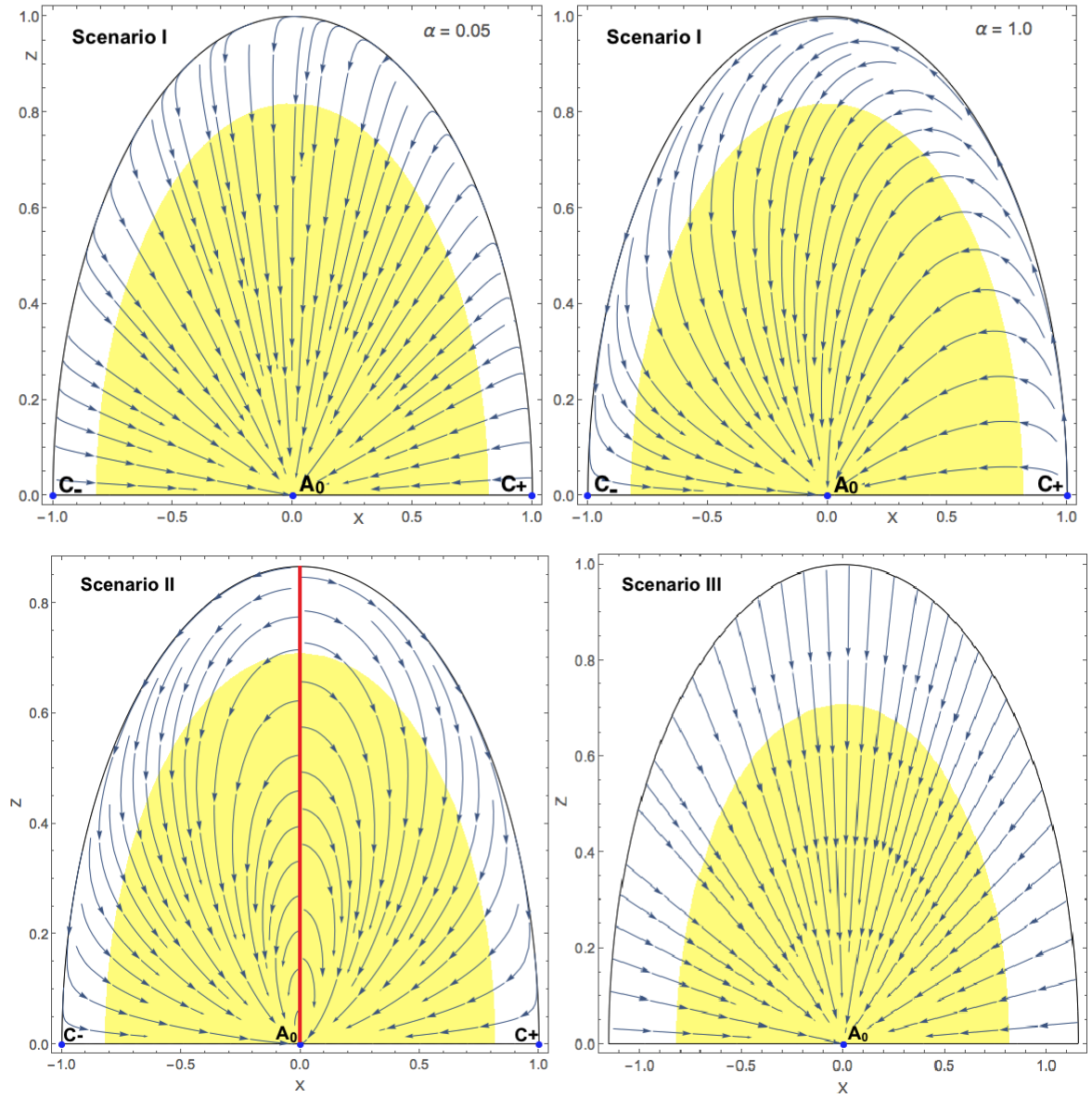

Figure 3.1: The trajectories of three dynamical systems for the Scenario I (i.e. $\tilde{w}_c = 0$ and $\tilde{w}_u = 0$), Scenario II (i.e $\tilde{w}_c = 1/3$ and $\tilde{w}_u = 0$), and Scenario III (i.e $\tilde{w}_c = 1/3$ and $\tilde{w}_u = 1/3$) are shown in the top, the bottom left and the bottom right panels respectively. The dynamical systems of Scenarios I, II and III are described by equations (3.37)-(3.38), equations (3.39)-(3.40), and equations (3.41)-(3.42) respectively. In all panels, the blue dots represents the fixed points, i.e., A_0 and $(C_\pm)$, which are the attractor and saddle points respectively. The yellow shaded region corresponds to a region of accelerated expansion, satisfying $w_{\text{eff}} < -1/3$. In the bottom left panel, where the red line is equilibrium line consisting of repeller fixed points and it separates $x < 0$ and $x > 0$. The Friedmann constraint (3.27) becomes $1 = x^2 + z^2$ (half-circle) for Scenario I, as $3 = 3x^2 + 4z^2$ (half-ellipse) for Scenario II, and $3 = 3x^2 + 4z^2$ (half-ellipse) for Scenario III.

evaluated according to Lyapunov theorem. Most of the trajectories seem to end at this fixed point. It always exists since it has no dependence on parameters α. It satisfies the acceleration condition of $w_{\text{eff}} < -1/3$.

2. Points $(C_{\pm})$, i.e. $(\pm 1, 0)$, which are two kinetic-dominated fixed points, which exist in Scenarios I and II, but not III. They are located on the xz plane at unit length of x. They have no dependence on the parameter α and always exists. In Scenario I, when $\alpha > 0$, Point $(C_{+})_{\mathbf{I}}$ is unstable and Point $(C_{-})_{\mathbf{I}}$ is saddle and when $\alpha < 0$, Point $(C_{+})_{\mathbf{I}}$ is unstable and Point $(C_{-})_{\mathbf{I}}$ is saddle. In Scenario II, Points $(C_{\pm})_{\mathbf{I}}$ are both saddle.

3. In Scenario II, the line $x = 0$ is an equilibrium line, which consist of repeller fixed points and it separates $x < 0$ and $x > 0$.

The trajectories of three dynamical systems (3.37)-(3.42) for the Scenario I (i.e., $\tilde{w}_c = 0$ and $\tilde{w}_u = 0$), Scenario II (i.e., $\tilde{w}_c = 1/3$ and $\tilde{w}_u = 0$), and Scenario III (i.e., $\tilde{w}_c = 1/3$ and $\tilde{w}_u = 1/3$) are shown in Figure 3.1. The Friedmann constraint (3.27) becomes $1 = x^2 + z^2$ (half-circle), as $3 = 3x^2 + 4z^2$ (half-ellipse), and $3 = 3x^2 + 4z^2$ (half-ellipse) for Scenarios I, II, III respectively.

In Scenario I, the values of α were constrained to be $\alpha = \pm 0.079^{+0.016}_{-0.019}$ using Bayesian statistics with the RSD data (Table A.1), as mentioned in section 2.5 [24]. Thus, two phase portraits were produced with $\alpha = 0.05$ and $\alpha = 1.0$ for illustrative purposes. In Scenarios II and III, the dynamical systems (3.39)-(3.40) and (3.41)-(3.42) do not depend on the parameters α and β at all.

3.7 Disformal Framework

We extend now our analysis of the fixed points and the phase portrait to a disformal framework for the three studied scenarios. The dynamical variable σ and the disformal constant β now play an important role. The form of the differential equations for (3.28), (3.29), (3.31) and the normalised interaction term (3.32) can be written for the respective scenarios as follows:

1. In Scenario I ($\tilde{w}_c = 0$ and $\tilde{w}_u = 0$): The dynamical system, described by the differential equations (3.43)-(3.46), has 9 fixed points; which are summarised in Table A.2 with respective eigenvalues in Table A.3.

$$x' = \frac{3x}{2}(x^2+z^2) - \frac{3x}{2} + \frac{\hat{Q}}{2\sqrt{3}}\,, \tag{3.43}$$

$$z' = \frac{3z}{2}(x^2+z^2) - \frac{3z}{2} - \frac{\hat{Q}}{2\sqrt{3}}\left(\frac{x}{z}\right)\,, \tag{3.44}$$

$$\sigma' = \left[\sqrt{3}x\left(\lambda_C-\lambda_D\right) - 3\left(x^2+z^2\right)\right]\sigma\,, \tag{3.45}$$

$$\hat{Q} = \frac{3z^2\left[\lambda_C\left(1-6\sigma x^2\right) + 3\sigma x\left(x\lambda_D+\sqrt{3}\right)\right]}{-6\sigma x^2+3\sigma z^2+2}\,. \tag{3.46}$$

2. In Scenario II ($\tilde{w}_c = 1/3$ and $\tilde{w}_u = 0$): The dynamical system, described by the differential equations (3.47)-(3.50), has 5 fixed points; which are listed with their Eigenvalues in the Table A.4 and A.5.

$$x' = +\frac{3}{2}x\left[x^2+\frac{z^2}{3}\left(4-3\sigma x^2\right)\right] - \frac{3x}{2\left(1-\sigma z^2\right)} + \frac{z^2\left(4-3\sigma x^2\right)\left(1-3\sigma x^2\right)}{6x\left(1-\sigma z^2\right)} + \frac{\sqrt{3}\sigma x^2 z^2\left(\lambda_C-\lambda_D\right)}{2\left(1-\sigma z^2\right)} + \frac{\left(4-3\sigma x^2\right)}{6\sqrt{3}\left(1-\sigma z^2\right)}\hat{Q}\,, \tag{3.47}$$

$$z' = +\frac{3}{2}z\left[x^2+\frac{z^2}{3}\left(4-3\sigma x^2\right)\right] - \frac{z}{2}\left(4-3\sigma x^2\right) - \frac{x}{2\sqrt{3}z}\hat{Q}\,, \tag{3.48}$$

$$\sigma' = \sigma\left\{\sqrt{3}x\left(\lambda_C-\lambda_D\right) - \left[3x^2+z^2\left(4-3\sigma x^2\right)\right]\right\}\,, \tag{3.49}$$

$$\hat{Q} = \frac{\sigma z^2\left\{9x^3(\lambda_D-\lambda_C) + \sqrt{3}\left[9\sigma x^4\left(\sigma z^2-2\right) + 3x^2\left(3\sigma z^2+5\right) - 4z^2\right]\right\}}{\sigma z^2\left(4-3\sigma x^2\right) + 2\left(1-3\sigma x^2\right)\left(1-\sigma z^2\right)}\,. \tag{3.50}$$

3. In Scenario III ($\tilde{w}_c = 1/3$ and $\tilde{w}_u = 1/3$), The dynamical system, described the differential equations (3.51)-(3.54), has 7 fixed points; which are summarised in Table A.6, together with their eigenvalues.

$$x' = +\frac{3}{2}x\left[x^2+\frac{z^2}{3}\left(4-3\sigma x^2\right)\right] - \frac{2x}{\left(1-\sigma z^2\right)} - \frac{\sigma x z^2\left(4-3\sigma x^2\right)}{2\left(1-\sigma z^2\right)} + \frac{\sqrt{3}\sigma x^2 z^2\left(\lambda_C-\lambda_D\right)}{2\left(1-\sigma z^2\right)} + \frac{\left(4-3\sigma x^2\right)}{6\sqrt{3}\left(1-\sigma z^2\right)}\hat{Q}\,, \tag{3.51}$$

$$z' = +\frac{3}{2}z\left[x^2+\frac{z^2}{3}\left(4-3\sigma x^2\right)\right] - \frac{z}{2}\left(4-3\sigma x^2\right) - \frac{x}{2\sqrt{3}z}\hat{Q}\,, \tag{3.52}$$

$$\sigma' = \sigma\left\{\sqrt{3}x\left(\lambda_C-\lambda_D\right) - \left(3x^2+z^2\left[4-3\sigma x^2\right)\right]\right\}\,, \tag{3.53}$$

$$\hat{Q} = \frac{3\sigma x z^2\left\{3x(\lambda_D-\lambda_C) + \sqrt{3}\left[3\sigma x^2\left(\sigma z^2-2\right) + 2\sigma z^2+6\right]\right\}}{3\sigma x^2\left(\sigma z^2-2\right) + 2\sigma z^2+2}\,. \tag{3.54}$$

All the disformal fixed points and features of the general dynamical system (3.28)-(3.32), which appear in Figures 3.2-3.4, are iterated below with the following remarks:

1. Point A_0, is a scalar field dominated fixed point, which exists in Scenarios I, II and III (same as in the conformal framework). It is located at the origin of the phase space. It is an attractor when evaluated according to Lyapunov theorem. Most of the trajectories end at this fixed point. It always exists since it does not depend on parameters α and β. It satisfies the acceleration condition of $w_{\text{eff}} < -1/3$. This fixed point has a null eigenvalue and it was found to be stable by using Lyapunov theorem instead.

2. Points $(C_\pm)$, i.e., $(\pm 1, 0, 0)$, are two kinetic-dominated fixed points which exist in Scenarios I and II, but not Scenario III. They are located on the xz plane at unit length of x. They are similar as in the conformal framework except that β can now influence their nature.

   (i) In Scenario I, Points $(C_\pm)$ always exist for all values of α and β but their different choices determine whether the fixed points are either unstable or saddle points. For Point $(C_+)_{\mathbf{I}}$, the conditions are the following:

$$\begin{aligned} \text{Unstable:} \quad & \beta > \frac{\sqrt{3}}{2} \text{ and } \alpha > 0 \,. \\ \text{Saddle:} \quad & \beta < \frac{\sqrt{3}}{2} \text{ and } \alpha < 0 \text{ OR } \beta < \frac{\sqrt{3}}{2} \text{ and } \alpha > 0 \text{ OR } \beta > \frac{\sqrt{3}}{2} \text{ and } \alpha < 0 \,. \end{aligned} \tag{3.55}$$

   For Point $(C_-)_{\mathbf{I}}$, the conditions are the following:

$$\begin{aligned} \text{Unstable:} \quad & \beta < -\frac{\sqrt{3}}{2} \text{ and } \alpha < 0 \,. \\ \text{Saddle:} \quad & \beta > -\frac{\sqrt{3}}{2} \text{ and } \alpha > 0 \text{ OR } \beta > -\frac{\sqrt{3}}{2} \text{ and } \alpha < 0 \text{ OR } \beta < -\frac{\sqrt{3}}{2} \text{ and } \alpha > 0 \,. \end{aligned} \tag{3.56}$$

   (ii) In Scenario II, the fixed points always exist as saddle points and the conditions are:

$$\begin{aligned} \text{For } (C_+)_{\mathbf{II}} \quad &: \quad \beta < \frac{\sqrt{3}}{2} \text{ OR } \beta > \frac{\sqrt{3}}{2} \,. \\ \text{For } (C_-)_{\mathbf{II}} \quad &: \quad \beta > -\frac{\sqrt{3}}{2} \text{ OR } \beta < -\frac{\sqrt{3}}{2} \,. \end{aligned} \tag{3.57}$$

3. Point $(B_\pm)$ are two disformal scaling points which are possible solutions in Scenarios I and II. They both can only exist if either $\beta \leq -\frac{\sqrt{3}}{2}$ or $\beta \geq \frac{\sqrt{3}}{2}$. The location of

the two fixed points depends on the parameter β. When $\beta = 0$ in conformal case, and those fixed points do not exist at all, so there is no issue of singularity at all. Nonetheless unfortunately, the Points $(B_\pm)_{\mathbf{I}}$ and $(B_\pm)_{\mathbf{II}}$ are unable to satisfy the condition (3.36), which means the points are neither real nor physical points. In Scenario I, these fixed points could only be saddle points and the conditions are:

$$0 < \beta < \frac{\sqrt{3}}{2} \text{ if } \alpha < 0 \text{ and } -\frac{\sqrt{3}}{2} < \beta < 0 \text{ if } \alpha > 0 \qquad (3.58)$$
$$\text{OR } \beta > \frac{\sqrt{3}}{2} \text{ if } \alpha < 0 \text{ and } \beta < -\frac{\sqrt{3}}{2} \text{ if } \alpha > 0.$$

4. Points $(D_\pm)_{\mathbf{III}}$, i.e., $(0, \pm 1, 0)$, are two radiation-dominated fixed points which exist only in Scenario III. They are located on the xz plane at $z = \pm 1$. It is an unstable point when evaluated according to Lyapunov theorem. The point $(D_-)_{\mathbf{III}}$ is unphysical because the energy density must be positive. The point $(D_+)_{\mathbf{III}}$ always exists as an unstable point. Since its effective EOS $w_{\text{eff}} = 1/3$, this fixed point leads to a decelerated expansion.

5. Points $(S_\pm)$, i.e., $(0, 0, \pm\infty)$, arise due to the restriction imposed by the condition (3.36) since they lie at $x = 0$, and $\sigma = \pm\infty$. Hence these fixed points exist in each Scenario I, II and III. Since the phase portrait is compactified and defined by (3.34), and by the definition of the σ variable is only positive, the Point (S_-) is unphysical. Point (S_+) is a Saddle.

6. Points $(T_\pm)$, i.e., $(0, +1, \pm\infty)$, arise due to the restriction imposed by the condition (3.36) since they lie at $x = 0$, and $\sigma = \pm\infty$. These fixed points exist in Scenario I and III only but not in Scenario II. Since the phase portrait is compactified and defined by (3.34), and by the definition of the σ variable is only positive, Point (T_-) is unphysical. Point (T_+) is a repeller.

7. The line L_{E} i.e., $(x = 0, z = 0, \forall\ \sigma)$ constitutes a line of equilibrium points and it connects the fixed points A_0 and (S_+). This equilibrium line exists in every of the three Scenario I, II and III.

8. In Scenario II, the $z\sigma$ surface at $(x = 0\ \forall\ \sigma)$ forms a topological plane surface of repeller points.

3.8 Disformal Trajectories

3.8.1 Disformal Scenario I: For various Initial Conditions

After having studied the fixed points, we move to the analysis of the non-static solutions of the dynamical system (3.28)-(3.32) in the Scenario I (i.e., $\tilde{w}_c = 0$ and $\tilde{w}_u = 0$). In this subsection, we fix (α, β) values and investigate various initial conditions.

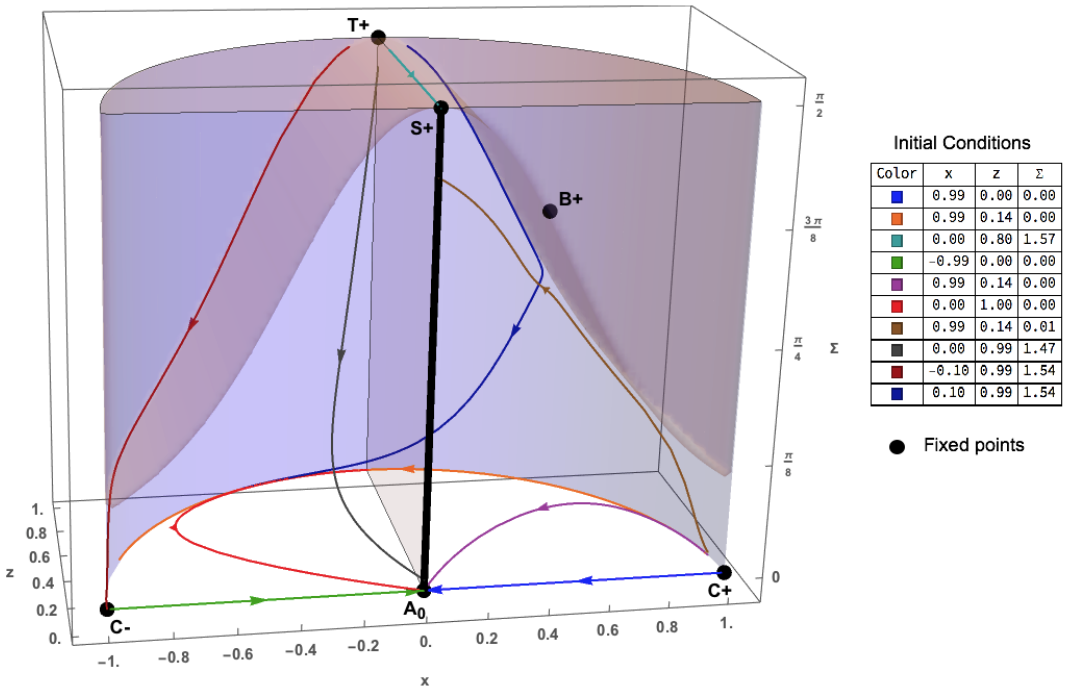

Figure 3.2: This figure shows Scenario I, where the quintessence is disformally coupled to a pressureless fluid (i.e., $\tilde{w}_c = 0$ and $\tilde{w}_u = 0$) with $\alpha = 0.5$, and $\beta = 1.5$ and the $x\sigma z$ phase portrait is shown with the different trajectories, which correspond to different chosen initial conditions (including the fixed points $(C_\pm)_\mathbf{I}$ and $(T_+)_\mathbf{I}$). At the boundary of the phase space, the Friedmann contraint (3.27) becomes $1 = x^2 + z^2$ and represents the surface for the half cylinder. The black solid line is the equilibrium line L_E i.e. $(x = 0, z = 0, \forall\, \sigma)$. The xz plane $(\sigma = 0)$ is the conformal invariant submanifold and the fixed point A_0 is an attracting end point. The shaded region corresponds to the forbidden region, where condition (3.36) is not satisfied.

Let us now fix the values $\alpha = 0.5$ and $\beta = 1.5$ (considering that $\beta \geq \sqrt{3}/2$ for Point $(B_+)_\mathbf{I}$ to exist), and analyse how the dynamical system (3.43)-(3.46) evolves from different sets of IC because the IC pre-determines the endpoints of the trajectories. The remarks were found from analysing Figure 3.2:

1. The dynamical system (3.43)-(3.46) flows from one fixed point to another within this closed compactified space, where the Points $(S_+)_\mathbf{I}$ and $(T_+)_\mathbf{I}$ are asymptotes, and trajectories tend towards that limit.

2. If the starting point is near or on the xz plane and satisfying $x^2 + z^2 \leq 1$, the end point is only the attractor point A_0, as in the conformal case. The conformal invariant sub-manifold is preserved.

3. The dynamical system (3.43)-(3.46) is sensitive to the chosen IC, i.e., different IC around the proximity of the fixed points can lead to different endpoints. For example, when the IC is chosen near $(C_+)_{\mathbf{I}}$, the dynamical system can end up at either A_0 or on the equilibrium line near$(S_+)_{\mathbf{I}}$. Similarly, IC is chosen near $(T_+)_{\mathbf{I}}$, the endpoints could be either at A_0 or $(S_+)_{\mathbf{I}}$ or on the equilibrium line L_{E}. $(C_-)_{\mathbf{I}}$ is a saddle fixed point where the dynamical system can be momentarily at rest such that point A_0 is the final end point.

3.8.2 Disformal Scenario I: For various (α, β) values

In this subsection, we fix the IC and investigate the effect of various choice of parameters. It is preferable to choose an IC close to a fixed point, because then, we know whether the chosen IC behaves like a saddle or a repeller. Moreover, it is preferable not to choose the IC near an attractor. The aim here is to investigate any deviation from the conformal case. Thus, it is in our interest to chose the IC set near to the repeller point $(T_+)_{\mathbf{I}}$, i.e., located at ($x_{\mathrm{ic}} = 0.0, z_{\mathrm{ic}} = +1.0$, and $\Sigma_{\mathrm{ic}} = \pi/2$). The different combination of parameters (α, β) can now be tested in order to determine how they affect the evolution of the dynamical system (3.43)-(3.46) and are shown in Figure 3.3 and the following remarks are made:

1. For $\alpha > 0$, the trajectories flow in the region bounded by $x < 0$ and for $\alpha < 0$, the trajectories flow in the region bounded $x > 0$. A larger value of α causes the trajectory to pass nearer to the conformal point$(C_\pm)_{\mathbf{I}}$ before ending at the attractor A_0 or on the equilibrium line L_{E}.

2. For $\alpha < 0$ and for $\beta > 0$, a larger value of β causes the trajectory to end nearer the disformal saddle point $(S_+)_{\mathbf{I}}$, otherwise for smaller value of β, it ends on equilibrium line L_{E}, nearer to the attractor A_0.

3. For $\alpha > 0$ and for $\beta > 0$, any value of β causes the trajectory to repel away from the disformal saddle point $(S_+)_{\mathbf{I}}$ and nearer to the attractor A_0.

4. For $\alpha < 0$ and for $\beta < 0$, any value of β causes the trajectory to repel away from the disformal saddle point $(S_+)_{\mathbf{I}}$ and end unto the attractor A_0.

5. The parameters (α, β) determine how much the dynamical system (3.43), (3.44) and (3.45) gets influenced by either the conformal fixed points $(C_{\pm})_{\mathbf{I}}$ or disformal fixed point $(S_{+})_{\mathbf{I}}$, as it evolves on its trajectory within the phase space.

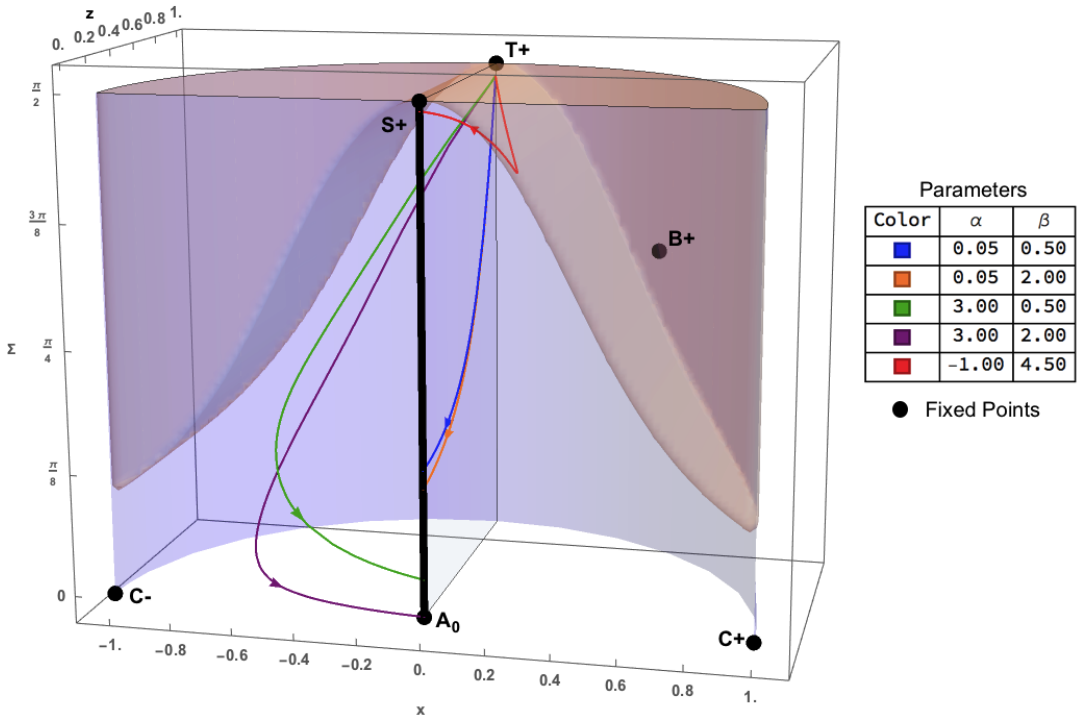

Figure 3.3: This figure shows Scenario I, where the quintessence is disformally coupled to pressureless fluid (i.e., $\tilde{w}_c = 0$ and $\tilde{w}_u = 0$). Given $(T_{+})_{\mathbf{I}}$ as the same initial condition, the evolution of the dynamical system (3.43)-(3.46) depend on the choice of parameters (α and β). At the boundary of the phase space, the Friedmann contraint (3.27) becomes $1 = x^2 + z^2$ and represents the surface for the half cylinder. The different trajectories in the $xz\sigma$ phase space correspond to different combination of parameters.

3.8.3 Disformal Scenario II: For various Initial Conditions

The two subsections 3.8.3 and 3.8.4 now consider the dynamical system (3.28)-(3.32) in the Scenario II (i.e., $\tilde{w}_c = 1/3$ and $\tilde{w}_u = 0$). For the sake of comparison with the other scenarios, we also fix $\alpha = 0.5$, $\beta = 1.5$ and analyse the dynamical system (3.47)-(3.50), evolving from different sets of IC. The remarks based on Figure 3.4 are noted:

1. We recover the conformal behaviour (compare with bottom left panel of Figure 3.1) on the plane of $\sigma = 0$ as expected. The dynamical variable Σ gives an additional degree of freedom for the dynamical system to evolve. The equilibrium line of repeller points in Figure 3.4 extends to a $z\sigma$ plane constitutes a topological separation between $x < 0$ and $x > 0$.

2. All the trajectories starting on that $z\sigma$ plane end on the equilibrium line $L_{\rm E}$, which connects both $(S_+)_{\mathbf{II}}$ and attractor point A_0.

3. If IC are set close to $z\sigma$ surface for $x > 0$ and further away from the equilibrium line $L_{\rm E}$, the trajectory gets attracted to the saddle point $(S_+)_{\mathbf{II}}$ than A_0 before ending onto the equilibrium line $L_{\rm E}$. If IC are set close to $z\sigma$ surface for $x < 0$ and further away from the equilibrium line $L_{\rm E}$, the trajectory gets repelled by the saddle point $(S_+)_{\mathbf{II}}$ but also attracted to the attractor point A_0 before ending onto the equilibrium line $L_{\rm E}$.

4. For $z = 0$, and $x < 0$ and $\forall\ \Sigma$, all trajectories end up at the attractor A_0. For $z = 0$, and $x > 0$ and $\Sigma > 0$, all trajectories end near to the saddle point $(S_+)_{\mathbf{II}}$, but if $\Sigma = 0$, the trajectory end up at the attractor A_0 as in the conformal behaviour.

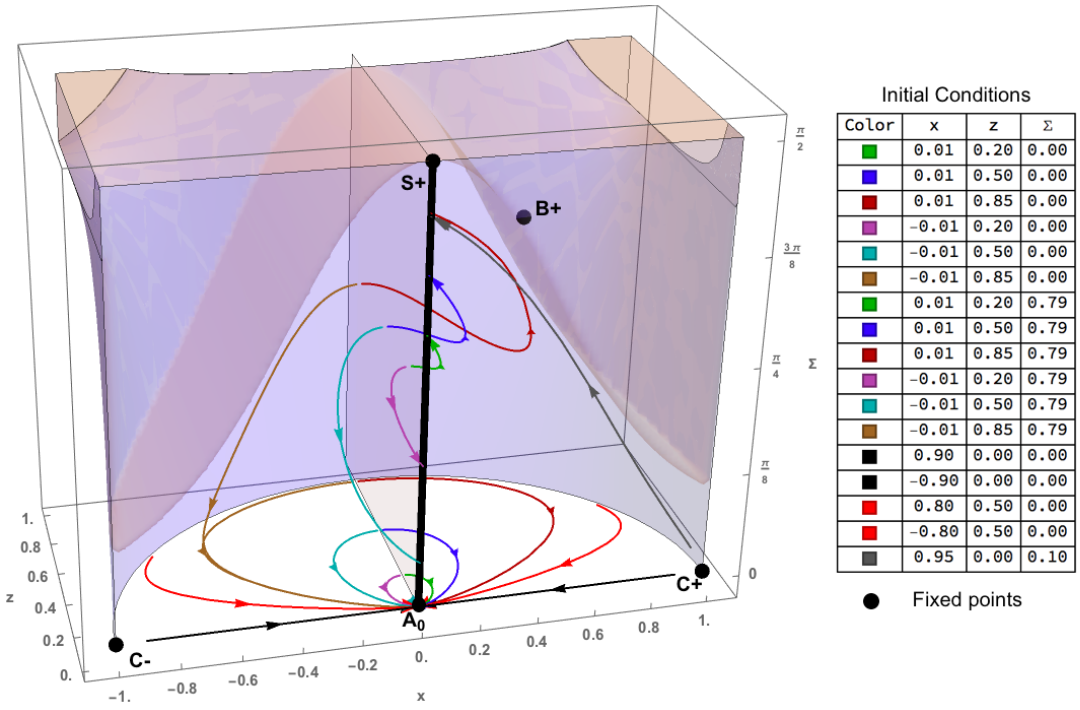

Figure 3.4: This figure shows Scenario II, where the quintessence is disformally coupled to relativistic fluid (i.e., $\tilde{w}_c = 1/3$ and $\tilde{w}_u = 0$) with $\alpha = 0.5$, and $\beta = 1.5$ and the $x\sigma z$ phase portrait is shown with the different trajectories, which correspond to different chosen initial conditions from the repeller $z\sigma$ plane surface. The blue surface represents the boundary of the phase space and satisfies the Friedmann contraint (3.27), which becomes $3x^2\left(\sigma z^2 - 1\right) + 3 = 4z^2$. The black solid line is the equilibrium line $L_{\rm E}$ i.e. $(x = 0, z = 0, \forall\ \sigma)$. The xz plane $(\sigma = 0)$ is the conformal invariant submanifold and the fixed point A_0 is an attracting end point. The $z\sigma$ plane constitute a topological separation between $x < 0$ and $x > 0$. The shaded region correspond to the forbidden region as where the condition (3.36) is not satisfied.

3.8.4 Disformal Scenario II: For various (α, β) values

As done in subsection 3.8.2, we choose IC close to a disformal fixed point. However, the disformal point $(B_{\pm})_{\mathbf{II}}$ is not physical and the conformal framework ($\Sigma = 0$) for this Scenario II, does not depend on the parameters α and β. The $z\sigma$ surface (i.e., $x = 0$ and $\forall\sigma$), however, consists of a surface of repeller fixed points and any point on that surface should be adequate for analysing how our dynamical system behaves with different combination of parameters.

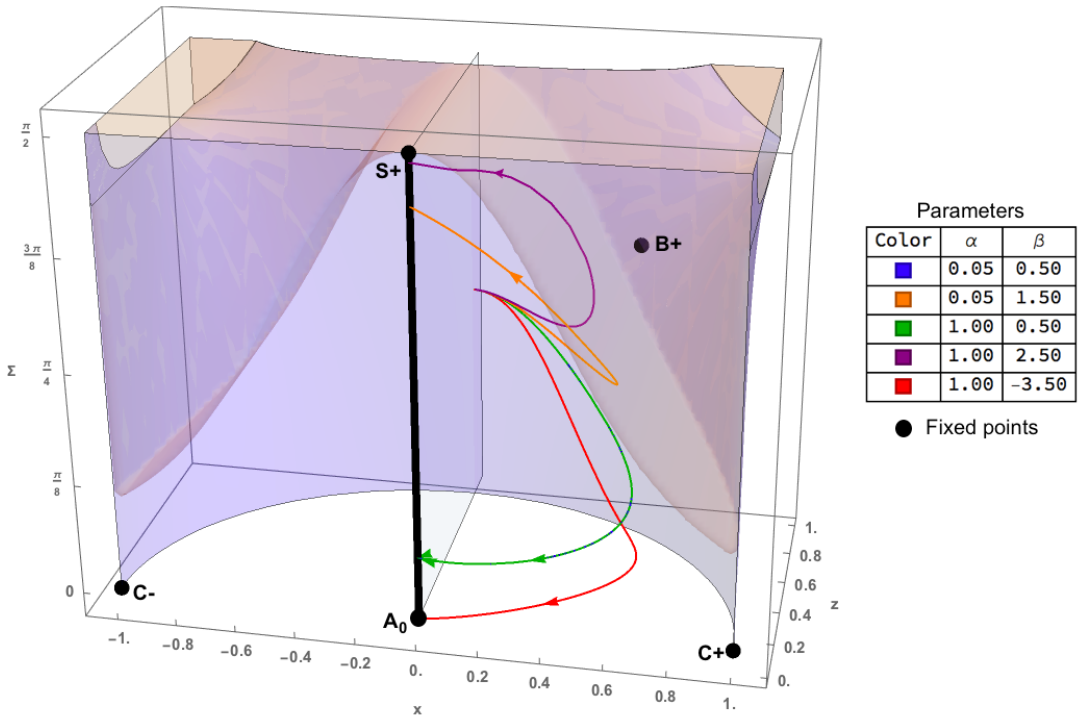

Figure 3.5: This figure shows Scenario II, where the quintessence is disformally coupled to relativistic fluid (i.e., $\tilde{w}_c = 1/3$ and $\tilde{w}_u = 0$). Given the same initial condition of $x = 0.01, z = 0.85, \Sigma = \pi/4$) on the surface of repeller points, the evolution of the dynamical system (3.47), (3.48) and (3.49) depend on the choice of parameters (α and β). The blue surface represents the boundary of the phase space and satisfies the Friedmann contraint (3.27), which becomes $3x^2(\sigma z^2 - 1) + 3 = 4z^2$. The different trajectories in the $xz\sigma$ phase space correspond to different combination of parameters. The blue trajectory ($\alpha = 0.05$) and green trajectory ($\alpha = 1.00$) overlap implying that α does not affect the trajectories on the dynamical system.

Since IC which are further away from the equilibrium line L_{E} produce appreciable trajectories, we choose the IC as ($x_{\mathrm{ic}} = 0.01,\ z_{\mathrm{ic}} = 0.85,\ \Sigma_{\mathrm{ic}} = \pi/4$). The different combination of parameters (α, β) can now be tested and we make the following remarks according to Figure 3.5:

1. The IC are set close to $z\sigma$ with $x \geq 0$ and further away from the equilibrium line $L_{\rm E}$, the trajectory gets attracted, as expected nearer to the saddle point $(S_+)_{\mathbf{II}}$ than A_0 before ending onto the equilibrium line $L_{\rm E}$.

2. The blue trajectory ($\alpha = 0.05$) and green trajectory ($\alpha = 1.00$) overlap each other which implies that α does not affect the trajectories on the dynamical system (3.47), (3.48) and (3.49).

3. The value of β determines, where trajectory ends on the equilibrium line $L_{\rm E}$. If the value β is large, the trajectory ends near the saddle point $(S_+)_{\mathbf{II}}$ and if the value β is small, the trajectory ends near A_0.

4. There is also no effect on the trajectories when the parameter $\alpha \to -\alpha$. In the event that $\beta \to -\beta$, then the trajectory ends up only at A_0, such that they are repelled from $(S_+)_{\mathbf{II}}$.

3.8.5 Disformal Scenario III: For Various Initial Conditions

We now analyse the dynamical system (3.28)-(3.32) in the Scenario III (i.e., $\tilde{w}_c = 1/3$ and $\tilde{w}_u = 1/3$) in the two subsections 3.8.5 and 3.8.6 . The values $\alpha = 0.5,\ \beta = 1.5$ are fixed for sake of comparison. Few different IC were chosen near the fixed points e.g. $(T_+)_{\mathbf{III}}$ and $(D_+)_{\mathbf{III}}$. Additionally, few other different IC were chosen on edge of the phase portrait on the line of intersection between the boundary surface satisfying the Friedmann constraint i.e. $4 = 4z^2 + 3x^2(1 - \sigma z^2)$ and the region satisfying (3.36). The reason to choose those IC is to appreciate how the trajectories of dynamical system (3.51)-(3.54) span out unto the phase portrait. The remarks are written according to Figure 3.6:

1. We recover the conformal behaviour (compare with Figure 3.1) on the plane of $\Sigma = 0$ as expected. The dynamical variable Σ gives an additional degree of freedom for the dynamical system to evolve.

2. When the IC is chosen from the fixed point $(T_+)_{\mathbf{III}}$, the trajectory ends at $(S_+)_{\mathbf{III}}$ and when the IC is chosen from the fixed point $(D_+)_{\mathbf{III}}$, the trajectory ends at A_0.

3. All these trajectories whose IC are on the line of intersection between the surface of the blue surface shown as $4 = 4z^2 + 3x^2(1 - \sigma z^2)$ and the surface satisfying (3.36), flow away from the repelling point $(T_+)_{\mathbf{III}}$ originally towards an endpoint on the equilibrium line $L_{\rm E}$.

4. All trajectories for all the IC without exception end eventually on the equilibrium line $L_{\rm E}$. If the IC have $x_{ic} < 0$, the trajectories tend to approach the attractor A_0 and if the IC have $x_{ic} > 0$, the trajectories tend to approach the saddle fixed point $(S_+)_{\mathbf{III}}$.

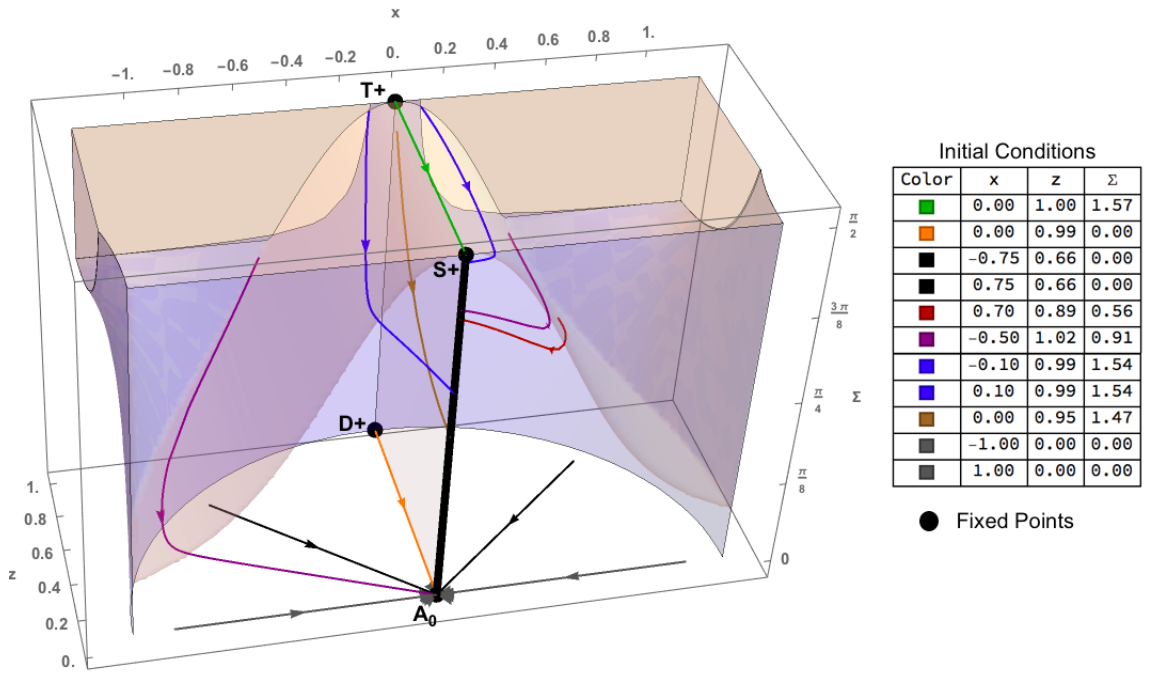

Figure 3.6: This figure shows the Scenario III, where the quintessence is disformally coupled to relativistic fluid (i.e., $\tilde{w}_c = 1/3$ and $\tilde{w}_u = 1/3$) with $\alpha = 0.5$, and $\beta = 1.5$ and the $x\sigma z$ phase portrait is shown with the different trajectories, which correspond to different chosen IC. The blue surface represents the boundary of the phase space and satisfies the Friedmann constraint (3.27), which becomes $4 = 4z^2 + 3x^2(1 - \sigma z^2)$. The black solid line is the equilibrium line $L_{\rm E}$ i.e. $(x = 0, z = 0, \forall\ \sigma)$. The xz plane $(\sigma = 0)$ is the conformal invariant submanifold and the fixed point A_0 is an attracting end point. The $z\sigma$ plane constitutes a topological separation between $x < 0$ and $x > 0$. The shaded region is where the condition (3.36) is not satisfied.

3.8.6 Disformal Scenario III: For various (α, β) values

Similar to the previous subsections 3.8.2 and 3.8.4, we fix the IC close to a fixed point and evaluate the dependence of the trajectories for dynamical system (3.51)-(3.54) on the parameters α and β. The IC was not chosen at $(T_+)_{\mathbf{III}}$ but near it, otherwise the behaviour is assymptotic and regardless of the (α, β) values, the trajectory flows straight to $(S_+)_{\mathbf{III}}$. But instead, in order to have appreciable effect of the parameters, the IC are set near the disformal repeller point$(T_+)_{\mathbf{III}}$ i.e. $(x_{ic} = -0.1, z_{ic} = +1.0,$ and $\Sigma_{ic} = \pi/2)$.

Different set of parameters (α, β) was considered for the investigation in this subsection and the comments, which were made based upon Figure 3.7 are given below:

1. The blue trajectory and green trajectory overlap each other, which implies that α does not affect the trajectories on the dynamical system (3.51)-(3.54).

2. The value of β determines, where trajectory ends on the equilibrium line $L_{\rm E}$. If the value β is large, the trajectory ends further away from the saddle point $(S_+)_{\mathbf{III}}$ and if the value β is small, the trajectory ends close to $(S_+)_{\mathbf{III}}$

3. There is also no effect on the trajectories when the parameter $\alpha \to -\alpha$. but if $\beta \to -\beta$, then the trajectory ends up only at $(S_+)_{\mathbf{III}}$.

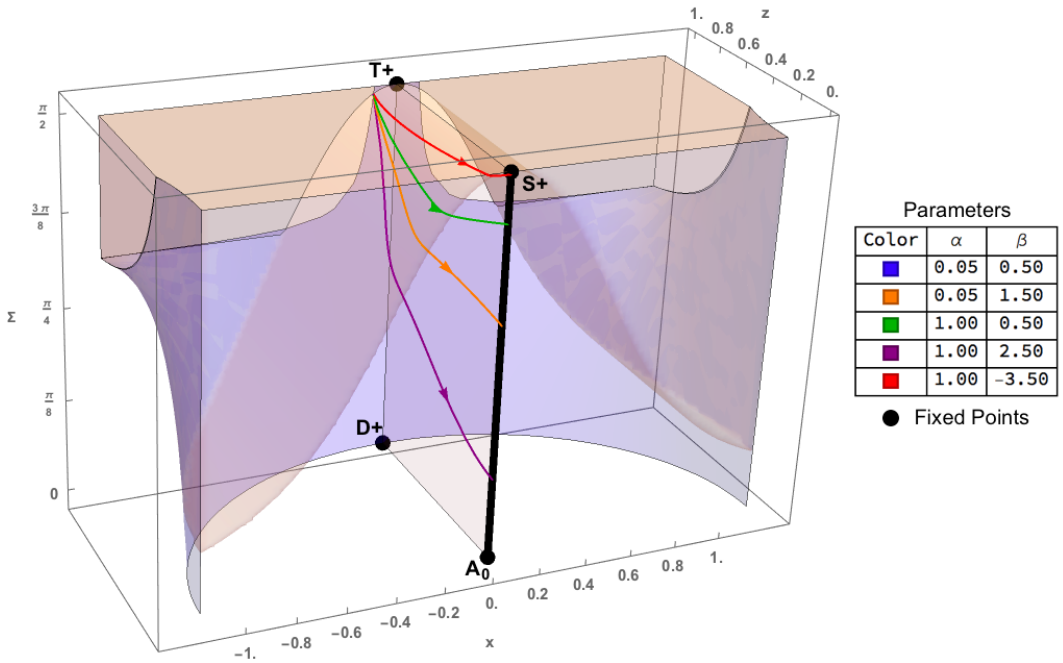

Figure 3.7: This figure shows the Scenario III, where the quintessence is disformally coupled to relativistic fluid (i.e., $\tilde{w}_c = 1/3$ and $\tilde{w}_u = 1/3$). Given the same initial condition of $(x = -0.1, z = 0.85, \Sigma = \pi/4)$ on the surface of repeller points, the evolution of the dynamical system (3.51)-(3.54) depends on the parameters α and β. The blue surface represents the boundary of the phase space and satisfies the Friedmann constraint (3.27), which becomes $4 = 4z^2 + 3x^2(1 - \sigma z^2)$. The blue trajectory and green trajectory overlap each other which implies that α does not affect the trajectories on the dynamical system.

In the sections 3.6-3.8, we have examined the DCQ model via the various theoretical possibilities for the dynamical system (3.28)-(3.32) in three scenarios. We have studied their disformal fixed points (summarised in Appendix A.5) and their trajectories for different IC and parameters. However, in section 3.9, we shall consider a more realistic investigation of the dynamical system, as it evolves through out the cosmological timeline.

3.9 Cosmological Analysis

In section 3.9, the expansion history of the DCQ model is studied in terms of cosmological redshift Z^*. In other words, we consider a DCQ model which evolves through a radiation-dominated phase and then a DM dominated phase, before it enters a de-Sitter evolution. With the assumption that the evolution of the background of the DCQ model mimics exactly that of ΛCDM as per equations (3.10) and (3.12), it is implied that the DCQ model fit the Planck data and the Supernovae Ia data. The quintessence is coupled to DM throughout the cosmological timeline and this implies that z represents the energy density of DM. Thus, we are dealing with the DCQ model in the Scenario I, whose dynamical system is described by the differential equations (3.43)-(3.46).

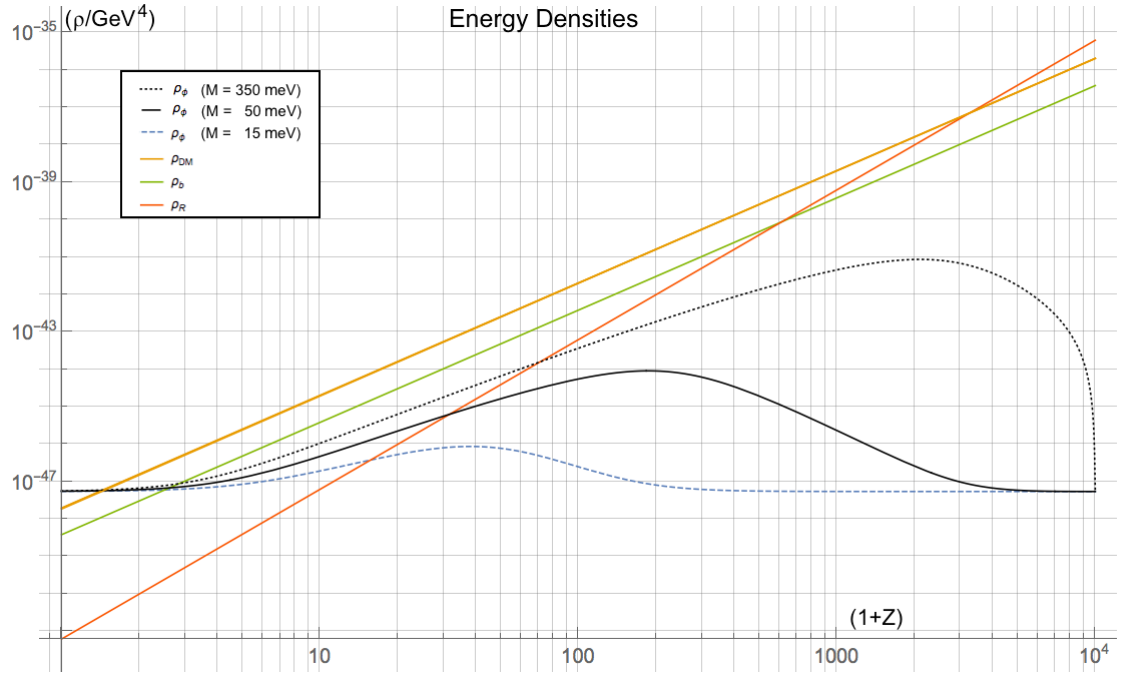

Figure 3.8: The energy density for the quintessence, radiation, DM and baryons, obtained when the dynamical system is evolved from the early universe ($Z_i = 10^4$) to present using three different mass scales of the quintessence.

Contrary to the three previous sections 3.6-3.8, where the initial values were theoretical and motivated by the fixed points on the phase space, it makes sense to consider more realistic IC for our universe, similar to ΛCDM background at redshift $Z_i = 10^4$. From the above definition (3.25), one evaluates the initial values of the dynamical variables as well at redshift Z_i for an early universe according to the relations,

*The redshift Z is not to be confused with dynamical variable z.

$$x_i = 0,\ \ y_i = \sqrt{\frac{\Omega_{\Lambda 0}}{h_i^2}},\ \ z_i \ = \ \sqrt{\frac{\Omega_{\mathrm{cdm}0}(1+Z_i)^3}{h_i^2}},\ \ \sigma_i = \frac{DH_0^2}{\kappa^2 C}h_i^2,\ \ h_i = h(Z_i), \quad (3.59)$$

where $h(Z) \equiv H/H_0$, is the reduced Hubble function and H_0 is Hubble's constant. The density parameters $\Omega_{\mathrm{cdm}0}$ and $\Omega_{\Lambda 0}$ correspond to DM and DE evaluated today. The parameters are set to $\alpha = 0.05$ from Ref. [24] and $\beta = 1.5$, which are chosen similar to the section 3.8.1 and the value of x_i is set to zero, as suggested by Ref. [24]. Additionally from equation (3.23), it can be noticed that $D(\phi_i) \propto M^{-4}$, thus the mass scale of the coupled quintessence becomes relevant in specifying the initial value for σ_i in equations (3.59). In the literature [65, 67], it has been constrained that the mass scale M is at least larger than $M \geq M_1 = 15$ meV. In addition to this mass M_1, we consider two hypothetical mass scales ($M_2 = 50$ meV, and $M_3 = 350$ meV) to test how large M must be in order to render the disformal contribution negligible. We hence investigate how the different mass scales M_1, M_2 and M_3 influence the dynamical system (3.43)-(3.46). Figure 3.8 shows the expansion history of the DCQ model in terms of cosmological redshift and how the energy densities of the quintessence, radiation, DM and baryons evolves from $Z_i = 10^4$ to the present. The following remarks were noted based on the results from Figure 3.8:

1. The features of ΛCDM are reproduced as expected such as the radiation-matter transition and the DM-DE transition.

2. The effect of different mass scales clearly affects the evolution of the energy density for quintessence ρ_ϕ as seen in Figure 3.8 and its density parameter $\Omega_\phi = x^2 + y^2$. However, from definition (3.25), the dynamical variables x and y do not depend on the mass. Rather, this effect only happens because of σ, which measures the strength of the disformal coupling, and depends on the mass M, given the definition of $D(\phi)$ in (3.23). This effect shows the deviation from the conformal framework ($\sigma = 0$), which is more apparent and important at early times.

3. The energy density of the quintessence traces that of a cosmological constant, when low mass scale is utilised. A larger mass scale causes deviation from the conformal framework.

Now that we understand that the disformal framework plays a more important role at early times, it becomes relevant to investigate how the disformal nature of the dynamical system (3.43)-(3.46) evolves from the early times to present. As mentioned in section 3.6, in a purely conformal framework, the interaction term Q does reduce to $Q = \alpha\rho\nabla^b\phi$ [36],

which is function of α only. In essence, the general form of $Q(\phi)$ (see equation (3.22)) is a function of α and β and thus behold both the disformal and conformal character of the dynamical system. Therefore, one can define an effective conformal coupling α_{eff}.

While the parameter α only characterises the rescaling of the metric via the conformal transformation (2.2) and the parameter β only characterises the deviation from pure conformal framework, i.e., distortion of angles of the metric by the disformal transformation (3.1), the effective coupling α_{eff} provides an interplay of both these characteristics. Similar to the Ref. [62], we also consider an α_{eff} of the form:

$$\alpha_{\text{eff}} = -\frac{Q}{\kappa\rho}\,, \tag{3.60}$$

where $Q(\phi)$ is initially defined as in equation (3.32) but reduces to equation (3.46) for Scenario I and ρ is related to dynamical variable z, as per equation (3.25). Figure 3.9 shows the evolution of the α_{eff} with redshift Z for the three different mass scales M_1, M_2 and M_3. From the results of Figure 3.9, the following interpretation was noted:

1. When the α_{eff} is close to zero, the disformal coupling is cancelling the conformal coupling as shown in [68].

2. There exists a turn over point, which indicates the redshift at which the contribution from the disformal coupling is of the same magnitude as the conformal coupling.

3. After the turn over point, the decay of the disformal coupling continues until it becomes insignificant and the α_{eff} becomes the chosen value of the conformal coupling constant $\alpha = 0.05$. The framework can be approximated as nearly conformal and the dynamical system (3.43)-(3.46) reduces to a system described by (3.37) and (3.38) at late times.

4. The α_{eff} is sensitive to the mass scale, which alters the redshift of the turnover point at which the disformal coupling becomes insignificant. A higher (lower) mass scale would cause turnover to occur at a much higher (lower) redshift.

The dynamical variable σ, which represents the strength of the disformal coupling, starts with large value initially but then decays at constant logarithmic rate throughout the whole expansion history as seen in Figure 3.10. From definition (3.23) and taking the logarithm of σ in (3.25), one can find that the mass scale does not affect the rate of decay but only the time when σ becomes $\mathcal{O}(1)$.

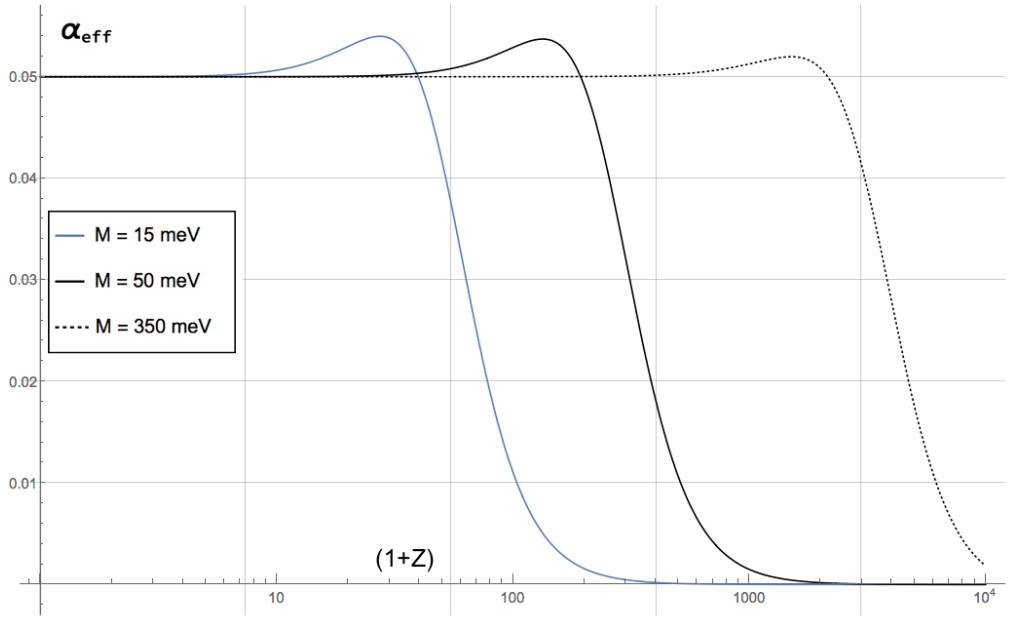

Figure 3.9: The evolution of the effective conformal coupling (α_{eff}), as defined in equation (3.59), was carried out from initial redshift $Z_i = 10^4$ to present for three mass scales M_1, M_2 and M_3. The turn over point, i.e., when the bump occurs, indicates the redshift when the contribution of the disformal coupling is of the same magnitude as the conformal coupling. After the turn over point, the effective conformal coupling $\alpha_{\text{eff}} \to \alpha$, because the disformal coupling becomes insignificant.

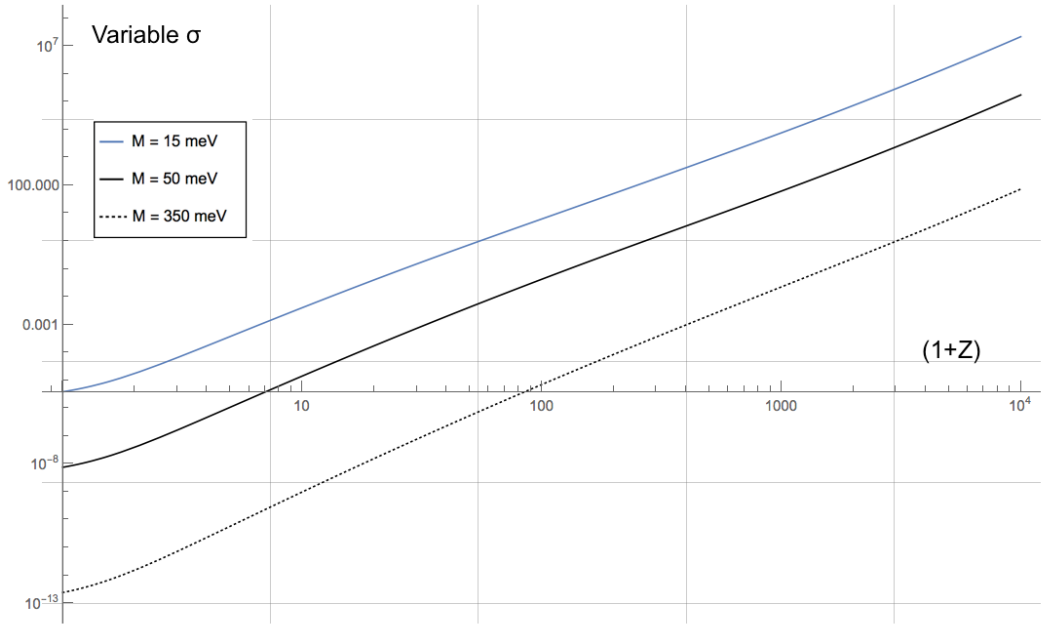

Figure 3.10: The decay of the dynamical variable σ, which represent the strength of the disformal coupling, is shown to occur at approximately a constant logarithmic rate throughout the whole expansion history for the three mass scales.

We end the Chapter 3 by highlighting that the disformal coefficient $D(\phi)$ from the disformal transformation brings more contributions in the coupling $Q(\phi)$ of the coupled quintessence (as per equation (3.8)) and in the construct of the DCQ model. In section 3.3, we find that the quintessence is coupled with a generic fluid in the DCQ model, which mimics a background that consists of a cosmological constant and another uncoupled generic fluid. Therefore, the EOS parameters of both generic fluids, the conformal and disformal coefficients determine the uniqueness of the disformal couplings and the DCQ model. The dynamical system analysis allowed us to study the static and non-static solutions of DCQ model on a 3D phase portrait. We study how the dynamical system could be influenced by the IC as well as the conformal and disformal parameter α and β, for the various scenarios. This help us understand the various theoretical possibilites of how DCQ model could evolve. Amongst all the theoretical possibilities, it is worth pointing that the dynamical system (3.43)-(3.46) could actually end towards a cosmological acceleration, when its trajectories eventually tends towards the attractor A_0, as shown in Figure 3.2. Finally, we investigated the expansion history of the DCQ model, where the quintessence was coupled with DM (Scenario I). After performing the cosmological analysis for the DCQ model mimicking ΛCDM background, we find that different mass scales clearly affect the evolution of the energy density for quintessence ρ_ϕ in a similar way to what was found in previous studies with an exponential potential [62, 68]. More specifically, the presence of a disformal coupling has the effect of screening the interaction between matter and the scalar field at high redshifts. The time of crossover to the dominant conformal coupling might be revealed when studying the evolution of density perturbations [68].

In Chapter 4, we will consider the DCQ model (Scenario I) in a perturbed space-time, while keeping a ΛCDM background. We will revisit the modified perturbation equations for the quintessence, baryons and coupled DM for the DCQ model. It is imperative that we also perturb the disformal coupling $Q(\phi)$ as indicated in equation (2.20)-(2.22). We shall study the effect of the parameters α, β and M on the evolution of total matter density perturbations and the growth rate respectively. The perturbation theory of the DCQ model brings new perspectives on the formation of large-scale structures via the $f\sigma_8(Z)$ function, which also depends on the matter fluctuation amplitude σ_8^0, as per equation (1.43). It is not ruled out that, the predicted σ_8^0 value by extensions of the Concordance model, might be able to resolve the σ_8 tension (see Ref. [24]). Similar to Figure 2.4, we shall constrain the plausible values of σ_8^0 for the DCQ model (see Figure 4.3) in order to understand the σ_8 tension better.

Chapter 4

Constraining disformal couplings with Redshift Space Distortion data

In section 2.5, we have reviewed how a CCQ model with a ΛCDM background attempts to alleviate the σ_8 tension (investigated by Ref. [24]). In Chapter 3, the disformal couplings in ΛCDM background cosmology were studied. This Chapter 4 extends the scalar perturbations of the CCQ model in section 2.5 towards the disformal framework, while it builds upon the expansion history of the DCQ model, which was investigated in section 3.9. In other words, the evolution of density perturbations is reviewed for a quintessence model, which is disformally coupled with DM. Since the background of the studied model mimics the ΛCDM cosmological evolution, the quintessential potential is not specified. In the following, we shall see a disformal effect due to the quintessential mass M, in the growth rate of the cosmological structures on large scales. The disformal parameter β renders no appreciable effect on the evolution of the total matter perturbation. Additionally, a Bayesian analysis of the relevant free parameters (i.e., σ_8^0, α and M) for the perturbative DCQ model is then carried out using the RSD data (Table A.1) to constrain the best-fit parameters, which might explain the σ_8 tension. We also conclude, via the best fit set of parameters, that the RSD data prefers the model to behave conformally.

This chapter is organised in the following order; section 4.1 reviews the background cosmology of the DCQ model, mimicking ΛCDM. Section 4.2 revisits the modified perturbation equations of the quintessence, baryons and coupled fluid for the studied DCQ model. Section 4.3 presents the results, observational constraints and the concluding remarks. We also mention few prospective works that will carried out in the future.

4.1 The DCQ background cosmology

The foundations of DCQ background cosmology were described by section 3.2. Assuming the spatially flat FLRW metric (1.24), the Friedmann and Raychaudhuri equations are given by the equations (2.7), such that the coupled fluid is the CDM in this Chapter. The continuity equations (2.9) indicate the flow of the energy-momentum between the CDM and quintessence, where $Q(\phi)$ is given by the interaction term (3.8). The mimicry of this DCQ model toward the ΛCDM model is described by equations (3.10)-(3.13) in section 3.3, but it simplifies as in Ref. [24] because the coupled fluid is the CDM:

$$\begin{aligned} H^2 = H^2_{\Lambda\text{CDM}} &\Rightarrow \rho_\phi = \rho_\Lambda \,, \\ \dot{H} = \dot{H}_{\Lambda\text{CDM}} &\Rightarrow P_\phi = -\rho_\Lambda, \\ &\Rightarrow \quad V(\phi) = \frac{1}{2}\dot{\phi}^2 + \rho_\Lambda \;\text{ and }\; V_{,\phi} = \ddot{\phi}\,. \end{aligned} \tag{4.1}$$

In the section 3.7 for the Scenario I, where the quintessence is disformally coupled with DM, the dynamical system (3.28)-(3.32) reduces to the set of equations (3.43)-(3.46), which can also be re-expressed :

$$x' = -\frac{H'}{H}x - \frac{3x}{2} + \frac{\sqrt{3}\tilde{Q}_0 z^2}{2}\,, \tag{4.2}$$

$$z' = -\frac{H'}{H}z - \frac{3z}{2} - \frac{\sqrt{3}\tilde{Q}_0}{2}xz\,, \tag{4.3}$$

$$\sigma' = \left[\sqrt{3}x\left(\lambda_C - \lambda_D\right) - 3\left(x^2 + z^2\right)\right]\sigma\,, \tag{4.4}$$

$$\tilde{Q}_0 \equiv \frac{\kappa Q_0}{3H^2 z^2} = \frac{\lambda_C\left(1 - 6\sigma x^2\right) + 3\sigma x\left(x\lambda_D + \sqrt{3}\right)}{2 - 6\sigma x^2 + 3\sigma z^2}\,, \tag{4.5}$$

where the dynamical variables x, y, z and σ have been defined by equations (3.25), and $\tilde{Q}_0$ is the normalised interaction term. These dynamical variables (3.25) are constrained to obey the Friedmann and Raychaudhuri equations (3.27), which become (Scenario I):

$$1 = x^2 + y^2 + z^2\,, \quad \text{and} \quad \hat{H} \equiv \frac{H'}{H} = -\frac{3}{2}\left(x^2 + z^2\right) \quad \text{and} \quad \frac{H''}{H} = 6(x^2 + z^2)\,, \tag{4.6}$$

such that the derivative of the Raychaudhuri equation is also computed for later derivations in subsection 4.2.3. It is additionally useful to define the variables Λ_C and Λ_D and the derivative of the variables λ_C and λ_D below:

$$\Lambda_C \equiv \frac{C_{,\phi\phi}}{\kappa^2 C}, \quad \Lambda_D \equiv \frac{D_{,\phi\phi}}{\kappa^2 D}\,, \quad \lambda'_C = \sqrt{3}x(\lambda_C^2 - \Lambda_C) \quad \text{and} \quad \lambda'_D = \sqrt{3}x(\lambda_D^2 - \Lambda_D). \tag{4.7}$$

The numerical background solutions for the dynamical system (4.2)-(4.5) was analysed from the early universe to present and this study was detailed in section 3.9.

4.2 The DCQ perturbative cosmology

In the section 4.2, we revisit the perturbations of a DCQ model, whose background mimics ΛCDM (See section 4.1). The Ref. [69] has already derived the second-order perturbation theory of a scalar field which is disformally coupled with CDM in a Horndeksi model, defined in terms of α basis (in the unitary gauge). Although the derivations in Ref. [69] are more general and apply to many models, we still provide the steps to obtain the perturbation equations of our DCQ model for the sake of completeness. We only consider the scalar perturbations in the FLRW metric as per equation (1.34). The perturbed components of the affine connections, Ricci tensor and the Einstein tensor can be found in the Appendix A.2. Similarly, the n^{th} cosmological fluids and the quintessence ϕ are perturbed as per the equations (1.35) and (2.15) respectively. Hence, their perturbed energy-momentum tensors are given by equations (A.15) and (A.16), such that one can define the density contrast $\delta_n \equiv \delta\rho_n/\bar{\rho}_n$ and the sound speed as $c_s^2 \equiv \delta P_n/\delta\rho_n$.

The scalar modes of the perturbed Einstein equations (i.e., $\delta G^{\mu}_{\nu} = \kappa^2 \delta T^{\mu}_{\nu}$) in the DCQ model for different combination of (μ, ν) are still given by the equations (2.16)-(2.19), which is re-expressed in cosmic time (inspired from Ref. [25]):

$$\nabla^2(\dot{\Psi} + H\Psi) = \frac{\kappa^2\dot{\phi}}{2}\nabla^2\chi - \frac{3}{2}aH^2(\Omega_c\theta_c + \Omega_{\mathtt{B}}\theta_{\mathtt{B}}) \,, \tag{4.8}$$

$$a^{-2}\nabla^2\Psi - 3H(\dot{\Psi} + H\Psi) = \frac{3}{2}H^2(\Omega_c\delta_c + \Omega_{\mathtt{B}}\delta_{\mathtt{B}}) + \frac{\kappa^2}{2}(\dot{\phi}\dot{\chi} - \Psi\dot{\phi}^2 + V_{,\phi}\chi) \,, \tag{4.9}$$

$$\ddot{\Psi} + 4H\dot{\Psi} + (2\dot{H} + 3H^2)\Psi = \frac{3}{2}H^2c_s^2(\Omega_c\delta_c + \Omega_{\mathtt{B}}\delta_{\mathtt{B}}) + \frac{\kappa^2}{2}(\dot{\phi}\dot{\chi} - \Psi\dot{\phi}^2 - V_{,\phi}\chi) \,, \tag{4.10}$$

whereby the equations (4.8)-(4.10) make use of the relation $\Psi = \Phi$, which has been obtained from the traceless spatial components of the perturbed Einstein equations. The subscripts "c" and "$\mathtt{B}$" denote the coupled CDM and baryons respectively. For the DCQ model, the perturbed Euler equation, the perturbed Continuity equation and the perturbed Klein-Gordon equation are still given by set of equations (2.20)-(2.22) respectively [48]. The variable $\theta_n \equiv \nabla^2 v_n$ is the perturbed comoving velocity. The term Q_1, which appears in equations (2.20) and (2.22), is the perturbation of the interaction term $Q(\phi)$ from the equation (3.8), and it is defined in cosmic time as the following [48, 69]:

$$Q_1 = \frac{-\rho_c}{C + D(\rho_c - \dot{\phi}^2)}\left(\mathcal{B}_1\delta_c + \mathcal{B}_2\dot{\Phi} + \mathcal{B}_3\Psi + \mathcal{B}_4\dot{\chi} + \mathcal{B}_5\chi\right) \,, \tag{4.11}$$

$$\text{with } \mathcal{B}_1 = \frac{C_{,\phi}}{2}(1 - 3c_s^2) - 3DH\dot{\phi}(1 + c_s^2) - D(V_{,\phi} - Q_0) - D\dot{\phi}^2\left(\frac{C_{,\phi}}{C} - \frac{D_{,\phi}}{2D}\right) , \tag{4.12}$$

$$\mathcal{B}_2 = 3D\dot{\phi}(1+w_f)\,, \tag{4.13}$$

$$\mathcal{B}_3 = 6DH\dot{\phi}(1+w_c) + 2D\dot{\phi}^2\left(\frac{C_{,\phi}}{C} - \frac{D_{,\phi}}{2D} + \frac{Q_0}{\rho_c}\right)\,, \tag{4.14}$$

$$\mathcal{B}_4 = -3DH(1+w_c) - 2D\dot{\phi}\left(\frac{C_{,\phi}}{C} - \frac{D_{,\phi}}{2D} + \frac{Q_0}{\rho_c}\right)\,, \tag{4.15}$$

$$\begin{aligned}\mathcal{B}_5 = {} & \frac{C_{,\phi\phi}}{2}(1-3w_c) + \frac{(1+w_c)D\nabla^2}{a^2} - DV_{,\phi\phi} - D_{,\phi}V_{,\phi} - 3D_{,\phi}H\dot{\phi}(1+w_c) \\ & -D\dot{\phi}^2\left[\frac{C_{,\phi\phi}}{C} + \left(\frac{C_{,\phi}}{C}\right)^2 + \frac{C_{,\phi}D_{,\phi}}{CD} - \frac{D_{,\phi\phi}}{2D}\right] + \left(C_{,\phi} + D_{,\phi}\rho_c - D_{,\phi}\dot{\phi}^2\right)\frac{Q_0}{\rho_c}\,,\end{aligned} \tag{4.16}$$

Such that the ∇^2 operator appearing in the second term of the coefficient $\mathcal{B}_5$ in (4.16) is acting upon the variable χ in equation (4.11). The perturbed Einstein equations (4.8)-(4.10) as well as the perturbed conservation and continuity equations (2.20)-(2.22) are used in deriving the second-order evolution equations of density perturbations. The corresponding evolution equations for the baryonic density perturbations are however much simpler, because they are not coupled with the quintessence, i.e., $Q_0 = Q_1 = 0$ for baryons, and therefore the equations (2.20)-(2.22) become of the form below:

$$\dot{\delta}_{\mathtt{B}} = -\frac{\theta_{\mathtt{B}}}{a} + 3\dot{\Psi} \quad \text{and} \quad \dot{\theta}_{\mathtt{B}} = -H\theta_{\mathtt{B}} - \frac{\nabla^2\Psi}{a}\,. \tag{4.17}$$

The evolution equation of baryonic density perturbations is then obtained as in Ref. [24].

$$\delta''_{\mathtt{B}} + \delta'_{\mathtt{B}}\left(2 + \hat{H}\right) - \frac{3}{2}\left(\Omega_{\mathtt{B}}\delta_{\mathtt{B}} + \Omega_c\delta_c\right) = 0\,. \tag{4.18}$$

4.2.1 The ODEs for the density perturbations of the coupled fluid

The derivation of the second-order evolution equations for the density perturbations of the coupled fluid is provided here. Since in our model, it is CDM which is coupled with the quintessence, and it is also assumed as a perfect fluid, one can set the variables $w_c = \dot{w}_c = \nabla^2\pi_c = 0$ and the equations (2.20)-(2.22) simplify to following equations (equivalent to equation (3.16)-(3.17) in Ref. [69]):

$$\dot{\delta}_c = -\frac{\theta_c}{a} + 3\dot{\Psi} + \frac{Q_0\,\dot{\phi}}{\rho_c}\delta_c - \frac{Q_0\,\dot{\chi}}{\rho_c} - \frac{Q_1\,\dot{\phi}}{\rho_c}\,, \tag{4.19}$$

$$\dot{\theta}_c = -\left(H - \frac{Q_0\,\dot{\phi}}{\rho_c}\right)\theta_c - \frac{\nabla^2\Psi}{a} + \frac{Q_0\nabla^2\chi}{\rho_c a}\,, \tag{4.20}$$

By taking the time-derivative of equation (4.19) and inserting $\dot{\theta}_c$ from the equation (4.20), one can obtain:

$$\ddot{\delta}_c = \left(2H - \frac{Q_0\,\dot{\phi}}{\rho_c}\right)\frac{\theta_c}{a} + \frac{\nabla^2\Psi}{a^2} - \frac{Q_0\nabla^2\chi}{\rho_c a^2} + 3\ddot{\Psi} + \frac{Q_0}{\rho_c}\Big[\ddot{\phi}\delta_c + \dot{\phi}\dot{\delta}_c - \ddot{\chi} + \left(\frac{\dot{\rho}_c}{\rho_c}\right)\left(\dot{\chi} - \dot{\phi}\delta_c\right)\Big] + \frac{\dot{Q}_0}{\rho_c}\left(\dot{\phi}\delta_c - \dot{\chi}\right) - \frac{Q_1}{\rho_c}\left[\ddot{\phi} - \left(\frac{\dot{\rho}_c}{\rho_c}\right)\dot{\phi}\right] - \frac{\dot{Q}_1\,\dot{\phi}}{\rho_c}\,. \quad (4.21)$$

Equation (4.19) can be re-inserted in equation (4.21) to substitute for θ_c/a and the perturbed Einstein equation (4.10), with $c_s^2 = 0$, can used to replace $\ddot{\Psi}$ (e.g., in Ref [69]):

$$\ddot{\delta}_c + \left(2H - \frac{Q_0\,\dot{\phi}}{\rho_c}\right)\left(\dot{\delta}_c - 3\dot{\Psi} - \frac{Q_0\,\dot{\phi}}{\rho_c}\delta_c + \frac{Q_0\,\dot{\chi}}{\rho_c} + \frac{Q_1\,\dot{\phi}}{\rho_c}\right) - \frac{\nabla^2\Psi}{a^2} + \frac{Q_0\nabla^2\chi}{\rho_c a^2} + 12H\dot{\Psi} + 3(2\dot{H} + 3H^2)\Psi - \frac{3\kappa^2}{2}(\dot{\phi}\dot{\chi} - \Psi\dot{\phi}^2 - V_{,\phi}\chi) - \frac{\dot{Q}_0\,\dot{\phi}}{\rho_c}\delta_c - \frac{Q_0\,\ddot{\phi}}{\rho_c}\delta_c - \frac{Q_0\,\dot{\phi}}{\rho_c}\dot{\delta}_c + \left(\frac{\dot{\rho}_c}{\rho_c}\right)\frac{Q_0\,\dot{\phi}}{\rho_c}\delta_c + \frac{\dot{Q}_0\,\dot{\chi}}{\rho_c} + \frac{Q_0\,\ddot{\chi}}{\rho_c} - \left(\frac{\dot{\rho}_c}{\rho_c}\right)\frac{Q_0\,\dot{\chi}}{\rho_c} + \frac{Q_1\,\ddot{\phi}}{\rho_c} + \frac{\dot{Q}_1\,\dot{\phi}}{\rho_c} - \left(\frac{\dot{\rho}_c}{\rho_c}\right)\frac{Q_1\,\dot{\phi}}{\rho_c} = 0\,. \quad (4.22)$$

The wave number k appears when performing the Fourier transformation of ∇^2 operator as in $\nabla^2 \to -k^2$. Under the approximation of $k^2\Psi \gg a^2H^2\Psi$ and $k^2\chi \gg a^2H^2\chi$, i.e., the Newtonian limit for sub-Hubble scales, equation (4.22) reduces into:

$$\ddot{\delta}_c + \left(2H - \frac{Q_0\,\dot{\phi}}{\rho_c}\right)\left(\dot{\delta}_c - \frac{Q_0\,\dot{\phi}}{\rho_c}\delta_c + \frac{Q_1\,\dot{\phi}}{\rho_c}\right) - \frac{\nabla^2\Psi}{a^2} + \frac{Q_0\nabla^2\chi}{\rho_c a^2} - \frac{\dot{Q}_0\,\dot{\phi}}{\rho_c}\delta_c - \frac{Q_0\,\ddot{\phi}}{\rho_c}\delta_c - \frac{Q_0\,\dot{\phi}}{\rho_c}\dot{\delta}_c + \left(\frac{\dot{\rho}_c}{\rho_c}\right)\frac{Q_0\,\dot{\phi}}{\rho_c}\delta_c + \frac{Q_1\,\ddot{\phi}}{\rho_c} + \frac{\dot{Q}_1\,\dot{\phi}}{\rho_c} - \left(\frac{\dot{\rho}_c}{\rho_c}\right)\frac{Q_1\,\dot{\phi}}{\rho_c} = 0\,. \quad (4.23)$$

Similarly, the perturbed Einstein equation (4.9) and the perturbed Klein-Gordon (2.22) can be approximated in the Newtonian limit to render the expressions below [69]. The $\nabla^2\dot{\chi}$ is also computed, which is useful for later derivations in subsection 4.2.3.

$$\frac{\nabla^2\Psi}{a^2} \approx \frac{3}{2}H^2(\Omega_c\delta_c + \Omega_{\mathtt{B}}\delta_{\mathtt{B}}) \quad \text{and} \quad \frac{\nabla^2\chi}{a^2} \approx -Q_1 \quad \text{and} \quad \frac{\nabla^2\dot{\chi}}{a^2} \approx -(\dot{Q}_1 + 2HQ_1) \quad (4.24)$$

The expressions in (4.24) are used to substitute $\nabla^2\Psi$ and $\nabla^2\chi$, which appear in the evolution equation (4.23). Thus, after inserting (4.24) and $\dot{\rho}_c/\rho_c$ (using equation (2.9)) into (4.23), one can obtain the form below.

$$\ddot{\delta}_c + 2\dot{\delta}_c\left(H - \frac{Q_0\,\dot{\phi}}{\rho_c}\right) - \delta_c\left[5H\left(\frac{Q_0\,\dot{\phi}}{\rho_c}\right) + \frac{\dot{Q}_0\,\dot{\phi}}{\rho_c} + \frac{\dot{Q}_0\,\ddot{\phi}}{\rho_c}\right] + 5H\left(\frac{Q_1\,\dot{\phi}}{\rho_c}\right) - \frac{3}{2}H^2(\Omega_c\delta_c + \Omega_{\mathtt{B}}\delta_{\mathtt{B}}) - \frac{Q_0Q_1}{\rho_c} + \frac{Q_1\,\ddot{\phi}}{\rho_c} + \frac{\dot{Q}_1\,\dot{\phi}}{\rho_c} = 0\,. \quad (4.25)$$

The functions and derivatives of equation (4.25) can be re-expressed in terms of the dynamical variables (3.25). One can use (4.5) and further define these normalised variables;

$$\tilde{Q}_0 \equiv \frac{\kappa Q_0}{3H^2z^2}, \qquad \tilde{Q}_1 \equiv \frac{\kappa Q_1}{3H^2z^2}, \qquad \hat{q}_0 \equiv \frac{\kappa Q_0'}{3H^2z^2}, \qquad \hat{q}_1 \equiv \frac{\kappa Q_1'}{3H^2z^2}, \tag{4.26}$$

so that the equation (4.25) yield the following expression:

$$\begin{aligned}\delta_c'' &= -\delta_c'\left(2-2\sqrt{3}\tilde{Q}_0x+\hat{H}\right)+\sqrt{3}\delta_c\left[5\tilde{Q}_0x+\hat{q}_0x+\tilde{Q}_0\left(x'+\hat{H}x\right)\right]-5\sqrt{3}\tilde{Q}_1x \\ &\quad+\frac{3}{2}(z^2\delta_c+\Omega_{\mathtt{B}}\delta_{\mathtt{B}})+3\tilde{Q}_0\tilde{Q}_1z^2-\sqrt{3}\tilde{Q}_1\left(x'+\hat{H}x\right)-\sqrt{3}\hat{q}_1x\,. \end{aligned}\tag{4.27}$$

While the tilde (i.e., in $\tilde{Q}_0$ and $\tilde{Q}_1$) denotes the normalisation of the interaction term Q_0 and of its perturbation Q_1, the hat (i.e., in $\hat{q}_0$ and $\hat{q}_1$) denotes the normalisation of the derivative of the interaction term Q_0' and the derivative of its perturbation Q_1'. After inserting the conservation equation (4.2) to replace $(x'+\hat{H}x)$ in equation (4.27), the second-order evolution equation for the density perturbations of the coupled DM is computed after some arrangements (This corresponds to equation (4.24) in Ref. [69]).

$$\begin{aligned}&\delta_c''+\delta_c'\left(2-2\sqrt{3}\,\tilde{Q}_0\,x+\hat{H}\right)-\delta_c\left[\sqrt{3}\,\hat{q}_0x+\frac{\tilde{Q}_0}{2}\left(7\sqrt{3}x+3\tilde{Q}_0z^2\right)\right] \\ &+\sqrt{3}\,\hat{q}_1x+\frac{\tilde{Q}_1}{2}\left(7\sqrt{3}x-3\tilde{Q}_0z^2\right)-\frac{3}{2}(z^2\delta_c+\Omega_{\mathtt{B}}\delta_{\mathtt{B}})=0\,,\end{aligned}\tag{4.28}$$

where the derivation of $\hat{q}_0$ and $\hat{q}_1$ is provided in the next two subsection 4.2.2 and 4.2.3. As expected, the equation (4.18) and (4.28) reduce to the perturbation equations (2.37)-(2.37) in section 2.5 for the conformal framework [24].

4.2.2 The normalised derivative of the interaction term

The interaction term $Q(\phi)$ as in equation (3.21) for a single coupled fluid can be computed by evaluating the covariant derivative of time components for the energy-momentum tensor (3.8). The derivation is kept general for arbitrary choices of λ_C and λ_D in the subsection 4.2.2. The dynamical variables (3.25) are inserted into equation (3.21) to yield:

$$\begin{aligned}(1-3\sigma x^2)\left(\frac{\kappa Q_0}{3H^2z^2}\right) &= \frac{\lambda_C}{2}(1-3w_c)+3\sqrt{3}w_c\sigma x-\sqrt{3}\frac{\sigma}{H}\left(\dot{x}+\frac{\dot{H}}{H}x\right) \\ &\quad+\frac{3}{2}\left(\lambda_D-2\lambda_C\right)\sigma x^2.\end{aligned}\tag{4.29}$$

The EOS for coupled DM is obtained by setting $w_c = 0$. When the equation (4.29) is expressed in terms of e-fold N and the conservation equation (4.2) is used to replace

$(x' + \hat{H}x)$, one obtains the interaction term (4.5) as expected. The derivative of the equation (4.29) with respect to cosmic time is carried out and is expressed in terms of e-fold N to yield the following:

$$\begin{aligned}
&\big(1-3\sigma x^2\big)\bigg(\frac{\kappa Q_0'}{3H^2z^2}\bigg) = 2\big(1-3\sigma x^2\big)\bigg(\frac{\kappa Q_0}{3H^2z^2}\bigg)\bigg(\frac{H'}{H}+\frac{z'}{z}\bigg) + \frac{\kappa Q_0}{H^2z^2}\left(\sigma' x^2 + 2\sigma x' x\right)\\
&+\frac{\lambda_C'}{2} + \frac{3}{2}(\lambda_D' - 2\lambda_C')\sigma x^2 + \frac{3}{2}(\lambda_D - 2\lambda_C)\big(\sigma' x^2 + 2\sigma x x'\big) - \sqrt{3}\left(\sigma' - \frac{H'}{H}\sigma\right)\bigg(x' + \frac{H'}{H}x\bigg)\\
&-\sqrt{3}\sigma\bigg(x'' + 2\frac{H'}{H}x' + \frac{H''}{H}x\bigg)\ . \qquad (4.30)
\end{aligned}$$

The conservation equations (4.2) and (4.3) are inserted in to substitute $(x' + \hat{H}x)$ and z'/z respectively. The derivative of Raychaudhuri equation in (4.6) is used to replace H''/H. Some of the terms get simplified with the normalised variables (4.26) and using $\lambda_C' = \lambda_D' = 0$ as per choices in equations (3.24) and (4.7). The normalised derivative $\hat{q}_0$, which is required in the evolution equation (4.28), is hence obtained.

$$\begin{aligned}
\hat{q}_0 \;=\;& -\tilde{Q}_0\left(3+\sqrt{3}\tilde{Q}_0 x\right) + \bigg(3\tilde{Q}_0 + \frac{3}{2}(\lambda_D - 2\lambda_C)\bigg)\bigg(\frac{\sigma' x^2 + 2\sigma x x'}{1-3\sigma x^2}\bigg)\\
&+\frac{\sqrt{3}}{2}\left(\frac{\sigma' - \hat{H}\sigma}{1-3\sigma x^2}\right)\Big(3x - \sqrt{3}\tilde{Q}_0 z^2\Big) - \sqrt{3}\sigma\left[\frac{x'' + 2\hat{H}x' + 6x(x^2+z^2)}{1-3\sigma x^2}\right]\ . \qquad (4.31)
\end{aligned}$$

4.2.3 The normalised derivative of the perturbed interaction

The perturbed interaction term Q_1, which is given by (4.11)-(4.16), is re-expressed in terms of the dynamical variables (3.25) in cosmic time as follows. The derivation is kept general for arbitrary choices of w_c, λ_C and λ_D in the subsection 4.2.3 as well.

$$\kappa Q_1 \;=\; \frac{-3H^2z^2}{(1-3\sigma x^2+3\sigma z^2)}\Big(\mathcal{A}_1\delta_c + \mathcal{A}_2\dot{\Phi} + \mathcal{A}_3\Psi + \mathcal{A}_4\dot{\chi} + \mathcal{A}_5\chi\Big) \qquad (4.32)$$

with

$$\mathcal{A}_1 \;=\; -\frac{\lambda_C}{2} - \frac{\sqrt{3}\sigma}{H}\left(\dot{x} + \frac{\dot{H}}{H}x\right) - \frac{3\sigma x^2}{2}\left(\lambda_D - 2\lambda_C\right)\ , \qquad (4.33)$$

$$\mathcal{A}_2 \;=\; \frac{3\sqrt{3}}{H}(1+w_c)\sigma x\,, \qquad (4.34)$$

$$\mathcal{A}_3 \;=\; 6\sqrt{3}(1+w_c)\sigma x + 3\sigma x^2\left(\lambda_D - 2\lambda_C + 2\frac{\kappa Q_0}{3H^2z^2}\right)\ , \qquad (4.35)$$

$$\mathcal{A}_4 \;=\; -3\frac{\kappa\sigma}{H}(1+w_c) - \sqrt{3}\frac{\kappa\sigma}{H}x\left(\lambda_D - 2\lambda_C + 2\frac{\kappa Q_0}{3H^2z^2}\right)\ , \qquad (4.36)$$

$$\mathcal{A}_5 = \frac{\kappa\Lambda_C}{2} - \frac{\kappa\sigma}{a^2H^2}(1+w_c)\nabla^2 - \frac{\kappa\sigma}{H^2}V_{,\phi\phi} + \lambda_D\frac{\kappa^2\sigma}{H^2}V_{,\phi} - 3\sqrt{3}\kappa\sigma\lambda_D x(1+w_c) \\ -3\kappa\sigma x^2\left(\Lambda_C + \lambda_C^2 + \lambda_C\lambda_D + \frac{\Lambda_D}{2}\right) - \kappa\left[\lambda_C + 3\lambda_D\sigma\left(z^2 - x^2\right)\right]\frac{\kappa Q_0}{3H^2z^2}\ , \quad (4.37)$$

such that the functions $\mathcal{A}_m$ are re-normalised as $\mathcal{A}_m \equiv \mathcal{B}_m/\kappa C$ with $m = 1, \ldots, 5$. The ∇^2 operator appearing in the second term of the coefficient $\mathcal{A}_5$ in (4.37) is acting upon the variable χ in equation (4.32). The relation $\Psi = \Phi$ was applied to equation (4.32) and the EOS was set to $w_c = 0$ since the coupled fluid is DM in this model. Under the approximation of the Newtonian limit, the perturbed interaction term (4.32) then reduces to the following.

$$\kappa Q_1\left(1 - 3\sigma x^2 + 3\sigma z^2\right) \approx -3H^2z^2\left[\mathcal{A}_1\delta_c + \mathcal{A}_5\chi\right] \approx -3H^2z^2\left[\mathcal{A}_1\delta_c - \frac{\kappa\sigma}{H^2}\left(\frac{\nabla^2\chi}{a^2}\right)\right]\ , \quad (4.38)$$

where only the second term of the coefficient $\mathcal{A}_5$ in equation (4.37) survives because it is of same order of $k^2\chi$. After having inserted $a^{-2}\nabla^2\chi \approx -Q_1$, i.e., from the approximation (4.24) of the pertubed Klein Gordon equation, and after having substituted for the normalised variable $\tilde{Q}_1$ (as defined in equation (4.26)), one can simplify to obtain:

$$\tilde{Q}_1 \approx -\frac{\mathcal{A}_1\delta_c}{1 - 3\sigma x^2 + 6\sigma z^2}\ . \quad (4.39)$$

The derivative of perturbed interaction (4.32) with respect to cosmic time is computed:

$$\kappa\dot{Q}_1\left(1 - 3\sigma x^2 + 3\sigma z^2\right) - \kappa Q_1\left(3\dot{\sigma}x^2 + 6\sigma x\dot{x} - 3\dot{\sigma}z^2 - 6\sigma z\dot{z}\right) = -6(H\dot{H}z^2 \\ + H^2z\dot{z})\left[\mathcal{A}_1\delta_c + \mathcal{A}_2\dot{\Phi} + \mathcal{A}_3\Psi + \mathcal{A}_4\dot{\chi} + \mathcal{A}_5\chi\right] - 3H^2z^2\left[\dot{\mathcal{A}}_1\delta_c\mathcal{A}_1\dot{\delta}_c + \dot{\mathcal{A}}_2\dot{\Phi}\right. \\ \left. + \mathcal{A}_2\ddot{\Phi} + \dot{\mathcal{A}}_3\Psi + \mathcal{A}_3\dot{\Psi} + \dot{\mathcal{A}}_4\dot{\chi} + \mathcal{A}_4\ddot{\chi} + \dot{\mathcal{A}}_5\chi + \mathcal{A}_5\dot{\chi}\right]\ . \quad (4.40)$$

Applying the relation $\Psi = \Phi$, the equation (4.40) is reduced under the Newtonian limit.

$$\kappa\dot{Q}_1\left(1 - 3\sigma x^2 + 3\sigma z^2\right) = \kappa Q_1\left(3\dot{\sigma}x^2 + 6\sigma x\dot{x} - 3\dot{\sigma}z^2 - 6\sigma z\dot{z}\right) - 6(H\dot{H}z^2 + H^2z\dot{z})\mathcal{A}_1\delta_c \\ -6(H\dot{H}z^2 + H^2z\dot{z})\mathcal{A}_5\chi - 3H^2z^2\left(\dot{\mathcal{A}}_1\delta_c + \mathcal{A}_1\dot{\delta}_c\right) - 3H^2z^2\dot{\mathcal{A}}_5\chi - 3H^2z^2\mathcal{A}_5\dot{\chi}\ , \quad (4.41)$$

where only the second term of the coefficient $\mathcal{A}_5$ as in equation (4.37) and its derivatives can survive because they are of same order of $k^2\chi$. The following four terms in equation (4.41) are approximated under the Newtonian limit and re-expressed using the relations (4.24) and become as below:

$$
\begin{aligned}
6H\dot{H}z^2\mathcal{A}_5\chi &\approx -6\kappa\sigma z^2\frac{\dot{H}}{H}\left(\frac{\nabla^2\chi}{a^2}\right)\approx +6\frac{\dot{H}}{H}\sigma z^2\kappa Q_1\ , \qquad (4.42)\\
6H^2z\dot{z}\mathcal{A}_5\chi &\approx -6z\dot{z}\kappa\sigma\left(\frac{\nabla^2\chi}{a^2}\right)\approx +6z\dot{z}\sigma\kappa Q_1\ ,\\
3H^2z^2\mathcal{A}_5\dot{\chi} &\approx -3z^2\kappa\sigma\left(\frac{\nabla^2\dot{\chi}}{a^2}\right)\approx +3z^2\sigma\kappa(\dot{Q}_1+2HQ_1)\ ,\\
3H^2z^2\dot{\mathcal{A}}_5\chi &\approx -3z^2\kappa\left[\dot{\sigma}-\left(2H+2\frac{\dot{H}}{H}\right)\sigma\right]\left(\frac{\nabla^2\chi}{a^2}\right)\ ,\approx +3z^2\left[\dot{\sigma}-\left(2H+2\frac{\dot{H}}{H}\right)\sigma\right]\kappa Q_1\ .
\end{aligned}
$$

Those four approximated terms (4.42) are inserted into equation (4.41). By dividing by $3H^2z^2$ and re-arranging the $\dot{Q}_1$ to one side, one can simplify equation (4.41) due to some cancelling terms. The simplified form of equation (4.41) is re-expressed in terms of N.

$$
\begin{aligned}
\frac{\kappa Q_1'}{3H^2z^2}\left(1-3\sigma x^2+6\sigma z^2\right) &= \frac{\kappa Q_1}{3H^2z^2}\left(3\sigma' x^2+6\sigma x x'-6\sigma' z^2-12\sigma z z'\right)\\
&\quad -2\left(\frac{H'}{H}+\frac{z'}{z}\right)\mathcal{A}_1\delta_c-\mathcal{A}_1'\delta_c-\mathcal{A}_1\delta_c'\ . \qquad (4.43)
\end{aligned}
$$

The conservation equation (4.3) is used to substitute z'/z and the normalised variables (4.26) are inserted into equation (4.43). The derivative $\hat{q}_1$, which is required to complete equation (4.28), is thus obtained after some arrangement of equation (4.43).

$$
\hat{q}_1 = \frac{3\tilde{Q}_1\left(\sigma' x^2+2\sigma x x'-2\sigma' z^2-4\sigma z z'\right)+\left[\left(3+\sqrt{3}\tilde{Q}_0 x\right)\delta_c-\delta_c'\right]\mathcal{A}_1-\mathcal{A}_1'\delta_c}{\left(1-3\sigma x^2+6\sigma z^2\right)}\ , \qquad (4.44)
$$

where,

$$
\begin{aligned}
\mathcal{A}_1' &= -\frac{\lambda_C'}{2}-\sqrt{3}\left(\sigma'-\frac{H'}{H}\sigma\right)\left(x'-\frac{H'}{H}x\right)-\sqrt{3}\sigma\left(x''+2\frac{H'}{H}x'+\frac{H''}{H}x\right)\\
&\quad -\frac{3}{2}\left(\sigma' x^2+2\sigma x x'\right)\left(\lambda_D-2\lambda_C\right)-\frac{3\sigma x^2}{2}\left(\lambda_D'-2\lambda_C'\right)\ . \qquad (4.45)
\end{aligned}
$$

4.3 Numerical analysis and observational constraints

The DCQ model, which is described by the system of evolution equations (4.18) and (4.28), is solved numerically in order to obtain the perturbations δ_c and δ_b in terms of cosmological redshift Z. The perturbation equation (4.28) includes the normalised interaction term $\tilde{Q}_0$ in equation (4.5), the derivative $\hat{q}_0$ in equation (4.31), the normalised perturbed interaction term $\tilde{Q}_1$ in equation (4.39), and the derivative $\hat{q}_1$ in equation (4.44). Since the perturbation equations (4.18) and (4.28) also depend on background dynamical

variables x and z, the numerical analysis requires solving the background dynamical system (4.2)-(4.5) first. From the above definition (3.25), one evaluates the initial values of the dynamical variables at redshift Z_i for an early universe according to the relations (3.59). In order to solve the system of evolution equations (4.18) and (4.28) numerically, we specify the initial values of redshift, density perturbations and their derivatives as:

$$Z_i = 10^4, \quad \text{and} \quad \delta_c(Z_i) = \delta_b(Z_i) = 10^{-3}, \quad \text{and} \quad \delta_c' = \delta_b' = 10^{-3}. \tag{4.46}$$

We can now investigate how the density contrasts will eventually grow or decrease for the given set of initial conditions (4.46). The derivation of the equation (4.28) was kept general for arbitrary choices of λ_C and λ_D, and thus the equation (4.28) relies on the constant parameters α and β, as well as the quintessential mass scale $M = D_m^{-1}$ as defined in (3.24). After obtaining the numerical solutions of δ_c and δ_b for a given choice of the parameters, one can plot the numerical $f\sigma_8(Z)$ curve with respect to redshift Z. From equation (1.43), we find that the $f\sigma_8(Z)$ function has dependence on the σ_8^0 parameter. Thus, this DCQ model has four free parameters: $\Theta_\mu = (\ \sigma_8^0,\ \alpha,\ \beta$ and $D_m\ )$.

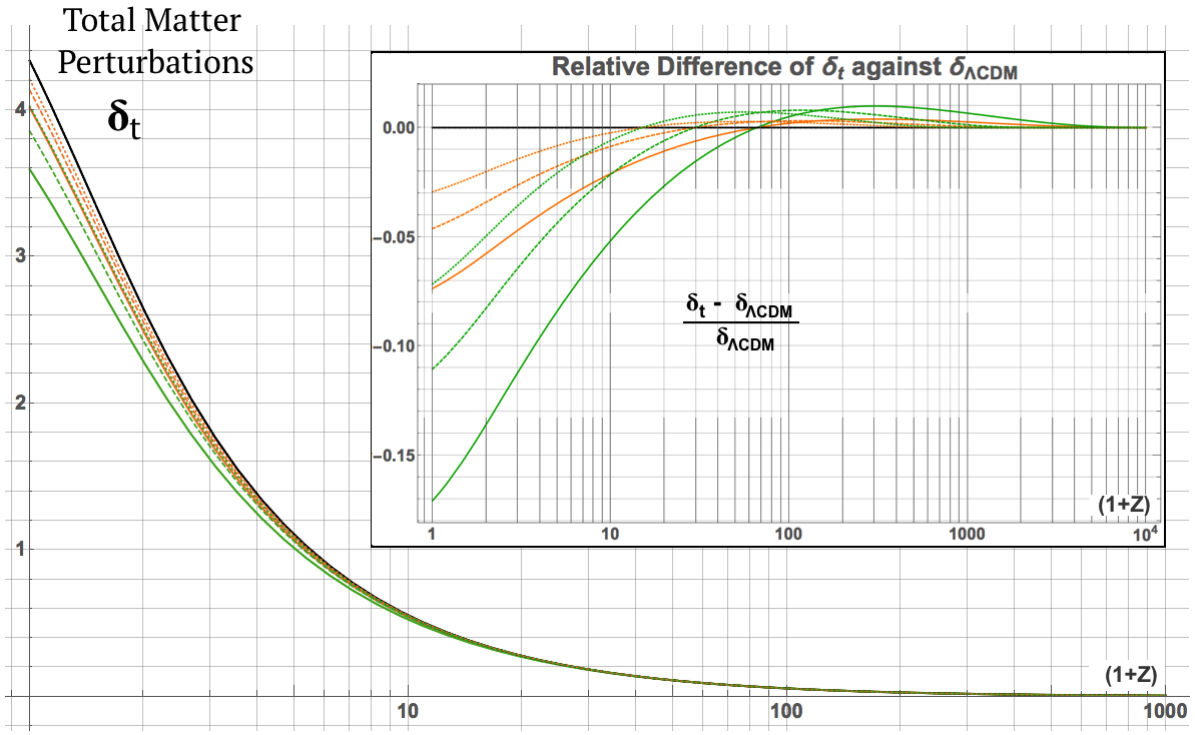

Figure 4.1: The effect of quintessential mass upon evolution of total matter perturbations. The black line represents ΛCDM while the orange lines and green solid lines correspond to $\alpha = 0.05$ and 0.08 respectively. For each color line, the solid, dashed, dotted lines correspond to $D_m = 0.001,\ 0.005,\ 0.01$ meV^{-1} respectively. The parameter β is set as unity.

However, the disformal parameter β was found to have no appreciable effect on the evolution of total matter perturbation δ_t and the amount of galactic clustering $f\sigma_8(Z)$. The relative difference by percentage of δ_t as well as $f\sigma_8(Z)$ against the simplest disformal framework (with $\alpha = 0.08, \beta = 0.0$ and $D_m = 1.0$) is found to be $\leq 0.5\%$ and $\leq 0.35\%$ respectively, for any value of β from a wide range of $0 < \beta < 1000$.

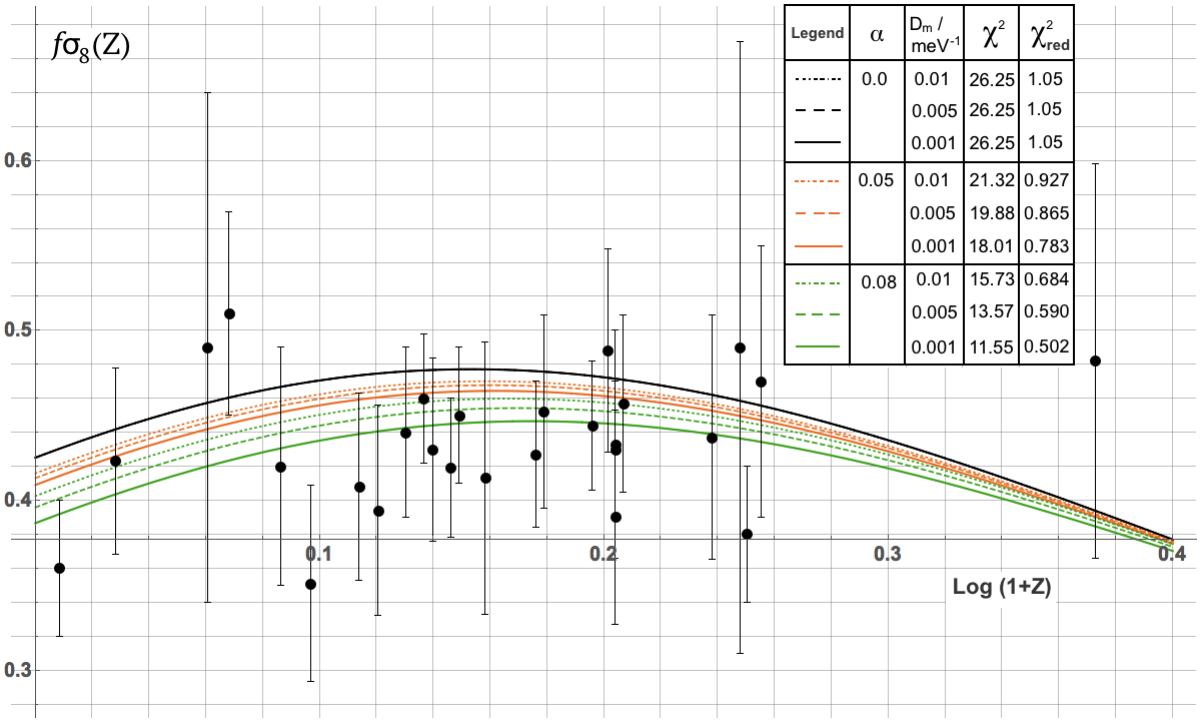

Figure 4.2: The effect of quintessential mass on the numerical $f\sigma_8(Z)$ curve of the disformally coupled quintessence model is shown with respect to redshift Z, together with RSD data (Table A.1). The black line represents ΛCDM while the orange lines and green solid lines correspond to $\alpha = 0.05$ and 0.08 respectively. For each color line, the solid, dashed, dotted lines correspond to $D_m = 0.001,\ 0.005,\ 0.01$ meV^{-1} respectively. Other parameters was set as $\sigma_8^0 = 0.818$ from Ref. [24] as per equation (1.44) and β as unity.

Figures 4.1 and 4.2 show the effect of the quintessential mass on the evolution of the total matter perturbations δ_t, and the numerical $f\sigma_8(Z)$ curve respectively, whereby the parameters σ_8^0 and β values are set as $\sigma_8^0 = 0.818$ from [24] and $\beta = 1.0$. Those following remarks are made for both Figures 4.1 and 4.2:

1. When the conformal parameter α is set to zero, the DCQ model approaches towards ΛCDM model in the limit $D_m \to 0$ (i.e., $M \to \infty$).

2. For non-zero values of α and β, the conformal nature of the model dominate at lower values of D_m (i.e., higher mass M) and disformal framework becomes more significant at higher values of D_m (i.e., lower mass M) as shown in section 3.9.

3. Hence with β set to unity and small D_m, the model behaves conformally such that the conformal results as in Ref. [24] are recovered for $\alpha = 0.05$ and 0.08 (Compare the Chi-square estimation with Figure 2.3).

4. For a fixed choice of α, the parameter D_m induces a gradual disformal effect. When D_m is very small (i.e., higher mass M), $f\sigma_8(Z)$ curve coincides with the purely conformal case, because the disformal coefficient $D(\phi)$ becomes zero, even if β is non-zero. As D_m is increased (i.e., decreasing mass M), a disformal effect is induced such that the rate of evolution of δ_t then increases leading to higher $f\sigma_8(0)$ value. The structures cluster faster when compared to the respective conformal case.

Parametrized Post-Newtonian analysis and the solar system tests produce stringent constraints on various conformal or disformal quintessence models, as these deal with couplings between a scalar field and baryons. To avoid these constraints, screening mechanisms such as the chameleon are invoked. In our study, however, the couplings arise between a scalar field and dark matter, for which the bounds come from cosmological effects only. Instead, a Bayesian analysis (see Appendix A.3) of this DCQ model was carried out to the find the set of the parameters, which will fit the RSD data (Table A.1), in a similar manner that was done in Figure 2.4. In our analysis, the likelihood $L(\beta)$ is found to be equally probable for all values β and this re-confirms that the parameter β does not affect the evolution of the total matter perturbation. For this reason, the disformal parameter β is fixed to unity, as an arbitrary choice. The set of parameters Θ_μ is then reduced to $\Theta_\mu \in \{\sigma_0,\ \alpha,\ D_m\}$ only. A three-dimensional grid of $75,000$ points was tabulated for the parameter space, and at each point (corresponding to a particular set of parameter), the Chi-square value was estimated. The bounds of the 3D parameters space are set as (i) $0 \leq \alpha \leq 0.5$ (ii) $0.65 \leq \sigma_8^0 \leq 1.2$, and (iii) $0.00001 \leq D_m \leq 1.0$. The best fit set of parameters is found to be (within 68% Confidence Level) :

$$\begin{aligned} \alpha_{\rm BF} &= 0.08 \pm 0.15, \\ \sigma_8^0|_{\rm BF} &= 0.80 \pm 0.17, \\ D_{m|\rm BF} &= 0.001^{+0.199}_{-0.001}\,. \end{aligned} \tag{4.47}$$

The Bayesian analysis is implying that the observed RSD data (Table A.1) favours a quite low numerical value of $D_{m|\rm BF}$ as best fit. As $D_m \to 0$, the quintessential mass $M \to \infty$, this implies that the disformal coefficient $D(\phi) \to 0$ as per equation (3.24) and from Figure 3.9, one finds that couplings are already conformal in those limits. Therefore, the observed RSD data (Table A.1) prefers the model when it behaves conformally.

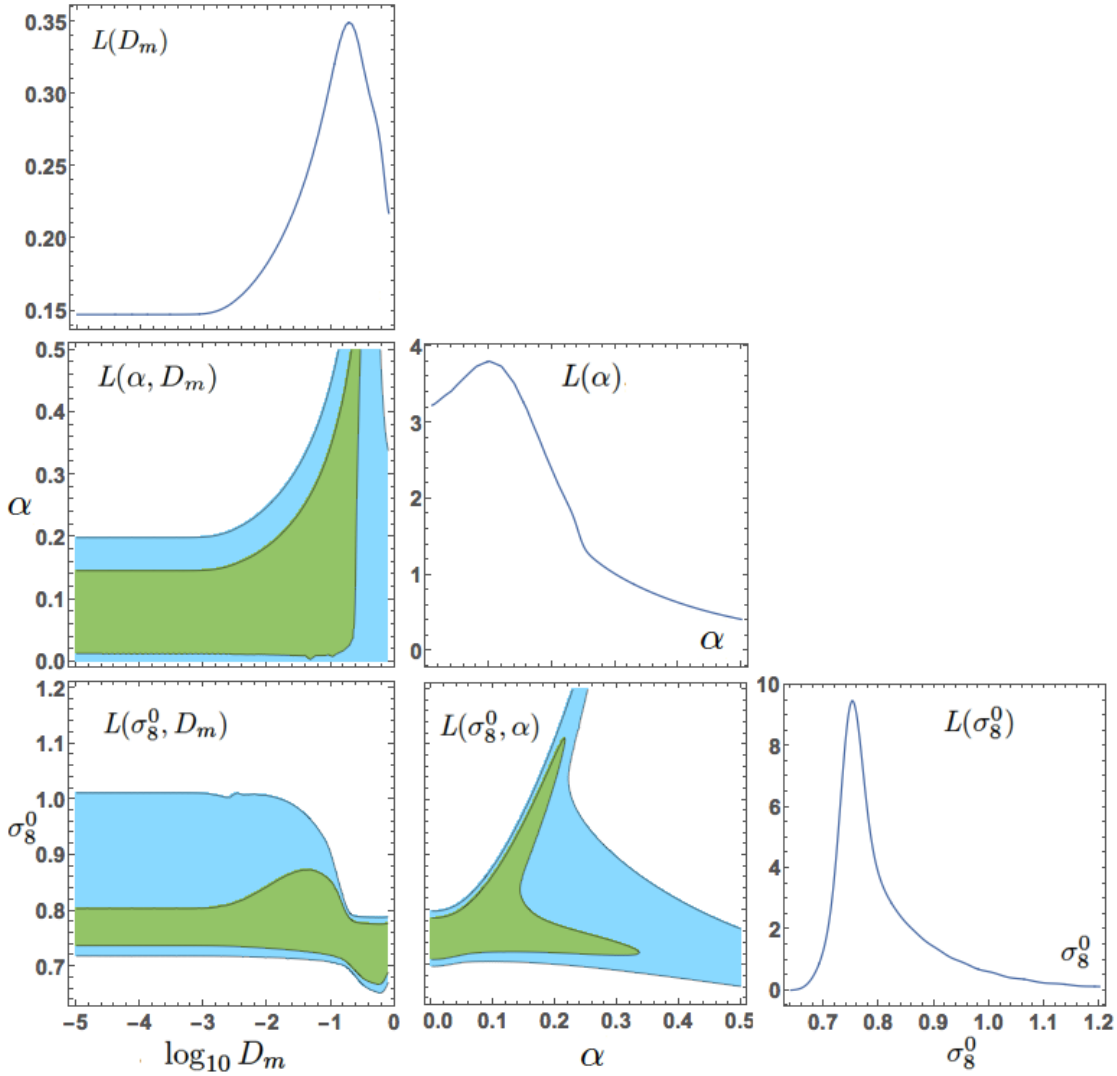

Figure 4.3: The marginalised surface Likelihoods $L(\alpha, D_m)$, $L(\sigma_8^0, D_m)$ and $L(\sigma_8^0, \alpha)$ are shown in topview, such that the green and the light blue regions indicate with 68% and 95% confidence as to where the correct set of parameters Θ_μ exists within each respective 2D parameters space. The $L(D_m)$, $L(\alpha)$, and $L(\sigma_8^0)$ are the marginalised likelihood curves.

Figure 4.3 shows the marginalisation of the main Likelihood $L(\Theta_\mu)$ over one parameter to yield the surface likelihoods $L(\alpha, D_m)$, $L(\sigma_8^0, D_m)$ and $L(\sigma_8^0, \alpha)$. These surface likelihoods are shown in topview, such that the green and the light blue regions indicate 68% and 95% confidence. Figure 4.3 also shows the marginalisation of the main Likelihood $L(\Theta_\mu)$ over two parameters to yield the 1D likelihood curves denoted by $L(D_m)$, $L(\alpha)$, and $L(\sigma_8^0)$. For range $0 < \alpha < 0.25$, the surface likelihood $L(\sigma_8^0, \alpha)$ maintains the characteristics of the conformal constraints with RSD data (Table A.1), as shown in Figure 2.4. The 1D Likelihood curves $L(\alpha)$ and $L(\sigma_8^0)$ also manifest this reasoning. Any deviation from Figure 2.4 is attributed to the disformal dependence of this DCQ model. In the limit

$D_m \to 0$, i.e., when the model starts to behave conformally, we find that there can be various values of D_m for a given value of σ_8^0 in the plot of the surface Likehood $L(\sigma_8^0, D_m)$ (See bottom left panel of Figure 4.3). This appears similarly in the plot of the surface Likehood $L(\alpha, D_m)$ for a given value of α (see left middle panel of Figure 4.3). This could suggest the parameter D_m is actually degenerate in that limit.

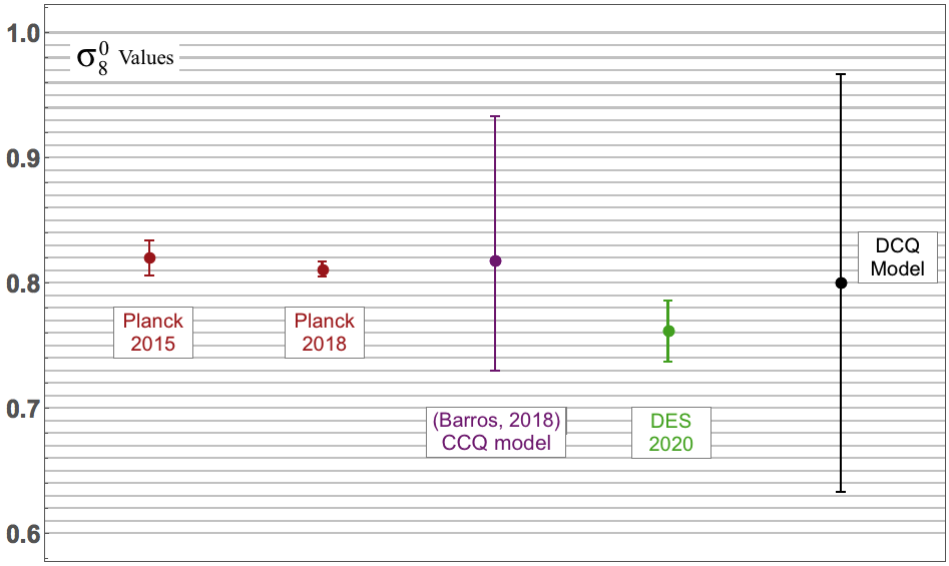

Figure 4.4: The predicted $\sigma_8^0|_{\rm BF}$ value of the DCQ model (Black) is visually compared against the predicted $\sigma_8^0|_{\rm BF}$ value of the CCQ model (purple) in Ref. [24] and against the observational constraints from Planck data (Red)[13, 49] and from the combination of the DES and KiDS+VIKING-450 (Green)[30]. The σ_8 tension, which is clearly shown between constraints of Plank and DES, seems to be loosened by the predicted $\sigma_8^0|_{\rm BF}$ value from the CCQ and DCQ models.

The Figure 4.4 shows a visual comparison of the predicted $\sigma_8^0|_{\rm BF}$ value by the DCQ model against the predicted σ_8^0 value by the CCQ model in Ref. [24], and against the observational constraints from Planck data [13, 49] as well as from the combination of the DES and KiDS+VIKING-450 [30]. We find that our obtained $\sigma_8^0|_{\rm BF}$ value (within 68% Confidence Level) seems to be consistent with the Planck (2018) value of $\sigma_8^0 = 0.811 \pm 0.006$ [13], although our $\sigma_8^0|_{\rm BF}$ value lies outside the 1σ error margin of Planck (2018)'s constraint and its error bars are quite large in the studied range of σ_8^0 values for σ_8 tension. While the best fit $\sigma_8^0|_{\rm BF}$ corresponds to when the DCQ model behaves conformally, we only obtain a $\sigma_8^0|_{\rm BF}$ value which is close to the conformal constraints from Ref. [24]. The Figure 4.4 clearly shows the σ_8 tension, in the sense that, the error margin of the DES's constraints do not overlap the error margin of the Plank (2018)'s constraints. However, the σ_8 tension seems to be relaxed by the predicted σ_8^0 values from CCQ and DCQ model, because their error margin are wide enough to overlap both constraint values by Planck and DES data.

The reduced Chi-square estimations of the best-fit parameters $\chi^2_{\rm red}$ as well as the number of fitted parameter $\rm N_f$ for the ΛCDM model, the CCQ model of section 2.5 and our studied DCQ model in ΛCDM background are summarised in Table 4.1. Compared to ΛCDM and the CCQ models, the minimum Chi-square $\chi^2_{\rm min}$ of the DCQ model is found to be lower but its reduced Chi-square $\chi^2_{\rm red}$ is in fact larger. This is counter-intuitive but could be accounted to the degeneracies of the parameters of the DCQ model, which are seen in the following: (i) the negligible relative difference of $f\sigma_8(Z)$ curve due to the effect of β, (ii) equi-probability of $L(\beta)$ for large range of β, (iii) the marginalised surface likelihoods appears as bands instead of Gaussian ellipses because within certain region of the parameter spaces, the surface likelihoods are actually equi-probable. The relatively higher value of reduced Chi-square for the DCQ model could also be due to large uncertainties associated with the values of the best fit parameters.

Model	$\sigma_8^0\vert_{\rm BF}$	$\alpha_{\rm BF}$	$D_{m\vert\rm BF}$	β	$\rm N_f$	$\chi^2_{\rm min}$	$\chi^2_{\rm red}$
ΛCDM [24]	0.750 ± 0.024	0	0	0	1	11.4413	0.4400
CCQ [24]	$0.818^{+0.115}_{-0.088}$	$0.079^{+0.059}_{-0.067}$	0	0	2	11.0946	0.4438
DCQ	0.80 ± 0.17	0.08 ± 0.15	$0.001^{+0.199}_{-0.001}$	1.0	4	10.6931	0.4649

Table 4.1: The Bayesian analyses provided the reduced Chi-square estimations $\chi^2_{\rm red}$ for the best-fit parameters for the ΛCDM model, the CCQ model of section 2.5 and our studied DCQ model in ΛCDM background. $\rm N_f$ is number of fitted parameters.

In conclusion from these facts, one cannot really state whether the DCQ model is better than ΛCDM or the CCQ model, until these degeneracies are clarified. The degeneracies may not necessarily imply that the studied disformal formalism is an incorrect model. In our RSD data (see Table A.1), we deal only with $f\sigma_8$ values and redshift Z. However, the Ref. [70] mentions that the combination of separate data of growth f and matter fluctuation amplitude σ_8^0 is capable of actually breaking degeneracies, which the quantity $f\sigma_8$ would not be able to do intuitively. As future work, we intend to elucidate the degeneracies of the DCQ model using the combination of $(f + \sigma_8^0)$ data, with the same methodology used in Ref. [70]. Moreover, it is also possible that the use of the late-time RSD data is indicating only one aspect of the big picture in understanding the σ_8 tension. Another way to further investigate and to reduce the degenerate variables is

for us to consider constraining the studied DCQ model with CMB data or BAO data or Supernovae surveys.

Moreover, the observational measurement of the $f\sigma_8$ value, inherently assumes that the power spectrum (defined as equation (1.44) in section 1.5) is from a GR framework and is well constrained with CMB experiments [13] at early redshifts (within the matter-dominated epoch). Thus, although the effect of the parameters α and D_m is seen as a relative difference of the total matter perturbation δ_t with respect to $\delta_{\Lambda\text{CDM}}$ throughout the cosmological timeline (see Figure 4.1), a correction of our $f\sigma_8$ function seems to be required to make sure that GR conditions are satisfied at early redshifts. As another prospective work, we will adopt the same approach as in Ref. [71, 72] to redress this issue in our $f\sigma_8$ function. Alternatively, the parameters of the DCQ model could also be re-normalised to recover GR conditions (as in equation (4.2) from Ref. [73]), such that $\alpha \to 0$, $\beta \to 0$ and $D_m \to 0$ in the limit $Z \to 10^3$ or higher within the matter-dominated epoch. In the next Chapter 5, we shall summarise all our results to conclude the thesis.

Chapter 5

Conclusion

This thesis attempts to address two main issues of the currently accepted ΛCDM cosmological model, described in section 1.6. These two main issues are the unknown nature of cosmological constant and the σ_8 tension. To address the latter issue in the literature, a scalar field (namely the quintessence ϕ) is often used to replace the cosmological constant. This thesis also uses the quintessence with the assumption that it is coupled with other cosmological fluids. In GR, one geometry is adequate to describe how a scalar field will propagate. The Scalar-Tensor theories, which are the modifications of GR, introduce the concept that the gravitational geometry is different but related to the physical geometry in which scalar field propagates. This relation between the two geometries is known as the conformal transformation (2.2). However in this thesis, the second assumption is the use of disformal transformation (3.1), which is an extension of conformal transformation. In Chapter 2, a review of the CCQ model is provided as the foundations for disformal formalism, which is then presented in Chapter 3. The literature review in Chapter 2 includes the construct of the conformal formalism, the background and perturbations of the CCQ model, the dynamical system analysis for three CCQ models and the case study of a CCQ model which is mimicking ΛCDM. The research question in this thesis is whether a disformally coupled quintessence model, which is mimicking ΛCDM, can attempt to resolve those two aforementioned issues since it has additional degrees of freedom compared to ΛCDM.

In Chapter 3, we investigate the cosmological dynamics of DCQ model (where the quintessence ϕ interacts with a generic fluid ρ_c), which is mimicking the cosmological constant Λ and an uncoupled fluid ρ_u. This brings the convenience of not having to specify the scalar field potential. The novelty in this body of work in Chapter 3 is that it extends the coupled quintessence model in ΛCDM background to, (i) include a disformal coupling,

and (ii) include these conformal and disformal couplings in a dynamical system analysis for the first time in the literature. The choice for EOS parameters in the Jordan frame for the coupled fluid and uncoupled fluid, i.e., $\tilde{w}$ and $\tilde{w}_u$ respectively give rise to different scenarios. There are three studied scenarios, which are Scenario I ($\tilde{w} = 0$ and $\tilde{w}_u = 0$), Scenario II ($\tilde{w} = 1/3$ and $\tilde{w}_u = 0$), and Scenario III ($\tilde{w} = 1/3$ and $\tilde{w}_u = 1/3$). The differential equations (3.28)-(3.32) which govern the behaviour for the dynamical system bring novel phenomenology in each scenario regarding the fixed points and trajectories. Section 3.6 entails the analysis of the conformal couplings in the three studied scenarios, which includes the conformal equations, i.e., (3.37)-(3.42), the nature of the fixed points, and 2D phase portraits in Figure 3.1. Sections 3.7 and 3.8 entail the analysis of the disformal couplings in the three studied scenarios, which includes the disformal equations, i.e., (3.43)-(3.54), the additional disformal fixed points (see Appendix A.5), the topological features and the investigation of the trajectories on a 3D phase portrait (See Figures 3.2-3.6). In all scenarios, we commonly find the invariant sub-manifold xz plane, the attractor A_0, $S_\pm$, and the equilibrium line $L_{\rm E}$, i.e., $(x = 0, z = 0, \forall\, \sigma)$, as well as the shaded region in which (3.36) is not satisfied. A more realistic numerical analysis of the DCQ model is then carried out, where the quintessence is disformally coupled with dark matter (i.e., Scenario I and described by (3.43)-(3.46)) throughout the cosmological evolution from the early times to present. The features of ΛCDM, such as the radiation-matter transition and the DM-DE transition, are reproduced as expected. Figure 3.8 shows the effect of different mass scales on the evolution of the quintessential energy density ρ_ϕ and its density parameter Ω_ϕ. This effect can be quantified by the effective conformal coupling (see Figures 3.9 and 3.10). Therefore, the energy density of the quintessence is effectively mimicking a cosmological constant, when low mass scale is utilised.

In Chapter 4, we revisit the perturbation theory for a DCQ model, whose background mimics the ΛCDM. The derivation of the perturbation equations for the disformally coupled dark matter i.e., equation (4.28), is reviewed in section 4.2.1. The equation (4.28) also reduces to the perturbation equations (2.37) in the conformal framework [24]. The DCQ model is analysed numerically by solving the system of evolution equations (4.18) and (4.28) to obtain δ_c and δ_b in terms of the cosmological redshift Z. Using the definition (1.43), we plot the numerical $f\sigma_8(Z)$ curve for several sets of parameters. The effect of the quintessential mass is seen in the evolution of total matter perturbation (See Figure 4.1) and the numerical $f\sigma_8(Z)$ curve (See Figure 4.2). For a given choice of α, when a decreasing quintessential mass is used for the model, a disformal effect seems to be induced. This disformal effect leads to a faster rate of evolution for total matter density

contrast and a higher $f\sigma_8(0)$ value, which imply that the large-scale structures cluster faster compared to the its respective conformal case. The free parameters of the DCQ model (i.e., $\sigma_8^0,\ \alpha,\ \beta,\ D_m$) are investigated with Bayesian statistics using the RSD data (Table A.1). The likelihood $L(\beta)$ is found to be constant for all values of β and confirms that β does not affect the evolution of the total matter perturbation. Figure 4.3 shows the marginalised surface likelihoods $L(\alpha, D_m)$, $L(\sigma_8^0, D_m)$ and $L(\sigma_8^0, \alpha)$ in topview, where the green and light blue indicate the 68% and 95% confidence regions. The best fit set of parameters is found to be $\sigma_8^0|_{\rm BF} = 0.80 \pm 0.17$, $\alpha_{\rm BF} = 0.08 \pm 0.15$ and $D_{m|\rm BF} = 0.001^{+0.199}_{-0.001}$ within 68% confidence level, at the minimum chi-square value $\chi_{\rm min} = 10.6931$. The best fit is close to the conformal results of the Ref. [24] and is consistent with latest Planck (2018) value of $\sigma_8^0 = 0.811 \pm 0.006$ [13]. The best fit set of parameters indicates that the RSD data (Table A.1) prefers the model to behave conformally.

In conclusion, we have explored the possibility of the disformally coupled quintessence, as a replacement for the cosmological constant, while it mimics the ΛCDM background. On one hand, the quintessence with low mass scale, could drive the dynamical system (3.43)-(3.46) towards a cosmological acceleration since the dynamical system eventually tends towards the attractor A_0 as seen in Figure 3.2. The energy density of the low-mass quintessence is effectively tracing a cosmological constant as shown in the expansion history (See Figure 3.8). Thus, this studied model might be able to bring few insights on the nature of the cosmological constant. On the other hand, despite that the low-mass quintessence induces the disformal effects of increasing the growth rate compared to its conformal case, the late-time RSD data (Table A.1) disfavours those disformal effects when the minimum chi-square is evaluated as a measure of fit. Moreover, the Figure 4.4 shows how the existent σ_8 tension seems to be relaxed by the predicted $\sigma_8^0|_{\rm BF}$ value from the studied DCQ model. Compared to ΛCDM and the CCQ models, the minimum Chi-square $\chi^2_{\rm min}$ of the DCQ model is found to be lower but its reduced Chi-square $\chi^2_{\rm red}$ is in fact larger (see Table 4.1). This is counter-intuitive but might be explained by the degeneracies of the parameters of the DCQ model. From these facts, one cannot really state whether the DCQ model is better than ΛCDM or the CCQ model, until these degeneracies are clarified. As future work, we shall clarify the degenerate variables of the DCQ model using the combination of $(f + \sigma_8^0)$ data (with same statistical techniques from Ref. [70]). As future endeavours, it would also be worthwhile to constrain this studied DCQ model with Planck CMB data and to investigate the disformal effects on the early universe. Another prospective work involves the correction of our $f\sigma_8$ function, similar to Ref. [71, 72], to recover GR conditions at early redshifts within matter-dominated era.

Appendix A

Useful cosmological quantities

A.1 Background tensor components

In this appendix, the computations of all tensor components (i.e., $\Gamma^{\alpha}_{\mu\nu}$, $R_{\mu\nu}$, G^{μ}_{ν} and T^{μ}_{ν}) are carried out in terms of conformal time $\tau = t/a$. For ΛCDM model, We still consider the FLRW metric (1.24), whose line element can be re-expressed as below [11]:

$$ds^2 = g_{\mu\nu}dx^{\mu}dx^{\nu} = a^2(\tau)\left[-d\tau^2 + \gamma_{ij}dx^i dx^j\right] \tag{A.1}$$

where $a(\tau)$ is the scale factor. There are only 10 background metric components because of its symmetric properties i.e. $g_{\mu\nu} = g_{\nu\mu}$. The components of the FLRW metric and its inverse metric are given by [11]:

$$\begin{aligned} &\text{Metric:} && \bar{g}_{00} = -a^2 && \bar{g}_{0i} = 0 && \bar{g}_{ij} = a^2\gamma_{ij} \\ &\text{Inverse Metric:} && \bar{g}^{00} = -a^{-2} && \bar{g}^{0i} = 0 && \bar{g}^{ij} = a^{-2}\gamma^{ij} \end{aligned} \tag{A.2}$$

The affine connection can be computed using Equation (1.4) and the background components are given below [11]:

$$\bar{\Gamma}^0_{00} = \mathcal{H} \quad \bar{\Gamma}^i_{00} = 0 \quad \bar{\Gamma}^0_{i0} = \bar{\Gamma}^0_{0i} = 0 \quad \bar{\Gamma}^0_{ij} = \mathcal{H}\delta_{ij} \quad \bar{\Gamma}^i_{0j} = \mathcal{H}\delta^i_j \quad \bar{\Gamma}^i_{jk} = \gamma^i_{jk} \tag{A.3}$$

Where $\mathcal{H} = \mathcal{H}(\tau)$ is the Hubble parameter in conformal timeand γ^i_{jk} denote the affine connection evaluated using the spatial metric. The Ricci Tensor $R_{\mu\nu} = R^{\alpha}{}_{\mu\alpha\nu}$ can be calculated using these affine connection as in Equation (1.5) from a Riemann Tensor, whose first and third components have been contracted.

Those background Ricci components are [11]:

$$\bar{R}_{00} = -3\frac{d\mathcal{H}}{d\tau} \qquad \bar{R}_{ij} = \left(\frac{d\mathcal{H}}{d\tau} + 2\mathcal{H}^2 + 2\mathcal{K}\right)\delta_{ij} \qquad \bar{R}_{0j} = 0 \tag{A.4}$$

The Ricci scalar can be deduced by $R = g^{\mu\nu}R_{\mu\nu} = 6a^{-2}\left(\frac{d\mathcal{H}}{d\tau} + \mathcal{H}^2 + \mathcal{K}\right)$. One can also raise the index of the Ricci Tensor $R_{\mu\nu}$ using the metric to obtain Ricci Tensor R^{μ}_{ν}. Thus, the background Einstein Tensor G^{μ}_{ν} are obtained as [11]:

$$a^2\bar{G}^0_0 = -3(\mathcal{H}^2 + \mathcal{K}) \qquad a^2\bar{G}^i_j = -\left(2\frac{d\mathcal{H}}{d\tau} + \mathcal{H}^2 + \mathcal{K}\right)\delta^i_j \qquad a^2\bar{G}^0_i = 0 \tag{A.5}$$

The ΛCDM model assumes the cosmological contents as perfect fluids, such that their energy-momentum tensor $T_{\mu\nu}$ was previously defined by Equation (1.11) Hence the heat flux q^{μ} and anisotropic stress $\pi_{\mu\nu}$ vanish. In order to evaluate the non-vanishing components of the Einstein Field equations (1.2), one compute $T^{\mu}_{\nu} = g^{\mu\eta}T_{\eta\nu}$[11]:

$$\bar{T}^0_0 = -\bar{\rho} \qquad \bar{T}^0_i = 0 \qquad \bar{T}^i_j = P\delta^i_j \tag{A.6}$$

For the coupled quintessence models, the energy-momentum tensor for the quintessence, $T^{\mu(\phi)}_{\nu} = g^{\eta\nu}T^{(\phi)}_{\eta\nu}$, are computed in conformal time using equation (2.6) [11]:

$$a^2\bar{T}^{0\,(\phi)}_0 = -\frac{1}{2}\left(\frac{d\phi}{d\tau}\right)^2 - a^2V\ , \quad a^2\bar{T}^{0\,(\phi)}_i = 0\ , \quad a^2\bar{T}^{i\,(\phi)}_j = \left[\frac{1}{2}\left(\frac{d\phi}{d\tau}\right)^2 - a^2V\right]\delta^i_j\ , \tag{A.7}$$

The energy density ρ_{ϕ} and pressure P_{ϕ} can be expressed in conformal time, whenever the quintessence is interpreted as a cosmological fluid via the equation (1.11) [11]:

$$\rho_{\phi} = \frac{1}{2a^2}\left(\frac{d\phi}{d\tau}\right)^2 + V\ , \qquad \text{and} \qquad P_{\phi} = \frac{1}{2a^2}\left(\frac{d\phi}{d\tau}\right)^2 - V\ , \tag{A.8}$$

A.2 Scalar Perturbations of tensor components

We assume the FLRW metric to be perturbed as per equation (1.35), which can be re-expressed in conformal time as:

$$ds^2 = a^2(\tau)\left[-(1+2\Phi)d\tau^2 + (1-2\Psi)\gamma_{ij}dx^i dx^j\ \right] \tag{A.9}$$

The components of the metric and inverse metric as well as the affine connection in this perturbed space-time are computed below. It is also useful to evaluate $\Gamma^k_{kk} = -\nabla_k\Psi$ and

$\Gamma^k_{wk} = -3\nabla_w\Psi$. The perturbed Ricci Tensor $R_{\mu\nu} = R^{\alpha}{}_{\mu\alpha\nu}$ is calculated using the affine connection using Equation (1.5).

$$\begin{array}{rccccc} \text{Metric [11]:} & g_{00} = -(1+2\Phi)a^2 & & g_{0i} = 0 & & g_{ij} = +(1-2\Psi)a^2\gamma_{ij} \\ \text{Inverse Metric:} & g^{00} = -(1+2\Phi)^{-1}a^{-2} & & g^{0i} = 0 & & g^{ij} = +(1-2\Psi)^{-1}a^{-2}\gamma^{ij} \end{array} \quad \text{(A.10)}$$

Affine connection [11]:

$$\begin{aligned} \Gamma^0_{00} = \mathcal{H} + \left(\frac{d\Phi}{d\tau}\right) \qquad \Gamma^0_{ij} &= \left[\mathcal{H} - \left(\frac{d\Psi}{d\tau}\right) - 2\mathcal{H}(\Psi+\Phi)\right]\delta_{ij} \\ \Gamma^i_{00} = \nabla^i\Phi \qquad \Gamma^i_{0j} &= \left[\mathcal{H} - \left(\frac{d\Psi}{d\tau}\right)\right]\delta^i_j \\ \Gamma^0_{i0} = \Gamma^0_{0i} = \nabla_i\Phi \qquad \Gamma^i_{jk} &= \delta_{jk}\nabla^i\Psi - \delta^i_k\nabla_j\Psi - \delta^i_j\nabla_k\Psi \end{aligned} \quad \text{(A.11)}$$

Ricci Tensor Components [11]:

$$\begin{aligned} R_{00} &= -3\left(\frac{d\mathcal{H}}{d\tau}\right) + 3\left(\frac{d^2\Psi}{d\tau^2}\right) + 3\mathcal{H}\left(\frac{d\Phi}{d\tau} + \frac{d\Psi}{d\tau}\right) + \nabla^2\Phi \\ R_{ij} &= \left[\left(\frac{d\mathcal{H}}{d\tau} + 2\mathcal{H}^2\right) - \left(\frac{d^2\Psi}{d\tau^2}\right) - 2\left(\Psi+\Phi\right)\left(\frac{d\mathcal{H}}{d\tau} + 2\mathcal{H}^2\right)\right. \\ &\quad \left. - \mathcal{H}\left(\frac{d\Phi}{d\tau} + 5\frac{d\Psi}{d\tau}\right) + \nabla^2\Psi\right]\delta_{ij} + \nabla_i\nabla_j(\Psi-\Phi) \\ R_{0j} &= 2\nabla_i\left(\frac{d\Phi}{d\tau} + \mathcal{H}\Phi\right) \end{aligned} \quad \text{(A.12)}$$

The Ricci scalar in the pertubed space-time can be deduced by $R = g^{\mu\nu}R_{\mu\nu}$ is given [11]:

$$\begin{aligned} a^2R &= 6\left(\frac{d\mathcal{H}}{d\tau} + \mathcal{H}^2\right) - 12\left(\frac{d\mathcal{H}}{d\tau} + \mathcal{H}^2\right)\Phi - 6\mathcal{H}\left(3\frac{d\Psi}{d\tau} + \frac{d\Phi}{d\tau}\right) - 6\frac{d^2\Psi}{d\tau^2} \\ &\quad -2\nabla^2(\Phi - 2\Psi) \end{aligned} \quad \text{(A.13)}$$

The Ricci Tensor R^μ_ν can be obtained by raising the index of $R_{\mu\nu}$, which are provided by Equation (1.43). The perturbed Einstein Tensor G^μ_ν are computed [11]:

$$\begin{aligned} a^2G^0_0 &= -3\mathcal{H}^2 + 6\mathcal{H}^2\Phi + 6\mathcal{H}\frac{d\Psi}{d\tau} - 2\nabla^2\Psi \\ a^2G^i_j &= -\left(2\frac{d\mathcal{H}}{d\tau} + \mathcal{H}^2\right)\delta^i_j + \left[2\left(2\frac{d\mathcal{H}}{d\tau} + \mathcal{H}^2\right)\Phi + 2\mathcal{H}\left(\frac{d\Phi}{d\tau} + 2\frac{d\Psi}{d\tau}\right) + 2\frac{d^2\Psi}{d\tau^2}\right. \\ &\quad \left. -\nabla^2(\Psi-\Phi)\right]\delta^i_j + \nabla^i\nabla_j(\Psi-\Phi) \\ a^2G^0_i &= -2\nabla_i\left(\frac{d\Psi}{d\tau} + \mathcal{H}\Phi\right) \end{aligned} \quad \text{(A.14)}$$

The perturbed energy-momentum tensor $T^{\mu}_{\nu} = g^{\mu\eta}T_{\eta\nu}$ is evaluated using (1.11)[11, 25]:

$$\begin{aligned} T^0_0 &= -\bar{\rho}_n - \delta\rho_n \,, \\ T^0_i &= +\bar{\rho}(1+w_n)(\tilde{\nabla}_i \mathbf{v}_n + V_i) = -T^i_0 \,, \\ T^i_j &= \left(\bar{P}_n + \delta P_n\right)\delta^i_j + \bar{P}_n \pi^i_j \,, \end{aligned} \tag{A.15}$$

where the velocity of the cosmological fluid is perturbed as $u^{\mu} = \bar{u}^{\mu} + \delta u^{\mu}$. In perturbed space-time, the temporal and spatial components of this velocity are $u^0 = a^{-1}(1-\Phi)$ and $u^i = a^{-1}v^i$ respectively [11], whereby v^i can be decomposed further into two vector degrees of freedom $v^i = \tilde{\nabla}^i \mathbf{v} + V^i$, with $\mathbf{v}$ as a scalar and V^i is divengenceless. For the coupled quintessence models, the energy-momentum tensor of quintessence in perturbed space-time is computed [11]:

$$\begin{aligned} a^2 T^{0\,(\phi)}_0 &= -\left[\frac{1}{2}\left(\frac{d\phi}{d\tau}\right)^2 + a^2 V\right] - \left(\frac{d\phi}{d\tau}\right)\left(\frac{d\chi}{d\tau}\right) + \Phi\left(\frac{d\phi}{d\tau}\right)^2 - a^2 V_{,\phi}\chi \,, \\ a^2 T^{0\,(\phi)}_i &= -\left(\frac{d\phi}{d\tau}\right)\nabla_i\chi = -a^2 T^i_0 \,, \\ a^2 T^{i\,(\phi)}_j &= +\left[\frac{1}{2}\left(\frac{d\phi}{d\tau}\right)^2 - a^2 V\right]\delta^i_j + \left[\left(\frac{d\phi}{d\tau}\right)\left(\frac{d\chi}{d\tau}\right) - \Phi\left(\frac{d\phi}{d\tau}\right)^2 - a^2 V_{,\phi}\chi\right]\delta^i_j \end{aligned} \tag{A.16}$$

A.3 A Bayesian analysis of the $f\sigma_8$ function

In cosmology, a well-known approach to compare the goodness of fitting for any curve with observational data is the Bayesian analysis. The probability of this data to have occurred given the numerical function $f\sigma_8(X_\nu, \Theta_\mu)$, with specific set of free parameters Θ_μ of the model, is referred the Likelihood of the parameters given the data [75]:

$$L(\Theta_\mu) \propto \prod_{\nu=1}^{\eta}\left\{\mathrm{Exp}\left[-\frac{\chi^2}{2}\right]\right\} \,, \quad \text{such that} \quad \chi^2(\Theta_\mu) = \sum_{\nu=1}^{\eta}\left(\frac{Y_\nu - f\sigma_8(X_\nu,\Theta_\mu)}{\epsilon_\nu}\right)^2 \tag{A.17}$$

where χ^2 is the Chi-square estimation, assuming the least-square method. The data points are expressed here as a vector $(X_\nu,\ Y_\nu \pm \epsilon_\nu)$, such that the index $\nu = 1, 2, 3 \ldots \eta$ with η as the total number of data points. The Y_ν corresponds the measured value of $f\sigma_8$, the ϵ_ν is error in the measurement of $Y_\nu(X_\nu)$ and the X_ν corresponds to the redshift Z. The reduced Chi-square is defined as $\chi^2_{\mathrm{red}} = \chi^2/(\eta - \mu)$. The best fit set of parameters occurs at minimum Chi-square estimation. The likelihood function is normalised to unity and can also be marginalised over certain parameters to consider a parameter sub-space [75]:

$$\int L(\Theta_\mu)\, d\Theta_\mu = 1 \,, \quad \text{and for e.g,} \quad L(\Theta_1) = \int L(\Theta_\mu)\, d\Theta_2 d\Theta_3 d\Theta_4, \tag{A.18}$$

A.4 Redshift Space Distortion Data

z	$f\sigma 8$	Survey	Refs.
0.02	0.36 ± 0.04	-	[90]
0.067	0.423 ± 0.055	6dF Galaxy Survey	[89]
0.15	0.49 ± 0.15	SDSS DR7 MGS	[88]
0.17	0.51 ± 0.06	2dF Galaxy Redshift Survey	[91][87]
0.22	0.42 ± 0.07	WiggleZ Dark Energy Survey	[86]
0.25	0.351 ± 0.058	SDSS II LRG	[85]
0.3	0.407 ± 0.055	SDSS I/II LRG + SDSS III BOSS CMASS	[83]
0.32	0.394 ± 0.062	SDSS III BOSS DR12 LOWZ	[82]
0.35	0.440 ± 0.05	SDSS DR5 LRG	[91][81]
0.37	0.460 ± 0.038	SDSS II LRG	[85]
0.38	0.430 ± 0.054	SDSS III BOSS DR12	[84]
0.4	0.419 ± 0.041	SDSS I/II LRG + SDSS III BOSS CMASS	[83]
0.41	0.45 ± 0.04	WiggleZ Dark Energy Survey	[86]
0.44	0.413 ± 0.080	WiggleZ Dark Energy Survey + Alcock-Paczynski distortion	[80]
0.5	0.427 ± 0.043	SDSS I/II LRG + SDSS III BOSS CMASS	[83]
0.51	0.452 ± 0.057	SDSS III BOSS DR12	[84]
0.57	0.444 ± 0.038	SDSS III BOSS DR12 CMASS	[82]
0.59	0.488 ± 0.06	SDSS III BOSS DR12 CMASS	[79]
0.60	0.43 ± 0.04	WiggleZ Dark Energy Survey	[86]
0.6	0.433 ± 0.067	SDSS I/II LRG + SDSS III BOSS CMASS	[83]
0.60	0.390 ± 0.063	WiggleZ Dark Energy Survey + Alcock-Paczynski distortion	[80]
0.61	0.457 ± 0.052	SDSS III BOSS DR12	[84]
0.73	0.437 ± 0.072	WiggleZ Dark Energy Survey + Alcock-Paczynski distortion	[80]
0.77	0.490 ± 0.18	VIMOS-VLT Deep Survey	[91][78]
0.78	0.38 ± 0.04	WiggleZ Dark Energy Survey	[86]
0.8	0.470 ± 0.08	VIMOS Public Extragalactic Redshift Survey	[76]
1.36	0.482 ± 0.116	FastSound	[77]

Table A.1: A summary of all RSD data (Compiled by Ref. [92]), used in the thesis.

A.5 Summary of all disformal fixed points

The following tables summarise all disformal fixed points as well as their eigenvalues, which were obtained from the three studied scenarios in the section 3.7. The conformal fixed points are a subset of the disformal fixed points, irrespective of the scenario. The notation " $-$ " means undetermined.

Point	x	z	σ	Ω_ϕ	w_ϕ	w_{eff}	Existence	Acceleration
A_0	0	0	0	1	-1	0	$\forall\beta,\alpha$	Yes
$(C_\pm)_{\mathbf{I}}$	±1	0	0	1	0	0	$\forall\beta,\alpha$	No
$(B_\pm)_{\mathbf{I}}$	$\frac{\sqrt{3}}{2\beta}$	$\pm\frac{\sqrt{4\beta^2-3}}{2\beta}$	$\frac{4\beta^2}{9}$	$\frac{3}{4\beta^2}$	0	$\frac{3}{4\beta^2}-1$	$\beta\leq-\frac{\sqrt{3}}{2}$ or $\beta\geq\frac{\sqrt{3}}{2}$	No
$(S_\pm)_{\mathbf{I}}$	0	0	$\pm\infty$	1	$-$	$-$	$\forall\beta,\alpha$	-
$(T_\pm)_{\mathbf{I}}$	0	±1	$\pm\infty$	0	$-$	$-$	$\forall\beta,\alpha$	-

Table A.2: This table shows a summary of all the fixed points which was obtained by solving the dynamical system (3.43)-(3.46) for a quintessence disformally coupled with pressureless fluid in the Scenario I ($\tilde{w}=0$ and $\tilde{w}_u=0$). For each fixed point, the existence and the effective equation of state, as defined in (3.33), are evaluated.

	Conformal		
Point	E_1	E_2	E_3
A_0	$-\frac{3}{2}$	$-\frac{3}{2}$	0
$(C_\pm)_{\mathbf{I}}$	$+3$	$+\frac{3}{2}$	$\pm\frac{\sqrt{3}\alpha}{2}$

	Disformal		
Point	E_1	E_2	E_3
A_0	$-\frac{3}{2}$	$-\frac{3}{2}$	0
$(C_\pm)_{\mathbf{I}}$	$+3$	$\pm\frac{\sqrt{3}\alpha}{2}$	$\pm2\sqrt{3}\beta-3$

Table A.3: This table shows all the eigenvalues, which are evaluated at each fixed point, for Scenario I ($\tilde{w}=0$ and $\tilde{w}_u=0$). The left and right tabular corresponds to the eigenvalues of the conformal dynamical system (3.37)-(3.38) and that of the disformal dynamical system (3.43)-(3.46) respectively. The eigenvalues of the disformal fixed points $(B_\pm)_{\mathbf{I}}$, $(S_\pm)_{\mathbf{I}}$ and $(T_\pm)_{\mathbf{I}}$ are undetermined.

Point	x	z	σ	Ω_ϕ	w_ϕ	w_{eff}	Existence	Acceleration
A_0	0	0	0	1	-1	-1	$\forall\beta,\alpha$	Yes
$(C_\pm)_{\mathbf{II}}$	±1	0	0	1	0	0	$\forall\beta,\alpha$	No
$(B_\pm)_{\mathbf{II}}$	$\frac{\sqrt{3}}{2\beta}$	$\pm\frac{\sqrt{4\beta^2-3}}{2\beta}$	$\frac{4\beta^2}{9}$	$\frac{3}{4\beta^2}$	0	$\frac{3}{4\beta^2}-1$	$\beta\leq-\frac{\sqrt{3}}{2}$ or $\beta\geq\frac{\sqrt{3}}{2}$	No
$(S_\pm)_{\mathbf{II}}$	0	0	$\pm\infty$	1	$-$	$-$	$\forall\beta,\alpha$	-

Table A.4: A summary of all the fixed points for the dynamical system (3.47)-(3.50) for a quintessence coupled with relativistic fluid in the Scenario II ($\tilde{w}=1/3$ and $\tilde{w}_u=0$).

	Conformal		
Point	E_1	E_2	E_3
A_0	-2	$-\frac{3}{2}$	0
$(C_\pm)_{\mathbf{II}}$	$+3$	$+\frac{3}{2}$	$-\frac{1}{2}$

	Disformal		
Point	E_1	E_2	E_3
A_0	-2	$-\frac{3}{2}$	0
$(C_\pm)_{\mathbf{II}}$	$+3$	$-\frac{1}{2}$	$\pm 2\sqrt{3}\beta - 3$
$(B_\pm)_{\mathbf{II}}$	-2	$-\frac{3}{2}$	$+3$

Table A.5: This table shows all the eigenvalues, which are evaluated at each fixed point, for Scenario II ($\tilde{w} = 1/3$ and $\tilde{w}_u = 0$). The left and right tabular corresponds to the eigenvalues of the conformal dynamical system (3.39)-(3.40) and that of the disformal dynamical system (3.47)-(3.50) respectively. The disformal eigenvalues of $(S_\pm)_{\mathbf{II}}$ are undertermined.

Point	x	z	σ	Ω_ϕ	w_ϕ	w_{eff}	Existence	Acceleration	E_1	E_2	E_3
A_0	0	0	0	1	-1	-1	$\forall\alpha, \beta$	Yes	-2	-2	0
$(D_\pm)_{\mathbf{III}}$	0	± 1	0	0	-	$\frac{1}{3}$	$\forall\alpha, \beta$	No	-4	-4	0
$(S_\pm)_{\mathbf{III}}$	0	0	$\pm\infty$	1	$-$	$-$	$\forall\alpha, \beta$	-	$-$	$-$	$-$
$(T_\pm)_{\mathbf{III}}$	0	± 1	$\pm\infty$	0	$-$	$-$	$\forall\alpha, \beta$	-	$-$	$-$	$-$

Table A.6: This table shows a summary of all the fixed points of the disformal dynamical system (3.51)-(3.54) for the Scenario III ($\tilde{w} = 1/3$ and $\tilde{w}_u = 1/3$). The nature of fixed point A_0 and $(D_\pm)_{\mathbf{III}}$ are found to be stable and unstable respectively. The Eigenvalues of A_0 is same for the dynamical system (3.41)-(3.42).

Bibliography

[1] M. Hobson, G. Efstathiou, & A. Lasenby, (Book): "General Relativity: An Introduction for Physicists." Cambridge University Press, (2006). doi:10.1017/CBO9780511790904

[2] T. Clifton, P. G. Ferreira, A. Padilla and C. Skordis, "Modified Gravity and Cosmology," Phys. Rept. **513** (2012), 1-189 doi:10.1016/j.physrep.2012.01.001 [arXiv:1106.2476 [astro-ph.CO]].

[3] R. V. Eotvos, D. Pekar and E. Fekete, "CONTRIBUTIONS TO THE LAW OF PROPORTIONALITY OF INERTIA AND GRAVITY," Annalen Phys. **68** (1922), 11-66

[4] S. K. Lamoreaux, J. P. Jacobs, B. R. Heckel, F. J. Raab and E. N. Fortson, "New limits on spatial anisotropy from optically pumped He-201 and Hg-199," Phys. Rev. Lett. **57** (1986), 3125-3128 doi:10.1103/PhysRevLett.57.3125

[5] G. D. Birkhoff and R. E. Langer, (Book): "Relativity and modern physics", Published in:Cambridge, Harvard University Press, (1923), Provided by the SAO/NASA Astrophysics Data System, URL: http://adsabs.harvard.edu/abs/1923rmp..book.....B

[6] D. Lovelock, "The Einstein tensor and its generalizations," J. Math. Phys. **12** (1971), 498-501 doi:10.1063/1.1665613

[7] D. Lovelock, "The four-dimensionality of space and the einstein tensor," J. Math. Phys. **13** (1972), 874-876 doi:10.1063/1.1666069

[8] R. M. Wald, "Final states of gravitational collapse," Phys. Rev. Lett. **26** (1971), 1653-1655 doi:10.1103/PhysRevLett.26.1653

[9] J. D. Bekenstein, "The Relation between physical and gravitational geometry," Phys. Rev. D **48** (1993) 3641 doi:10.1103/PhysRevD.48.3641 [gr-qc/9211017].

[10] G. F. R. Ellis and H. van Elst, "Cosmological models: Cargese lectures 1998," NATO Sci. Ser. C **541** (1999), 1-116 [arXiv:gr-qc/9812046 [gr-qc]].

[11] J.P. Uzan & P. Peter (Book): "Primordial Cosmology" Oxford University Press, (2013). ISBN: 9780199665150, 9780199209910

[12] A. G. Riess *et al.* [Supernova Search Team], "Observational evidence from supernovae for an accelerating universe and a cosmological constant," Astron. J. **116** (1998), 1009-1038 doi:10.1086/300499 [arXiv:astro-ph/9805201 [astro-ph]].

[13] N. Aghanim *et al.* [Planck Collaboration], "Planck 2018 results. VI. Cosmological parameters," arXiv:1807.06209 [astro-ph.CO].

[14] A. Porredon *et al.* [DES], "Dark Energy Survey Year 3 results: Cosmological constraints from galaxy clustering and galaxy-galaxy lensing using the MagLim lens sample," [arXiv:2105.13546 [astro-ph.CO]].

[15] E. Komatsu *et al.* [WMAP], "Seven-Year Wilkinson Microwave Anisotropy Probe (WMAP) Observations: Cosmological Interpretation," Astrophys. J. Suppl. **192** (2011), 18 doi:10.1088/0067-0049/192/2/18 [arXiv:1001.4538 [astro-ph.CO]].
[16]

[16] M. Kowalski *et al.* [Supernova Cosmology Project], "Improved Cosmological Constraints from New, Old and Combined Supernova Datasets," Astrophys. J. **686** (2008), 749-778 doi:10.1086/589937 [arXiv:0804.4142 [astro-ph]].

[17] A. Arbey and F. Mahmoudi, "Dark matter and the early Universe: a review," doi:10.1016/j.ppnp.2021.103865 [arXiv:2104.11488 [hep-ph]].

[18] E. Corbelli and P. Salucci, "The Extended Rotation Curve and the Dark Matter Halo of M33," Mon. Not. Roy. Astron. Soc. **311** (2000) 441 doi:10.1046/j.1365-8711.2000.03075.x [astro-ph/9909252].

[19] D. Clowe, A. Gonzalez and M. Markevitch, "Weak lensing mass reconstruction of the interacting cluster 1E0657-558: Direct evidence for the existence of dark matter," Astrophys. J. **604** (2004) 596 doi:10.1086/381970 [astro-ph/0312273].

[20] Peacock, J. A. 1999, Cosmological Physics

[21] J.-P Uzan, and R. Lehoucq, "A dynamical study of the Friedmann equations", European Journal of Physics, (2001), Vol. 22, no. 4, Pg. 371–384,. doi:10.1088/0143-0807/22/4/312.

[22] S. Bahamonde, C. G. Böhmer, S. Carloni, E. J. Copeland, W. Fang and N. Tamanini, "Dynamical systems applied to cosmology: dark energy and modified gravity," Phys. Rept. **775-777** (2018), 1-122 doi:10.1016/j.physrep.2018.09.001 [arXiv:1712.03107 [gr-qc]].

[23] H. E. S. Velten, R. F. vom Marttens and W. Zimdahl, "Aspects of the cosmological "coincidence problem"," Eur. Phys. J. C **74** (2014) no.11, 3160 doi:10.1140/epjc/s10052-014-3160-4 [arXiv:1410.2509 [astro-ph.CO]].

[24] B. J. Barros, L. Amendola, T. Barreiro and N. J. Nunes, "Coupled quintessence with a ΛCDM background: removing the σ_8 tension," JCAP **01** (2019), 007 doi:10.1088/1475-7516/2019/01/007 [arXiv:1802.09216 [astro-ph.CO]].

[25] C. P. Ma and E. Bertschinger, "Cosmological perturbation theory in the synchronous and conformal Newtonian gauges," Astrophys. J. **455** (1995), 7-25 doi:10.1086/176550 [arXiv:astro-ph/9506072 [astro-ph]].

[26] D. H. Weinberg, M. J. Mortonson, D. J. Eisenstein, C. Hirata, A. G. Riess and E. Rozo, "Observational Probes of Cosmic Acceleration," Phys. Rept. **530** (2013), 87-255 doi:10.1016/j.physrep.2013.05.001 [arXiv:1201.2434 [astro-ph.CO]].

[27] V. Motta, M. A. García-Aspeitia, A. Hernández-Almada, J. Magaña and T. Verdugo, "Taxonomy of Dark Energy Models," [arXiv:2104.04642 [astro-ph.CO]].

[28] L. Verde, T. Treu and A. G. Riess, "Tensions between the Early and the Late Universe," Nature Astron. **3**, 891 doi:10.1038/s41550-019-0902-0 [arXiv:1907.10625 [astro-ph.CO]].

[29] E. Di Valentino, O. Mena, S. Pan, L. Visinelli, W. Yang, A. Melchiorri, D. F. Mota, A. G. Riess and J. Silk, "In the Realm of the Hubble tension − a Review of Solutions," [arXiv:2103.01183 [astro-ph.CO]].

[30] S. Joudaki, H. Hildebrandt, D. Traykova, N. E. Chisari, C. Heymans, A. Kannawadi, K. Kuijken, A. H. Wright, M. Asgari and T. Erben, *et al.* Astron. Astrophys. **638** (2020), L1 doi:10.1051/0004-6361/201936154 [arXiv:1906.09262 [astro-ph.CO]].

[31] A. G. Riess, L. M. Macri, S. L. Hoffmann, D. Scolnic, S. Casertano, A. V. Filippenko, B. E. Tucker, M. J. Reid, D. O. Jones and J. M. Silverman, *et al.* Astrophys. J. **826** (2016) no.1, 56 doi:10.3847/0004-637X/826/1/56 [arXiv:1604.01424 [astro-ph.CO]].

[32] R. J. Adler, B. Casey, , and O. C. Jacob, "Vacuum catastrophe: An elementary exposition of the cosmological constant problem", American Journal of Physics (1995), vol. 63, no. 7, pp. 620–626,. doi:10.1119/1.17850.

[33] S. E. Rugh,and H., Zinkernagel, "The quantum vacuum and the cosmological constant problem", Studies in the History and Philosophy of Modern Physics, (2002), vol. 33, no. 4, pp. 663–705, doi:10.1016/S1355-2198(02)00033-3.

[34] M. Thorsrud, "Bianchi models with a free massless scalar field: invariant sets and higher symmetries," Class. Quant. Grav. **36** (2019) no.23, 235014 doi:10.1088/1361-6382/ab45b3 [arXiv:1905.11456 [gr-qc]].

[35] A. Nunes, J. P. Mimoso and T. C. Charters, "Scaling solutions from interacting fluids," Phys. Rev. D **63** (2001) 083506 doi:10.1103/PhysRevD.63.083506 [gr-qc/0011073].

[36] L. Amendola, "Scaling solutions in general nonminimal coupling theories," Phys. Rev. D **60** (1999), 043501 doi:10.1103/PhysRevD.60.043501 [arXiv:astro-ph/9904120 [astro-ph]].

[37] D. J. Holden and D. Wands, Phys. Rev. D **61** (2000), 043506 doi:10.1103/PhysRevD.61.043506 [arXiv:gr-qc/9908026 [gr-qc]].

[38] B. Wang, E. Abdalla, F. Atrio-Barandela and D. Pavon, "Dark Matter and Dark Energy Interactions: Theoretical Challenges, Cosmological Implications and Observational Signatures," Rept. Prog. Phys. **79** (2016) no.9, 096901 doi:10.1088/0034-4885/79/9/096901 [arXiv:1603.08299 [astro-ph.CO]].

[39] P. G. Bergmann, "Comments on the scalar-tensor theory", International Journal of Theoretical Physics, (1968), Vol 1, No 1, Pg 25-36 https://doi.org/10.1007/BF00668828

[40] K. Nordtvedt, Jr., "PostNewtonian metric for a general class of scalar tensor gravitational theories and observational consequences," Astrophys. J. **161** (1970), 1059-1067 doi:10.1086/150607

[41] R. V. Wagoner, "Scalar tensor theory and gravitational waves," Phys. Rev. D **1** (1970), 3209-3216 doi:10.1103/PhysRevD.1.3209

[42] R. H. Dicke, "Mach's principle and invariance under transformation of units," Phys. Rev. **125** (1962), 2163-2167 doi:10.1103/PhysRev.125.2163

[43] C. Brans and R. H. Dicke, "Mach's principle and a relativistic theory of gravitation," Phys. Rev. **124** (1961), 925-935 doi:10.1103/PhysRev.124.925

[44] C. van de Bruck, J. Mifsud, J. P. Mimoso and N. J. Nunes, "Generalized dark energy interactions with multiple fluids," JCAP **1611** (2016) 031 doi:10.1088/1475-7516/2016/11/031 [arXiv:1605.03834 [gr-qc]].

[45] L. Amendola, "Coupled quintessence," Phys. Rev. D **62** (2000), 043511 doi:10.1103/PhysRevD.62.043511 [arXiv:astro-ph/9908023 [astro-ph]].

[46] A. Leithes, K. A. Malik, D. J. Mulryne and N. J. Nunes, Phys. Rev. D **95** (2017) no.12, 123519 doi:10.1103/PhysRevD.95.123519 [arXiv:1608.00908 [astro-ph.CO]].

[47] M. Shahalam, S. D. Pathak, M. M. Verma, M. Y. Khlopov and R. Myrzakulov, Eur. Phys. J. C **75** (2015) no.8, 395 doi:10.1140/epjc/s10052-015-3608-1 [arXiv:1503.08712 [gr-qc]].

[48] C. van de Bruck and G. Sculthorpe, "Modified Gravity and the Radiation Dominated Epoch," Phys. Rev. D **87** (2013) no.4, 044004 doi:10.1103/PhysRevD.87.044004 [arXiv:1210.2168 [astro-ph.CO]].

[49] P. A. R. Ade *et al.* [Planck], Astron. Astrophys. **594** (2016), A13 doi:10.1051/0004-6361/201525830 [arXiv:1502.01589 [astro-ph.CO]].

[50] B. J. Barros, T. Barreiro and N. J. Nunes, "Spherical collapse in coupled quintessence with a ΛCDM background," Phys. Rev. D **101** (2020) no.2, 023502 doi:10.1103/PhysRevD.101.023502 [arXiv:1907.10083 [astro-ph.CO]].

[51] Brans, C. and Dicke, R. H., (1961), **Phys. Rev., American Physical Society**, Vol. 124, Pages 925-935, Mach's Principle and a Relativistic Theory of Gravitation.

[52] P. A. M Dirac, (1973), **Proceedings of the Royal Society of London. A. Mathematical and Physical Sciences**, Vol. 333, Pages 403-418, Long range forces and broken symmetries.

[53] G. T. Horowitz and A. Strominger, (1991), **Nuclear Physics B**, Vol. 360, Pages 197 - 209, Black strings and p-branes

[54] M. Zumalacirregui and J. Garcia-Bellido, "Transforming gravity: from derivative couplings to matter to second-order scalar-tensor theories beyond the Horndeski Lagrangian," Phys. Rev. D **89** (2014) 064046 doi:10.1103/PhysRevD.89.064046 [arXiv:1308.4685 [gr-qc]].

[55] D. Bettoni and S. Liberati, Phys. Rev. D **88** (2013), 084020 doi:10.1103/PhysRevD.88.084020 [arXiv:1306.6724 [gr-qc]].

[56] C. de Rham and G. Gabadadze, "Generalization of the Fierz-Pauli Action," Phys. Rev. D **82** (2010) 044020 doi:10.1103/PhysRevD.82.044020 [arXiv:1007.0443 [hep-th]].

[57] T. Q. Do, "Higher dimensional nonlinear massive gravity," Phys. Rev. D **93** (2016) no.10, 104003 doi:10.1103/PhysRevD.93.104003 [arXiv:1602.05672 [gr-qc]].

[58] T. Koivisto, D. Wills and I. Zavala, "Dark D-brane Cosmology," JCAP **1406** (2014) 036 doi:10.1088/1475-7516/2014/06/036 [arXiv:1312.2597 [hep-th]].

[59] L. Xiao, R. An, L. Zhang, B. Yue, Y. Xu and B. Wang, "Can conformal and disformal couplings between dark sectors explain the EDGES 21-cm anomaly?," Phys. Rev. D **99** (2019) no.2, 023528 doi:10.1103/PhysRevD.99.023528 [arXiv:1807.05541 [astro-ph.CO]].

[60] R. Gannouji, M. W. Hossain, N. Jaman and M. Sami, "Bigravity and Horndeski gravity connected by a disformal coupling," Phys. Rev. D **99** (2019) no.4, 043504 doi:10.1103/PhysRevD.99.043504 [arXiv:1808.04137 [gr-qc]].

[61] P. Brax, A. C. Davis and A. Kuntz, "Disformally Coupled Scalar Fields and Inspiralling Trajectories," Phys. Rev. D **99** (2019) no.12, 124034 doi:10.1103/PhysRevD.99.124034 [arXiv:1903.03842 [gr-qc]].

[62] E. M. Teixeira, A. Nunes and N. J. Nunes, "Disformally Coupled Quintessence," Phys. Rev. D **101** (2020) no.8, 083506 doi:10.1103/PhysRevD.101.083506 [arXiv:1912.13348 [gr-qc]].

[63] F. F. Bernardi and R. G. Landim, "Coupled quintessence and the impossibility of an interaction: a dynamical analysis study," Eur. Phys. J. C **77** (2017) no.5, 290 doi:10.1140/epjc/s10052-017-4858-x [arXiv:1607.03506 [gr-qc]].

[64] C. G. Boehmer, N. Tamanini and M. Wright, "Interacting quintessence from a variational approach Part II: derivative couplings," Phys. Rev. D **91** (2015) no.12, 123003 doi:10.1103/PhysRevD.91.123003 [arXiv:1502.04030 [gr-qc]].

[65] C. van de Bruck, J. Mifsud and N. J. Nunes, "The variation of the fine-structure constant from disformal couplings," JCAP **12** (2015), 018 doi:10.1088/1475-7516/2015/12/018 [arXiv:1510.00200 [astro-ph.CO]].

[66] J. Wainwright, G. Ellis, (Book): "Dynamical Systems in Cosmology", Cambridge University Press, (1997). doi:10.1017/CBO9780511524660

[67] C. van de Bruck, J. Morrice and S. Vu, "Constraints on Nonconformal Couplings from the Properties of the Cosmic Microwave Background Radiation", Phys. Rev. Lett. **111** (2013) 161302 doi:10.1103/PhysRevLett.111.161302 [arXiv:1303.1773 [astro-ph.CO]].

[68] C. van de Bruck and J. Morrice, "Disformal couplings and the dark sector of the universe," JCAP **04** (2015), 036 doi:10.1088/1475-7516/2015/04/036 [arXiv:1501.03073 [gr-qc]].

[69] J. Gleyzes, D. Langlois, M. Mancarella and F. Vernizzi, "Effective Theory of Interacting Dark Energy," JCAP **08** (2015), 054 doi:10.1088/1475-7516/2015/08/054 [arXiv:1504.05481 [astro-ph.CO]].

[70] L. Perenon, J. Bel, R. Maartens and A. de la Cruz-Dombriz, "Optimising growth of structure constraints on modified gravity," JCAP **06** (2019), 020 doi:10.1088/1475-7516/2019/06/020 [arXiv:1901.11063 [astro-ph.CO]].

[71] B. J. Barros, T. Barreiro, T. Koivisto and N. J. Nunes, Phys. Dark Univ. **30** (2020), 100616 doi:10.1016/j.dark.2020.100616 [arXiv:2004.07867 [gr-qc]].

[72] L. Kazantzidis and L. Perivolaropoulos, Phys. Rev. D **97** (2018) no.10, 103503 doi:10.1103/PhysRevD.97.103503 [arXiv:1803.01337 [astro-ph.CO]].

[73] J. Gleyzes, D. Langlois, M. Mancarella and F. Vernizzi, "Effective Theory of Dark Energy at Redshift Survey Scales," JCAP **02** (2016), 056 doi:10.1088/1475-7516/2016/02/056 [arXiv:1509.02191 [astro-ph.CO]]. 64 citations counted in INSPIRE as of 11 Feb 2022

[74] A. Dusoye, A. de la Cruz-Dombriz, P. Dunsby and N. J. Nunes, "Disformal couplings in a ΛCDM background cosmology," JCAP **03** (2021), 002 doi:10.1088/1475-7516/2021/03/002 [arXiv:2006.16962 [gr-qc]].

[75] William H. Press and Saul A. Teukolsky, (1992) (Book): "Numerical Recipes in C : the Art of Scientific Computing", Published in: Cambridge [Cambridgeshire] ; New York :Cambridge University Press, (ISBN 0-521-43108-5)
RSD DATA

[76] S. de la Torre, L. Guzzo, J. A. Peacock, E. Branchini, A. Iovino, B. R. Granett, U. Abbas, C. Adami, S. Arnouts and J. Bel, *et al.* "The VIMOS Public Extragalactic

Redshift Survey (VIPERS). Galaxy clustering and redshift-space distortions at z=0.8 in the first data release," Astron. Astrophys. **557** (2013), A54 doi:10.1051/0004-6361/201321463 [arXiv:1303.2622 [astro-ph.CO]].

[77] H. Okada, T. Totani, M. Tonegawa, M. Akiyama, G. Dalton, K. Glazebrook, F. Iwamuro, K. Ohta, N. Takato and N. Tamura, *et al.* "The Subaru FMOS Galaxy Redshift Survey (FastSound). II. The Emission Line Catalog and Properties of Emission Line Galaxies," Publ. Astron. Soc. Jap. **68** (2016) no.3, 47 doi:10.1093/pasj/psw043 [arXiv:1504.05592 [astro-ph.GA]].

[78] L. Guzzo, M. Pierleoni, B. Meneux, E. Branchini, O. L. Fevre, C. Marinoni, B. Garilli, J. Blaizot, G. De Lucia and A. Pollo, *et al.* Nature **451** (2008), 541-545 doi:10.1038/nature06555 [arXiv:0802.1944 [astro-ph]].

[79] C. H. Chuang, F. Prada, M. Pellejero-Ibanez, F. Beutler, A. J. Cuesta, D. J. Eisenstein, S. Escoffier, S. Ho, F. S. Kitaura and J. P. Kneib, *et al.* "The clustering of galaxies in the SDSS-III Baryon Oscillation Spectroscopic Survey: single-probe measurements from CMASS anisotropic galaxy clustering," Mon. Not. Roy. Astron. Soc. **461** (2016) no.4, 3781-3793 doi:10.1093/mnras/stw1535 [arXiv:1312.4889 [astro-ph.CO]].

[80] C. Blake, "The WiggleZ Dark Energy Survey: joint measurements of the expansion and growth history at $z < 1$", Mon. Not. Roy. Astron. Soc., **425** (2012) no. 1, pp. 405–414, doi:10.1111/j.1365-2966.2012.21473.x.

[81] M. Tegmark *et al.* [SDSS], "Cosmological Constraints from the SDSS Luminous Red Galaxies," Phys. Rev. D **74** (2006), 123507 doi:10.1103/PhysRevD.74.123507 [arXiv:astro-ph/0608632 [astro-ph]].

[82] H. Gil-Marín, W. J. Percival, J. R. Brownstein, C. H. Chuang, J. N. Grieb, S. Ho, F. S. Kitaura, C. Maraston, F. Prada and S. Rodríguez-Torres, *et al.* "The clustering of galaxies in the SDSS-III Baryon Oscillation Spectroscopic Survey: RSD measurement from the LOS-dependent power spectrum of DR12 BOSS galaxies," Mon. Not. Roy. Astron. Soc. **460** (2016) no.4, 4188-4209 doi:10.1093/mnras/stw1096 [arXiv:1509.06386 [astro-ph.CO]].

[83] R. Tojeiro, "The clustering of galaxies in the SDSS-III Baryon Oscillation Spectroscopic Survey: measuring structure growth using passive galaxies", Mon. Not. Roy. Astron. Soc., **424** (2012) no. 3, pp. 2339–2344 doi:10.1111/j.1365-2966.2012.21404.x.

[84] S. Satpathy *et al.* [BOSS], "The clustering of galaxies in the completed SDSS-III Baryon Oscillation Spectroscopic Survey: On the measurement of growth rate using galaxy correlation functions," Mon. Not. Roy. Astron. Soc. **469** (2017) no.2, 1369-1382 doi:10.1093/mnras/stx883 [arXiv:1607.03148 [astro-ph.CO]].

[85] , L. Samushia, W. J. Percival, and A. Raccanelli, "Interpreting large-scale redshift-space distortion measurements", Mon. Not. Roy. Astron. Soc. **420** (2012) no.3, pp. 2102–2119 doi:10.1111/j.1365-2966.2011.20169.x.

[86] C. Blake, "The WiggleZ Dark Energy Survey: the growth rate of cosmic structure since redshift z=0.9", Mon. Not. Roy. Astron. Soc. , **415** (2011) no.3, pp. 2876–2891 doi:10.1111/j.1365-2966.2011.18903.x.

[87] W. J. Percival *et al.* [2dFGRS], "The 2dF Galaxy Redshift Survey: Spherical harmonics analysis of fluctuations in the final catalogue," Mon. Not. Roy. Astron. Soc. **353** (2004), 1201 doi:10.1111/j.1365-2966.2004.08146.x [arXiv:astro-ph/0406513 [astro-ph]].

[88] C. Howlett, A. Ross, L. Samushia, W. Percival and M. Manera, "The clustering of the SDSS main galaxy sample II. Mock galaxy catalogues and a measurement of the growth of structure from redshift space distortions at $z = 0.15$," Mon. Not. Roy. Astron. Soc. **449** (2015) no.1, 848-866 doi:10.1093/mnras/stu2693 [arXiv:1409.3238 [astro-ph.CO]].

[89] F. Beutler, "The 6dF Galaxy Survey: z$\approx$ 0 measurements of the growth rate and σ_8", Mon. Not. Roy. Astron. Soc. **423** (2012) no.4, pp. 3430–3444,[arXiv:1204.4725 [astro-ph.CO]] doi:10.1111/j.1365-2966.2012.21136.x.

[90] M. J. Hudson and S. J. Turnbull, "The Growth Rate of Cosmic Structure from Peculiar Velocities at Low and High Redshifts", The Astrophysical Journal, (2012), vol. 751, no. 2, [arXiv:1203.4814 [astro-ph.CO]]. doi:10.1088/2041-8205/751/2/L30. [91]

[91] Y. S. Song and W. J. Percival, "Reconstructing the history of structure formation using Redshift Distortions," JCAP **10** (2009), 004 doi:10.1088/1475-7516/2009/10/004 [arXiv:0807.0810 [astro-ph]].

[92] I. Albarran, M. Bouhmadi-López and J. Morais, "Cosmological perturbations in an effective and genuinely phantom dark energy Universe," Phys. Dark Univ. **16** (2017), 94-108 doi:10.1016/j.dark.2017.04.002 [arXiv:1611.00392 [astro-ph.CO]].